Exploring the Effects of Fluoroalkyl Sidechains on Peptoid Secondary Structure

LEWIS JAMES PICKEN

Durham University

A thesis entitled

Exploring the Effects of Fluoroalkyl Sidechains on Peptoid Secondary Structure

Submitted by

Lewis James Picken

(Collingwood College)

Durham University

Department of Chemistry

A Candidate for the Degree Master of Science by Research

March 2023

Statement of Copyright

Declaration

This work was conducted in the Department of Chemistry of Durham University between October 2021 and September 2022. The work has not been submitted for a degree in this or any other university. Unless otherwise indicated, this is my own work.

Abstract

N-substituted glycines (peptoids) are a promising class of peptidomimetic that exhibit proteolytic resistance, enhanced lipophilicity, and greater structural diversity relative to their peptide counterparts. Peptoids have shown great potential as antimicrobials owing their advantageous properties, yet the development of novel antimicrobial sequences is hindered. This is due the presence of a tertiary amide backbone, which removes the capacity for hydrogen bonding interactions and thus renders many peptoids disordered in solution. Currently, the *de novo* design of extended sequences is reliant on a toolbox of peptoid monomers, capable of directing the tertiary amide bond to a single isomer. This selection of monomers is currently dominated by bulky, charged, chiral and aromatic sidechains.

This work describes the development of novel, fluoroalkyl sidechains capable of inducing the *cis* amide bond isomer in model dipeptoid systems. A series of 1D and 2D NMR experiments were performed to calculate $K_{cis/trans}$ for the library of monomers studied. Further NMR experiments evaluated the relationship between sidechain fluorination and lipophilicity. The fluorinated monomers investigated gave $K_{cis/trans}$ values up to 6.22 in CD_3CN and displayed an increase in lipophilicity upon higher degrees of fluorination. A selection of these new monomers were then incorporated into oligomers utilizing microwave irradiation to accelerate the solid-phase synthesis. Analysis of these extended sequences in solution gave characteristic, right-handed, alpha-helical spectra by CD spectroscopy.

Acknowledgements

Firstly, I must extend my greatest thanks to Professor Steven Cobb who supervised this project. Steven was kind enough to accept me into his group and provided a great deal of support, encouragement, and opportunity to develop my research and presentation skills. He has been an excellent mentor throughout my time in Durham and a voice of encouragement when I doubted my abilities. The same can be said for my secondary supervisor Dr William Brittain, who was always on hand and willing to provide practical advice as well as share his immense knowledge of organic chemistry.

Thank you to the technical staff at the chemistry department, namely: Dr Juan A Aguilar Malavia for helping me to execute and interpret my many NMR experiments, Dr David Parker and Mr Peter Stokes for advising on and running my mass spectrometry samples, and Dr Dmitry Yufit for generating and refining the crystal structures presented in this thesis. I would also like to acknowledge Dr Aileen Congreve and Professor Elizabeth Bromley for training me on and subsequently supporting me with the puriFlash purification system and CD spectrometer respectively, as these instruments were paramount to the work conducted in Chapter 3.

Thank you to the whole of the Cobb group for your guidance and motivation during my time in Durham. This is a fantastic group of young researchers with whom it has been a pleasure to work with. I would like to highlight Carissa Lloyd, Izzy Zawadzki and Diana Kolos who I spent much of my day to day working with. These three supported me throughout the entirety of my research, imparting endless advice as well as being friendly faces around the lab. My time in Durham would've been very different if not for Liam Beardmore, with whom I started and finished my masters. Liam is a fantastic chemist and friend who never failed to make me laugh even when the project was difficult. Thank you all for such an insightful and enjoyable experience.

Finally, I would like to thank my parents Andrew and Joanne Picken. Without them, this project would not have been possible. Thank you for always believing in me and everything you have given to get me where I am today. I hope I can make you proud.

Conferences

This work has been presented as part of the following conferences:

- 20th RSC Fluorine Interest Group Postgraduate Meeting 2022 (as a poster)
- The Durham Postgraduate Research Symposium 2022 (as a talk)
- 11th Peptoid Summit 2022 (as a poster)

Abbreviations

Ac	Acetyl
AcCl	Acetyl chloride
AMP	Antimicrobial peptide
Bn	Benzyl
Boc	*tert*-butyloxycarbonyl
CD	Circular dichroism
CD_3CN	Deuterated acetonitrile
CD_3OD	Deuterated methanol
$CDCl_3$	Deuterated chloroform
COSY	^1H-^1H Correlation spectroscopy
DCM	Dichloromethane
DIC	N,N'-Diisopropylcarbodiimide
DIPEA	N,N'-Diisopropylethylamine
DMF	Dimethylformamide
ESI	Electrospray ionization
EtOAc	Ethyl acetate
Fmoc	9-Fluorenylmethyl carbamate
gem	*Geminal*
HMBC	Heteronuclear multiple bond correlation
HPLC	High pressure liquid chromatography
HRMS	High resolution mass spectrometry
HSQC	Heteronuclear single quantum coherence spectroscopy
Hz	Hertz
LC/MS	Liquid chromatography/ mass spectrometry
Log D	Distribution coefficient

Log *P*	Partition coefficient
MeCN	Acetonitrile
MeOH	Methanol
MIC	Minimum inhibitory concentration
NMM	N-Methylmorpholine
NMR	Nuclear magnetic resonance
NOE/NOESY	Nuclear overhauser effect/ nuclear overhauser effect spectroscopy
PPI/PPII	Polyproline type 1/ polyproline type 2
Psyche	Pure shift yielded by chirp excitation spectroscopy
QToF	Quadrupole time of flight
RT	Retention time
S_N2	Bimolecular nucleophilic substitution reaction
^{t}Bu	*tert*-Butyl
TFA	Trifluoroacetic acid
TFE	Trifluoroethanol
THF	Tetrahydrofuran
TIPS	Triisopropylsilane
TLC	Thin layer chromatography
UPLC	Ultra-high performance liquid chromatography
UV	Ultraviolet
v/v	Volumetric ratio

Thesis Contents

Chapter 1: Introduction to Peptoids and their Secondary Structure

1.1 Background on Peptoids

1.1.1 Peptides to Peptidomimetics

Ubiquitous to living organisms, peptides are principal biomolecules comprised of repeating units known as amino acids. Nature typically utilizes just 20 unique variations of these monomers to form extended sequences, capable of self-assembly into complex secondary structures. Physiologically pertinent, structure-activity relationships of these polymers have found great significance in therapeutic research.[1]

Proportionally poised between small molecules and proteins, peptides can possess potent and selective pharmacological characteristics complimented by a relatively low toxicity.[1] Despite offering a rich source of therapeutic potential, peptide drugs show instability *in vivo*.[2] Rapid enzymatic degradation results in poor bioavailability, short half-lives and the need for administration via parenteral routes.[3]

Peptidomimetics are analogues of peptides, that tend to exhibit proteolytic resistance and enhanced bioavailability. Grossman arranged peptidomimetics into four divisions based on their similarity to the native substrate.[4,5] Classes A and B denote mimetics with significant peptide character, whereas classes C and D represent small molecules with unnatural frameworks.[5] Class A mimetics only possess minor backbone or sidechain alterations, including D- and β-amino acids as well as cyclized and stapled chains.[5] Compounds belonging to class B offer a more drastic deviation from the natural α-amino acid sequence, such as the incorporation of small molecules, like lipids[6] and PEG chains,[7] and foldamers which are a family of peptide analogues with non-natural backbone alterations.[8] The structures of a selection of class A and B peptidomimetics, as well as examples of foldamers with various backbone compositions, can be seen in **Figure 1.1**.

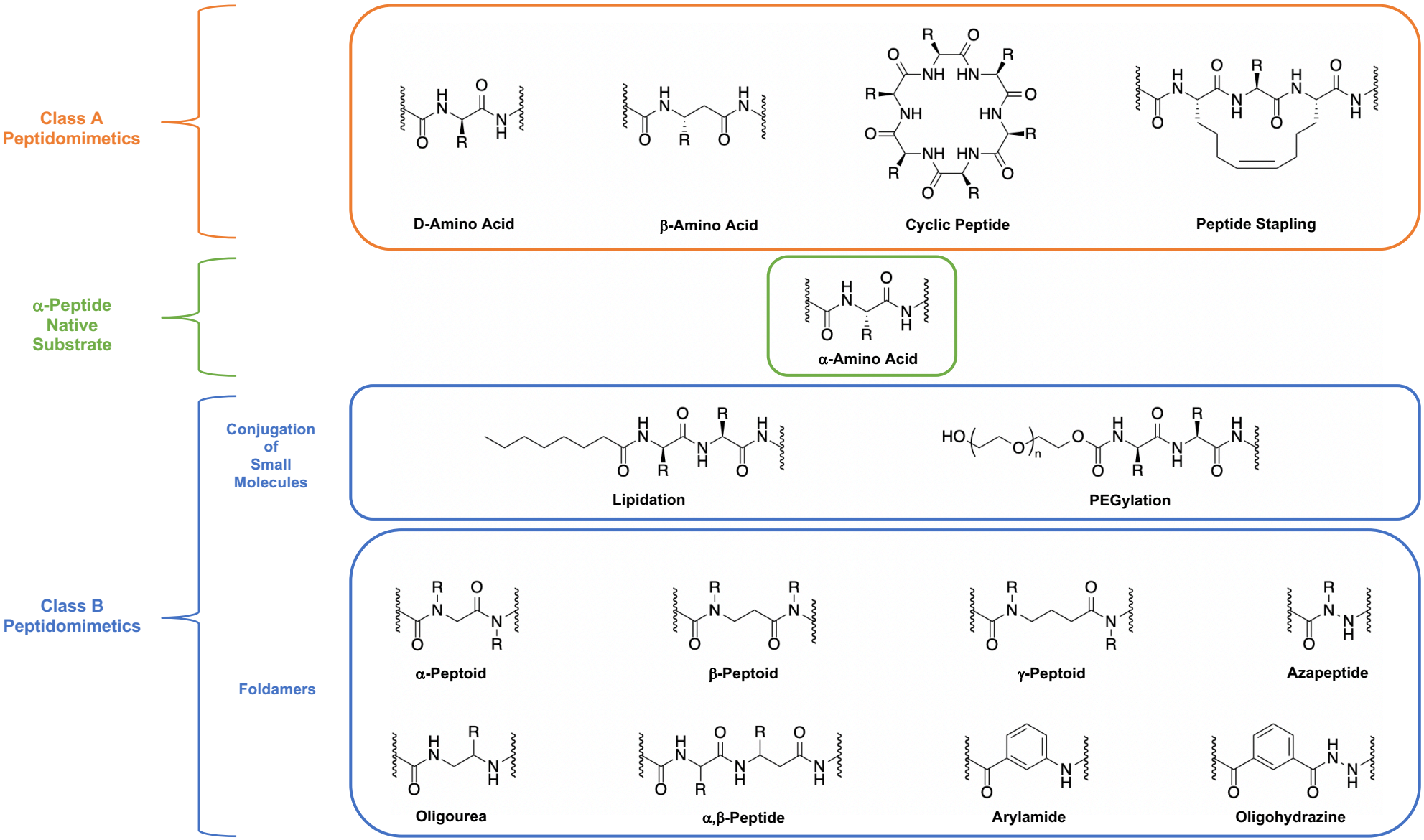

Figure 1.1: Structural composition of different class A and class B peptidomimetics including various foldamers with non-natural backbone compositions.[8]

1.1.2 Peptoids and their Structure

N-substituted glycines (peptoids) first came to light in the early 1990's[9] and see the variable R group on the alpha carbon in amino acids shifted and instead appended to the backbone amide nitrogen. Conserving the topology of the peptide sequence, peptoids impose divergence from the parent backbone discrete enough to retain significant peptide-like character.

Migration of the sidechain moiety to nitrogen affords three defining structural characteristics to the peptoid backbone: a lack of nitrogen bound protons, the presence of tertiary amides and elimination of chirality at C_α (**Figure 1.2**). Consequently, each of these distinctions collectively contribute to the inherent heterogeneity of peptoid oligomers.

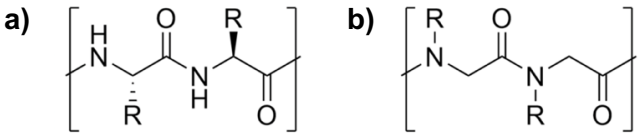

Figure 1.2: General backbone structure of **a)** an α-peptide and **b)** an α-peptoid.

Naturally occurring amino acids, excluding glycine, accommodate a stereogenic centre at the alpha carbon, conferring polypeptides with an intrinsic handedness. Lacking a C_β atom eliminates many of the steric clashes experienced by other amino acids, giving rise to extensive backbone flexibility as seen in glycine's Ramachandran plot (**Figure 1.3**).

Resonance across the amide engenders a 'double-bond' character between carbon and nitrogen,[10] bringing *cis*/*trans* nomenclature to peptide orientation. With the exception of proline, amino acids almost exclusively adopt a *trans* (ω = 180°) conformation in lieu of *cis* (ω = 0°), being separated by a rotational barrier of approximately 54-84 kJ/mol.[11,12]

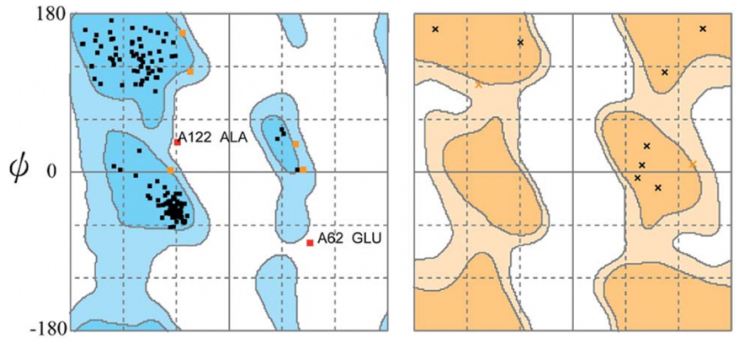

Figure 1.3: General Ramachandran plot of an amino acid (left) vs Ramachandran plot of glycine (right) showing larger regions of energetically allowed orientations. Darker regions denote allowed conformations. Figure sourced from Tang and Chen, 2015.[13]

In *cis* peptide arrangements, sidechains at C_α for adjacent amino acids clash whereas when *trans*, the amide hydrogen offers significantly reduced steric repulsion.[12] Tertiary amide bonds in peptoids isomerize between rotamers far more readily, as the bond experiences steric clashes for both conformations.[12,14] The tertiary amide architecture also removes hydrogen bond donors from the backbone, rendering peptoids unable to stabilize their high order folded structures via H-bonding networks.[15]

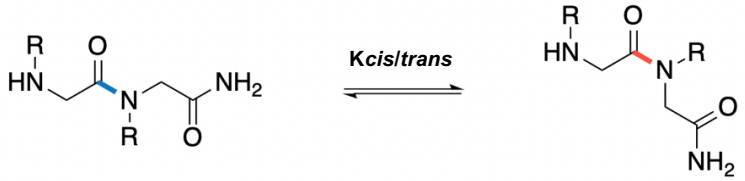

Figure 1.4: Isomerism between *cis*/*trans* conformations about the amide bond in α-peptoids. *Trans* amide bond shown in blue (ω = 180°) and *cis* amide bond shown in red (ω = 0°).

By virtue of their backbone composition, peptoids are constitutionally flexible and routinely exhibit either of the almost isoenergetic *cis* and *trans* arrangements (**Figure 1.4**). The *de novo* design of oligomers with stable secondary structures is at the frontier of current foldamer chemistry. Monomers that can force the backbone dihedral angles into a *cis* amide orientation can be utilized to form α-helix like structures capable of mimicking biopolymers.

1.1.3 The Peptoid Helix

Several secondary scaffolds have been documented for peptoid oligomers. For example, Crapster et al. found peptoid **1** to spontaneously arrange into antiparallel sheets, stabilized by intermolecular hydrogen bonding between *trans* inducing *N*-hydroxy amide sidechains (**Figure 1.5**).[16] Peptoid ribbons were also reported in hexamers by Crapster et al.,[17] having an alternating backbone of *cis* and *trans* inducing monomers. With the backbone extending in a single dimension, the peptoid adopts a spiral configuration as seen in **Figure 1.6**.

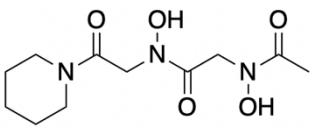

1

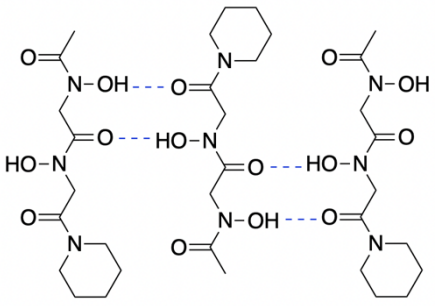

Figure 1.5: Structure of peptoid **1** reported by Crapster et al.[16] and a depiction of its self-assembly into the secondary sheet structure via intermolecular hydrogen bonding (dashed lines) between *N*-hydroxy amide sidechains.

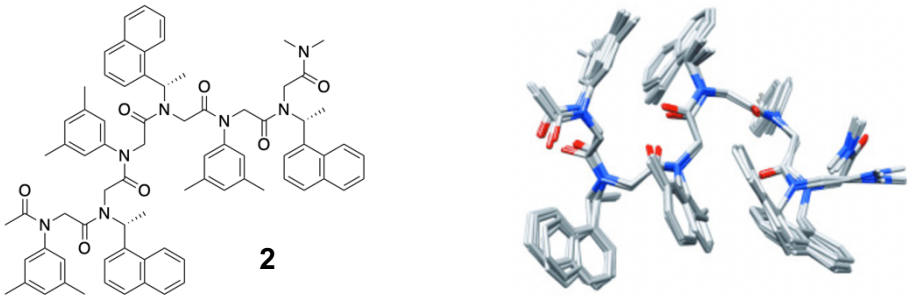

2

Figure 1.6: Left: Structure of hexamer **2** with alternating *cis* and *trans* amide bonds. Right: ten superimposed low energy NMR determined structures of **2** in $CDCl_3$ showing the peptoid ribbon structure (taken from Crapster et al. 2013).[17]

However, the peptoid helix remains the most extensively studied and understood. Early work by Kirshenbaum et al.[18] hypothesised sequence specific incorporation of *N*α-chiral substituents (**Figure 1.7**), possessing significant steric bulk, could predictably direct amide bond geometry.

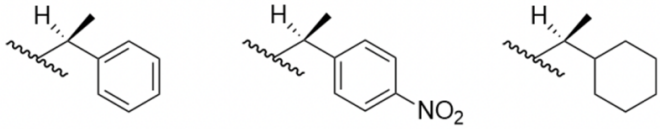

3, *N*spe **4**, *N*snp **5**, *N*sch

Figure 1.7: Examples of bulky *N*α-chiral substituents used to influence peptoid secondary structures.

The group prepared a library of oligomers, yielding stable folded frameworks 5 - 30 residues in length (**Figure 1.8**). Double minima at ~200 and ~220 nm with a maximum at ~190 nm gave characteristic right-handed helical circular dichroism (CD) profiles, apparent even in dodecamers incorporating 33% achiral monomers. Enantiomeric substitution was found to induce an inverted screw sense in the helix,[18] evidenced by mirror image CD spectroscopy (**Figure 1.9**).

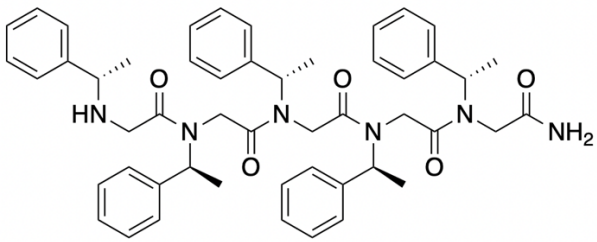

6

Figure 1.8: Example of a 5-mer peptoid (*N*spe)$_5$ (**6**) synthesized by the Kirshenbaum group.[18]

Notable from this study, a pentamer of *N*snp gave rise to all three typical CD peaks independent of peptoid concentration, as well as displaying sharp, well defined 1D ^{1}H-NMR

spectra, together inferring the helix to be monomeric and to stabilize without intermolecular affiliations.[18]

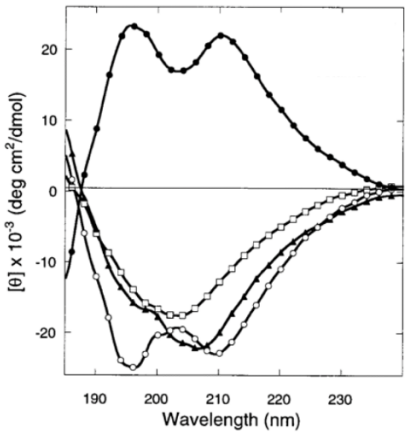

Figure 1.9: CD spectrum of trimer (*N*snp)$_3$ (▲), pentamer (*N*snp)$_5$ (○), octamer (*N*rnp)$_8$ (●), and the acetylated monomer Ac-*N*snp (□) showing octamer (*N*rnp)$_8$ in the opposite sign to the other peptoids owing its (*R*)-stereochemistry. Figure adapted from Kirshenbaum et al., 1998.[18]

Molecular modelling from the same group predicted an *N*spe decamer (**7**) would form an all *cis*-amide, right-handed helix with three residues per turn and dihedral angles ω = 0°, ϕ = -75°, ψ = 170° and χ1 = -120° (**Figure 1.10** and **Figure 1.11**).[19]

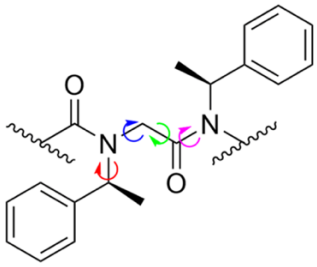

Figure 1.10: Depiction of the torsional angles present in the peptoid backbone using the *N*spe monomer as an example. ω shown in pink, ψ shown in green, ϕ shown in blue and χ1 shown in red.

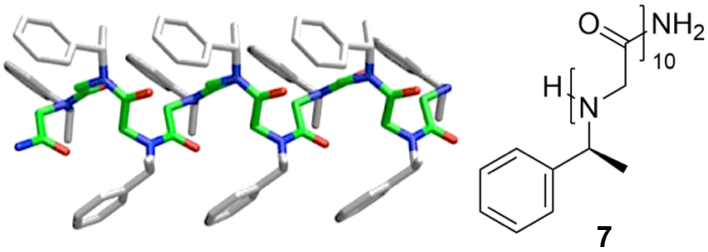

7

Figure 1.11: Molecular modelling of (*N*spe)$_{10}$ showing a right-handed α-helical structure, sourced from Fowler et al., 2009[20] alongside the chemical structure of the (*N*spe)$_{10}$ oligomer (**7**).

Asymmetry in the Ramachandran plot of (*N*spe)$_8$, relative to an octamer of sarcosine (*N*-methyl substituted glycine) affirmed the chiral centre imparts significant influence on the handedness

of the peptoid backbone. This is consistent with the CD spectra as a double minimum is indicative of backbone handedness. Contrary to sarcosine, mapping also exhibited a lower energy for the *cis* geometry in *N*spe, reasoned by the steric preference of bulkier substituents to be *trans* to each other i.e., Cα in residue *i* and *N*α in *i* + 1 (**Figure 1.12).**[19]

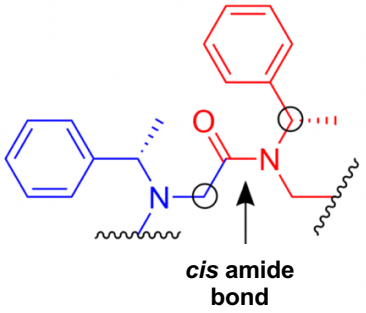

Figure 1.12: *Cis* amide bond geometry in (*N*spe)$_8$ showing Cα in residue *i* (blue) and *N*α in *i* + 1 (red) *trans* to each other as the bulkiest substituents on their respective side of the amide bond.

In solution state NMR studies, a modified derivative of the *N*snp pentamer was employed with various substitutions at the *para* position, as seen in **Figure 1.13** alongside its CD spectra. Substitutions increased chemical shift dispersions which, in conjunction with the relatively small size of the oligomer, allowed for 2D conformational interrogation of the helix.[21]

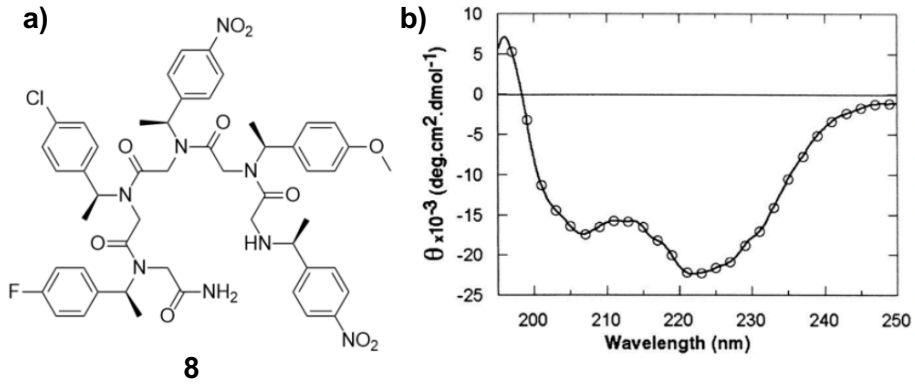

Figure 1.13: a) Structure of the modified *N*snp pentamer (**8**) used for NMR studies by Armand et al. **b**) CD spectra of the modified *N*snp pentamer showing three distinct peaks at ~190 nm, ~205 nm and ~220 nm characteristic of an alpha helix, recorded in 100% MeOH, at 10 °C and 0.1 mM. Taken from Armand et al., 1998.[21]

Structural predictions from the (*N*spe)$_8$ model were confirmed, showing a right-handed, all *cis* helix with three residues per turn and a pitch of ~6 Å. Although NMR cannot decipher the method of folding, such similarities with the model imply that steric factors indeed play an important role. Also detected was a minor isomer with the *trans* configuration, elucidating that the energetic separation between rotamers was not great enough to exclusively populate a

single geometry.[21] This reiterates *cis*/*trans* isomerisation as being a source of flexibility in peptoid scaffolds.

1.1.4 Exploring the Roles of Bulky Sidechains and α-Chirality.

Building from the ability of the *N*spe group to induce the *cis* conformation, Stringer et al. reported unprecedented $K_{cis/trans}$ values of 6.27 for a model *N*-s-1-Naphthylethyl (*N*s1npe) (**9**) aromatic system (**Figure 1.14**), and >19 for its tetramer in MeCN.[22] These rate constants, typically derived from NMR, measure the position of the equilibrium between the *cis* and *trans* rotamers, with values below 1 indicating a *trans* preference and those above 1 showing a preference for *cis*. In this case, the increased $K_{cis/trans}$ value can be attributed to the added steric bulk proximal to the amide bond, forcing the backbone into a *cis* conformation. Further ratifying this steric effect is the substantially smaller $K_{cis/trans}$ value of the *N*-s-2-Naphthylethyl (*N*s2npe) (**10**) model system (2.21 in MeCN) (**Figure 1.14**).[23] Oligomers of 1 - 4 *N*s1npe units (**11** – **14**) all gave crystal structures (**Figure 1.14**), with the tetramer adopting a right-handed α-helix with 3 residues per turn and a pitch of ~6 Å.[22]

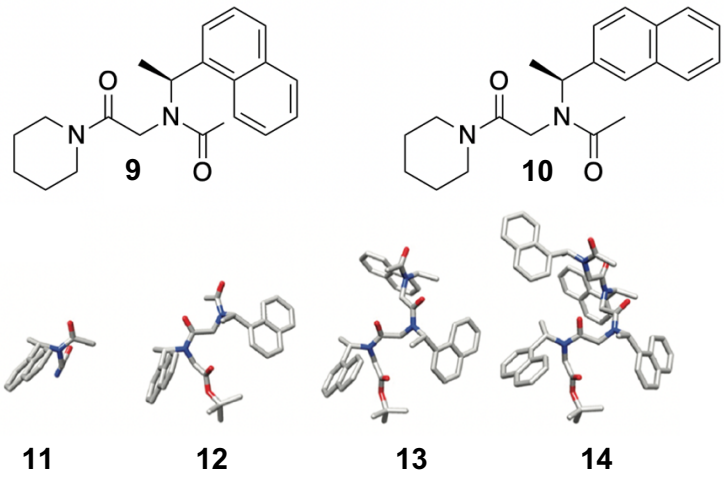

Figure 1.14: Model peptoid systems of *N*s1npe (**9**) and *N*s2npe (**10**) used to determine $K_{cis/trans}$ as well as crystal structures of peptoids containing (from left to right) 1, 2, 3 and 4 *N*s1npe residues (**11** – **14**). View is perpendicular to the helical axis. Hydrogen atoms have been removed for clarity. Image taken from Stringer et al., 2011.[22]

Significantly, CD spectroscopy of **13** and **14** showed the minimum at ~230 nm to greatly intensify moving from 3 residues to 4, which continued to increase as the chain extended further. This can be attributed to the first *i* to *i* + 3 overlap of the side chains, suggesting helix formation is a cooperative process i.e. *N*s1npe groups can sterically exclude regions of space for adjacent residues.[22]

Barron and co-workers probed the effect of *N*α-chiral aromatic sidechains, developing rules for the construction of stable peptoid helices.[24] Firstly, at least half of constituent monomers should be aromatic α-chiral, one of which should be located at the carboxy terminus as it is structurally less stable than the amino end. In studying hexamers composed of the α-chiral *N*rpe monomer (the enantiomer of **3**) and the achiral aliphatic *N*me monomer (*N*-(methoxyethyl)glycine), chains with only one or two terminal *N*rpe units exhibited no net CD. However, a 50:50 composition of these two monomers gave nascent chiral helical spectra (**Figure 1.15a**). CD spectra were also generated for the hexamer *N*pm-*N*rpe-*N*pm$_2$-*N*rpe$_2$ and its retro-sequence, clearly displaying a much greater helicity is inferred when the α-chiral aromatic *N*rpe residue is placed at the carboxy terminus (**Figure 1.15b**). Further, these side chains should be sequentially incorporated every third residue to 'stack' the aromatic faces down the longitudinal axis. Comparing compounds **15** and **16** (**Figure 1.15c**), **16** displayed sharper, more well-defined CD peaks despite both sequences comprising 67% α-chiral aromatic residues with one of these at the carboxy terminus. With three residues per turn, **16** creates a more stacked aromatic face to the helix, which in turn increases helicity.

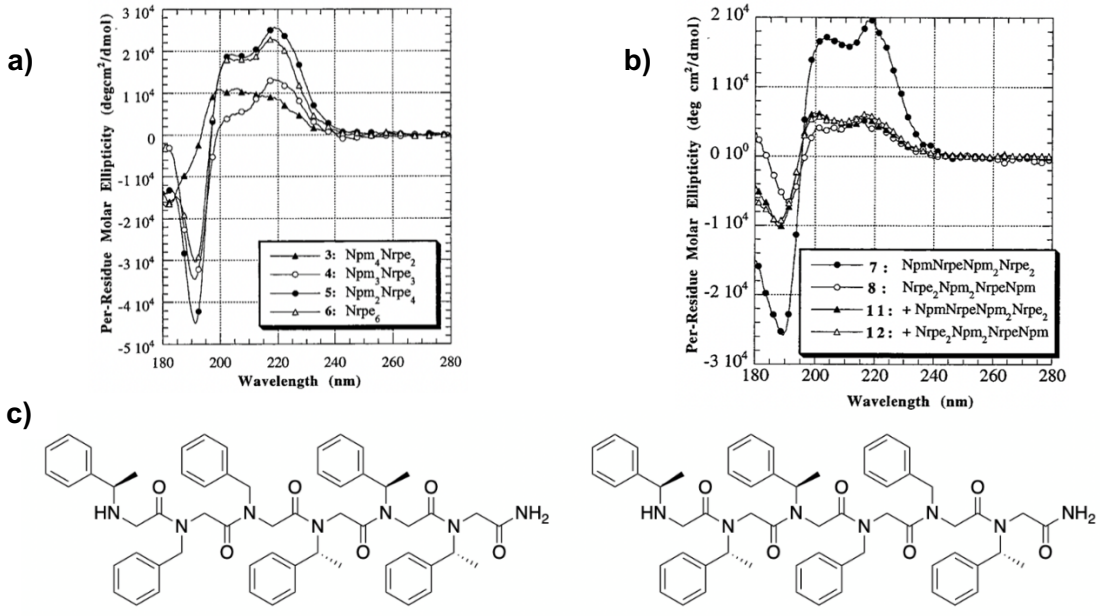

*N*rpe-*N*pm$_2$-*N*rpe$_3$, **15**

*N*rpe$_3$-*N*pm$_2$-*N*rpe, **16**

Figure 1.15: a) CD spectra showing an increase in helicity as the percentage of α-chiral aromatic *N*rpe residues in a peptoid hexamer increases relative to an achiral aliphatic *N*me residue. Figure taken from Wu et al., 2001.[24] **b)** CD spectra showing increased helicity for a peptoid hexamer possessing an α-chiral aromatic *N*rpe residue at the carboxy terminus compared to its retro-sequence which does not. Figure taken from Wu et al., 2001.[24] **c)** structures of compounds **15** and **16**.

Wu et al. performed spectroscopic studies on non-aromatic *N*α-chiral monomers; yielding a fully resolved peptoid crystal structure.[25] A pentamer of *N*rch (**Figure 1.16**) displayed backbone dihedral angles implicative of a PPI helix, though accordingly in the opposite sign due to its *R*-stereochemistry. The crystal exhibited a *cis*-amide, left-handed PPI helix with three residues per turn and a helical pitch of ~6.7Å,[25] slightly larger than the *para*-substituted *N*snp pentamer discussed in section **1.2.2**. This increase can be attributed to the deviation from planarity moving from a phenyl group to cyclohexane.

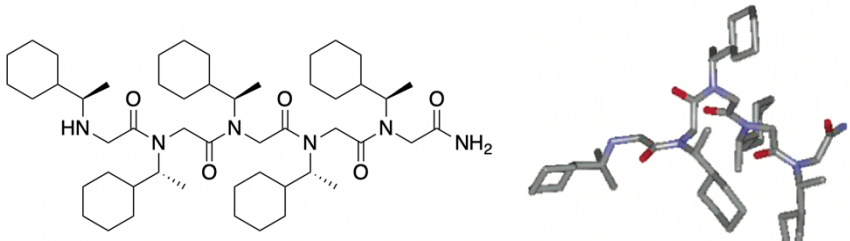

17a, (*N*rch)$_5$ **17b**, (*N*rch)$_5$

Figure 1.16: Structure of the Nrch pentamer (**17a**) and its fully resolved crystal structure (**17b**) taken from Wu et al., 2003.[25]

Mimicking the stereochemistry of natural peptides, the Wu group utilized CD spectroscopy to study oligomers of the *N*sch enantiomer. Distinct PPI type peaks at 210 nm, 200 nm and 225 nm grew in intensity with the lengthening chain, consistent with α-chiral aromatic studies.[24] Oligomers of *N*sch displayed intense bands at 200 and 225 nm, showing strong conformational order and that its lowest free energy conformation is a *cis* amide PPI type helix (**Figure 1.17a**). However, at the same wavelength in oligomers of *N*ssb ((*S*)-*N*-(2-butyl)glycine)), these bands were significantly less intense, owing its less bulky side chain and subsequently increased flexibility (**Figure 1.17b**).[25] The *N*sch sidechain demonstrates that *cis*-amide helix formation is not dependent on aromatic moieties, though relative to the likes of *N*spe, homogeneity is greatly reduced.

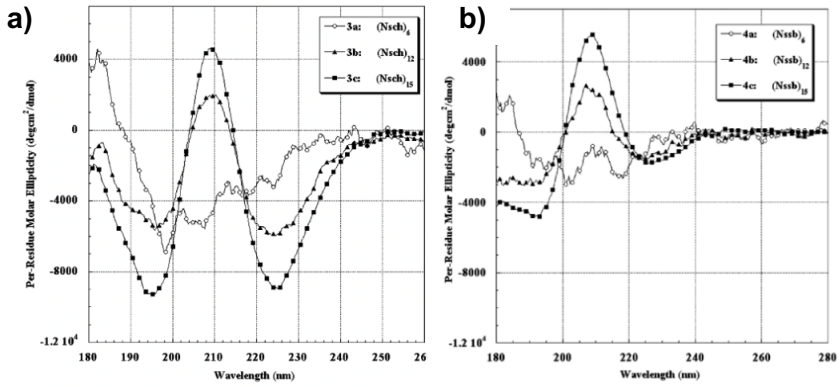

Figure 1.17: Comparison of CD spectra for oligomers of **a**) *N*sch and **b**) *N*ssb. Recorded at 100% MeCN, room temp. and ~60 μM. Figure taken from Wu et al., 2003.[25]

Impressively, Roy et al. demonstrated that robust helices of *N*^{t}Bu exclusively populate a *cis* conformation.[26] Single model peptoids of *N*^{t}Bu (**Figure 1.18a**) gave $K_{cis/trans}$ values >19 in MeCN, compared to 6.3 in a single model of *N*s1npe. Crystal structures of the *N*^{t}Bu dimer resembled a PPI-type helix and were superimposed onto the *N*rch pentamer with great accuracy.[26] The *tert*-butyl group is widely utilised in organic chemistry for its profound steric influence, and direct appendage to nitrogen affords such proximity to the amide that *trans* rotamers are spectroscopically undetectable. While this dismisses the requisite for 50% aromatic substituents, the lack of chirality in ^{t}Bu allows the formation of either left or right-handed PPI helices. Therefore, homooligomers of *N*^{t}Bu cannot be analysed by CD.

More recently, the same group devised the *N*stbe monomer, introducing handedness to the ^{t}Bu group by branching the sidechain at the *N*α position. Predictably, steric influences were less pronounced being further from the amide bond, with a peptoid monomer showing $K_{cis/trans}$ = 0.67 in MeCN. However, the corresponding hexamer **19** (**Figure 1.18a**) gave $K_{cis/trans}$ values of >19 in $CDCl_3$,[27] in line with previously discussed effects of chain extension on peptoid folding. Indeed, introduction of a stereogenic centre allowed for CD examination. Oligomers with the general structure Ac-(*stbe*)$_n$-COO^{t}Bu were analysed where n = 1 – 9. Chains with n = 1 – 4 displayed weak bands, indicating no robust structure in the molecule. As n increases (i.e., the length of the peptoid chain increases) to between 5 – 9 *N*stbe residues, a maximum and minimum at 209 and 225 nm respectively grew in intensity, giving clear bands indicative of a robust PPI type helix (**Figure 1.18b**). Strategic incorporation of a single *N*^{t}Bu at the carboxy terminus of *N*s1tbe hexamers offered complete suppression of the *trans* rotamer, consequently reinforcing the helical fold.[28]

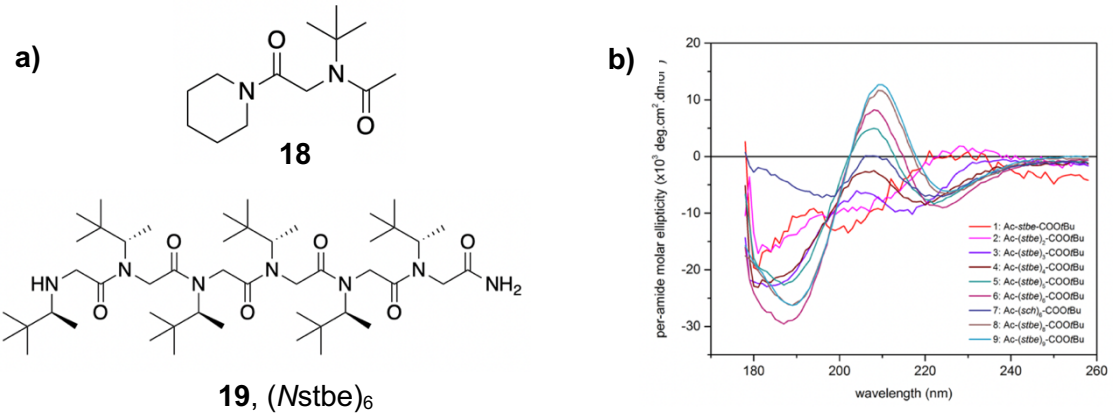

Figure 1.18: a) Structure of the *N*^{t}Bu model peptoid **(18)** and (*N*stbe)$_6$ hexamer **(19). b)** CD spectra of oligomers of *N*stbe showing distinct PP1 type peaks. Recorded at 100% MeCN, room temp. and ~500 μM. Image taken from Roy et al., 2017.[27]

Though helix formation can be induced regardless, chirality necessitates peptoid handedness and allows for characterisation by CD spectroscopy. Shin et al. analysed helical modulation by specific placement of chiral monomers.[29] Heptamers of *N*pm, an achiral derivative of *N*spe (**3**), were doped with *N*spe substitutions at varying positions in the chain. Remarkably, it was found that inclusion of one chiral monomer at the 2nd residue from the N-terminus (**Figure 1.19**) was enough to 'lock' the helicity of the peptoid and give α-helix type spectra.[29]

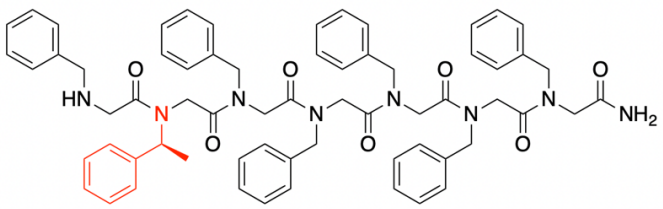

20, *N*pm-*N*spe-(*N*pm)$_5$

Figure 1.19: Structure of an Npm heptamer doped with a single Nspe monomer two residues from the N-terminus, found by Shin et al.[29] to be sufficient to lock the helicity of the peptoid.

As seen in **Figure 1.20**, a heptamer with 100% *N*spe residues gives a fully helical CD trace with a strong maximum at ~190 nm and two distinct minima at ~200 and ~220 nm whereas a heptamer comprising only *N*pm monomers (0% *N*spe) lacks any trace at all. Increasing the content of *N*spe strengthens these characteristic peaks that are still clearly present at only 14% *N*spe, which corresponds to peptoid **20**. Interestingly, inclusion of monomers with opposite handedness i.e., both *N*spe and *N*rpe residues, gave atypical traces with no clear secondary structure.[29] This work allows for achiral, *cis* inducing peptoid monomers to be developed, essentially 'stapling' helicity into oligomers by inclusion of one chiral side chain.

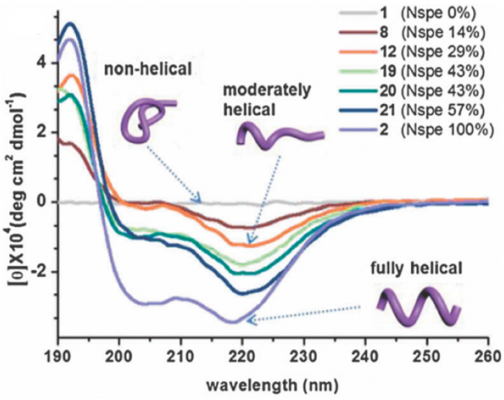

Figure 1.20: CD spectra of *N*pm heptamers with increasing *N*spe content showing α-helix character. Note that in the legend, oligomer 8 corresponds to a peptoid with a single *N*spe substitution two residues from the N-terminus (i.e., peptoid **20**). Recorded at 100% MeCN, room temp. and ~50 μM. Figure taken from Hye-Min Shin et al., 2014.[29]

Monomers with relatively large sidechains close to the amide bond can impart a substantial *cis* preference. Curiously, though an *N*sch pentamer (**15**) produced a helical CD spectrum, a model peptoid of this monomer gave a $K_{cis/trans}$ value of 1.22 (NMR determined) in MeCN, compared to 2.04 for a model peptoid of *N*spe in the same solvent.[23] Both possess a 6-membered carbon ring, with the cyclohexane group in *N*sch actually having a greater molecular weight than the benzene ring in *N*spe. Regardless, *N*sch is still populating the *cis* geometry less. It is therefore implied that aromaticity is imparting a stereoelectronic effect on the peptoid backbone.

1.1.5 Electronic Effects Governing Peptoid Conformation

Although steric bulk is introduced closer to the amide bond, *N*-aryl glycines, such as **21**, exclusively adopt the *trans* configuration.[30] It is well established that α-branched aryl containing monomers, such as *N*spe (**3**), impose a strong *cis* preference. Therefore, isomerism between rotamers must additionally be governed by electronic interactions between the amide group and the side chain.

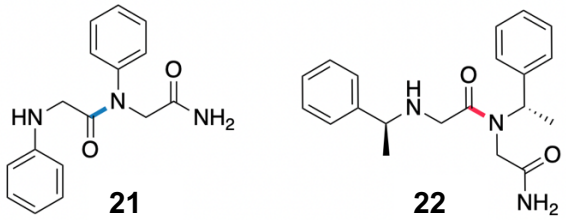

Figure 1.21: Structure of peptoid dimers containing *N*-aryl glycine monomers (**21**) and *N*spe monomers (**22**) which adopt the *trans* and *cis* conformation respectively.

Quantum mechanical modelling of substituted *N*-methylacetanilides displayed an energetic disposition towards the *trans* conformation, ranging from 1.05 - 3.55 kcal/mol.[30] This preference was increased when electron donating groups, such as NO_2 (**23**), were appended to phenyl and conversely supressed for electron withdrawing groups such as OMe (**25**) (**Figure 1.22**). Pedersen et al. proposed the electron dense centre of phenyl repelled the amide oxygen,[31] which would be much closer if the amide were to be *cis*. Modelling further showed the lowest energy conformation of an *N*-aryl glycine hexamer (**26**) to be an all *trans* PPII helix with 3.1 residues per turn and a helical pitch of ~9 Å (**Figure 1.23**).[30] Branching at the α-position of the nitrogen appended side chain offers increased flexibility, allowing *N*pe's *cis* inducing effects to overcome the energetic penalty experienced by the relatively rigid *N*-aryl glycine.

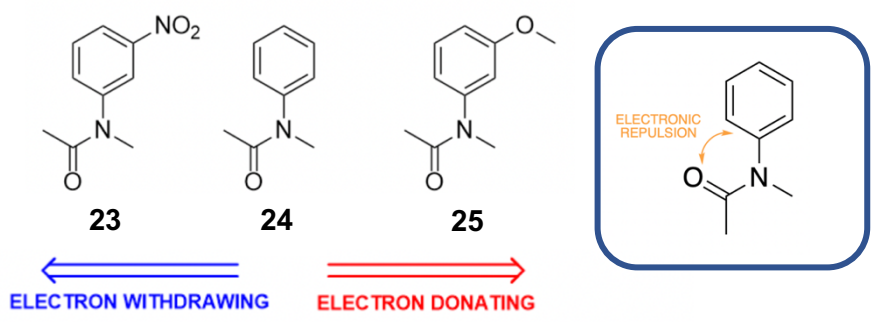

Figure 1.22: Structures of *N*-methylacetanilides with electron withdrawing and donating substitutions and depiction of the electronic repulsion between the carbonyl and electron dense phenyl experienced in the *cis* orientation.

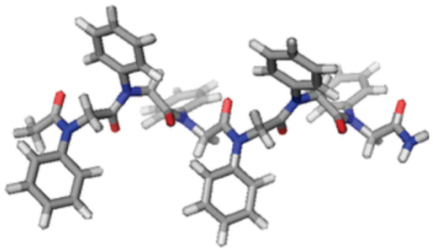

26

Figure 1.23: Molecular modelling of unsubstituted *N*-aryl glycine hexamer in its lowest energy state showing an all trans PPII type helix. Taken from Shah et al., 2008.[30]

Gorske et al. demonstrated that competing n $\rightarrow \pi^*_{Ar}$ and n $\rightarrow \pi^*_{Am}$ interactions operate in peptoids containing aromatic monomers.[32] The former involves donation of electron density from a carbonyl oxygen lone pair into the π^* orbital of an adjacent aromatic sidechain. This interaction can only stabilise the *cis* conformation, as this satisfies the geometrical requirements for orbital overlap (**Figure 1.24a**). Stabilization of the *trans* conformer is promoted by n $\rightarrow \pi^*_{Am}$ donation of electron density from the backbone carbonyl and the π^* orbital of an adjacent carbonyl group (**Figure 1.24b**).

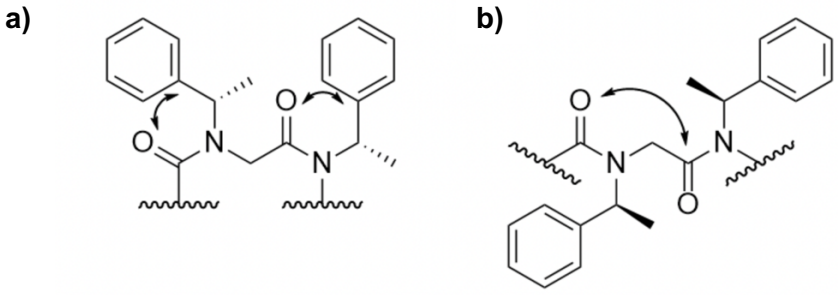

Figure 1.24: a) Depiction of the n $\rightarrow \pi^*_{Ar}$ interaction and **b)** the n $\rightarrow \pi^*_{Am}$ interaction which stabilize the *cis* and *trans* conformations for *N*spe respectively.

Gorske et al. demonstrated modulation of this n → π^*_{Ar} effect by modifying the well characterised *N*pe substituent. Electron withdrawing *N*np (**27**) and *N*4mpy (**28**) groups stabilised the *cis* conformation relative to *N*spe, whereas the electron rich *N*mph (**29**) decreased $K_{cis/trans}$ by 40% relative to *N*spe in MeCN (**Figure 1.25**).[32] This proves n → π^*_{Ar} interactions to be occurring in the backbone. Most notably, the positively charged *N*4mpy increased the *cis* amide preference by 270% relative to *N*spe in MeCN.[32]

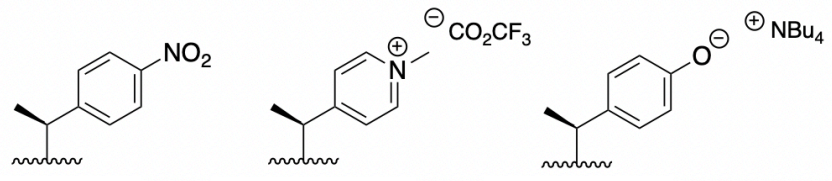

27, *N*np **28**, *N*4mpy **29**, *N*mph

Figure 1.25: Substituents studied by Gorske et al.[32] on the inductive effects modulating n → π^*_{Ar}.

The effect of cationic side chains was probed further by Caumes et al.,[33] exploiting triazolium type motifs. Models were synthesised by alkyne post side chain modification using copper catalysed azyde-alkyne click chemistry (**Figure 1.26**). This was followed by methylation with MeI. These positively charged rings induced profound suppression of the *trans* rotamer in $CDCl_3$ with $K_{cis/trans}$ > 19, exceeding the capabilities of *N*4mpy.[33]

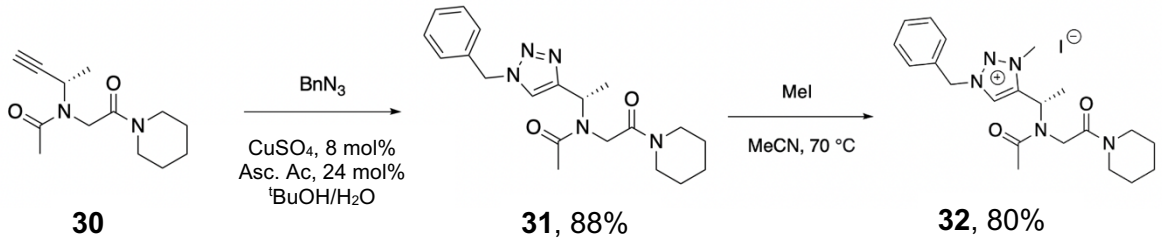

30 **31**, 88% **32**, 80%

Figure 1.26: Two step click chemistry post modification of alkyne groups to synthesize cationic triazolium peptoid sidechains. Yields for **31** and **32** taken from Caumes et al., 2012.[33]

Unmethylated precursors gave $K_{cis/trans}$ values in the range of 1 - 2, affirming the presence of an n → π^*_{Ar} interaction and its dependence on electron deficiency.[33] Unsurprisingly, the α-branched precursor gave the greatest *cis* preference. The downfield chemical shift of the triazolium proton suggests secondary interactions were possible in this *cis* conformation. Although this shift was not seen when using CD_3CN, NOE's were reproduced in all solvents indicating that the model peptoid was still adapting the same orientation for n → π^*_{Ar} donation.[33] This suggests that these secondary forces and electronic interactions act

cooperatively, as shown for model peptoid **32** (**Figure 1.27**). To date, these charged moieties offer one of the greatest *cis* preferences of all peptoid monomers, with **32** having $K_{cis/trans} > 19$ in $CDCl_3$.[33]

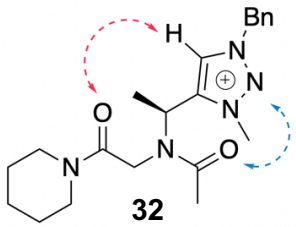

Figure 1.27: Depiction of n $\rightarrow \pi^*_{Ar}$ interaction (blue) and secondary interaction (red) stabilizing the *cis* conformation in a triazolium model peptoid.

Hydrogen bonding between the backbone carbonyl and sidechain was investigated by Stringer et al. in their *N*-aryl motifs.[34] Addition of a functional group, such as OH, at the *ortho* position on the aromatic ring (**33**) could reinforce the pre-existing proclivity for this group to adopt a *trans* conformation to a preference of 93%. This interaction takes place between the hydrogen bonding group appended to the monomer at position *i* + 1 and the carbonyl group at position *i* (**Figure 1.28**).

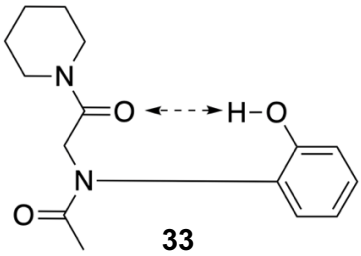

Figure 1.28: Depiction of the hydrogen bond between proximal carbonyl and *ortho* substituted aryl promoting the *trans* conformation induced by the *N*-aryl group.

1.2 Using Fluorine as a Conformational Tool and to Modulate Lipophilicity

1.2.1 Introduction to Fluorine and the C-F Bond

By virtue of its $1s^2 2s^2 2p^5$ electron configuration, fluorine dominates the Pauling scale as the most electronegative element on the periodic table. A proton dense nucleus and near saturated valence shell assumes fluorine with a relatively small van der Waals radius, similar to that of hydrogen (**Table 1.1**). It stems that an exchange for fluorine presents the most conservative substitution of hydrogen on the grounds of sterics.

Table 1.1: Van der Waals radius and average C-X bond lengths in some common elements.[35]

Van der Waals radii (Å)	H (1.20)	C (1.70)	N (1.55)	O (1.52)	Si (2.10)	P (1.80)	S (1.80)	Cl (1.74)	F (1.47)
Bond Length (Å)	C-H (1.09)	C-C (1.54)	C-N (1.47)	C-O (1.43)	C-Si (1.85)	C-P (1.84)	C-S (1.82)	C-Cl (1.77)	C-F (1.35)

Possessing a bond dissociation energy of up to 130 kcal/mol,[36] fluorine forms the strongest single bond to carbon in organic chemistry. Its electronic composition induces a highly polarised C-F bond, such that the uneven electron density creates a 'semi-ionic' character between C (δ+) and F (δ-).

Typically seen in other electronegative elements, such as oxygen and nitrogen, fluorine is reluctant to participate in resonance or as a hydrogen bond acceptor, owing its strong attraction for the three outer lone pairs. However, with a dipole moment of 1.51 D,[37] a H to F transaction at carbon can impart significant structural influences on the local environment, essentially pre-organising it without drastically increasing steric volume.

Fluorine finds broad applications in pharmaceutical design by exploitation of its unique characteristics. From 1954 - 2020, around 340 fluoro-pharmaceuticals were registered ranging in use from antimicrobials, anti-inflammatories, and anti-tumour drugs.[38] As well as being a conformational control element, fluorine can productively increase a drug's potency and membrane permeability (hence improving oral bioavailability). Partly recognised as a result of the C-F bond strength, fluorine can strategically be incorporated to replace labile protons in both aromatic and aliphatic environments. Electron rich phenyl rings, inherently prone to metabolic oxidation, may exhibit enhanced *in vivo* stability following the installation of a fluorine atom.[39] Aromatic fluorination has in fact shown to increase the metabolic stability of drug molecules with established patterns of *ortho*- and *para*-substitution, such as in Ayvakit (**34**) and Tabrecta (**35**) (**Figure 1.29**).[40]

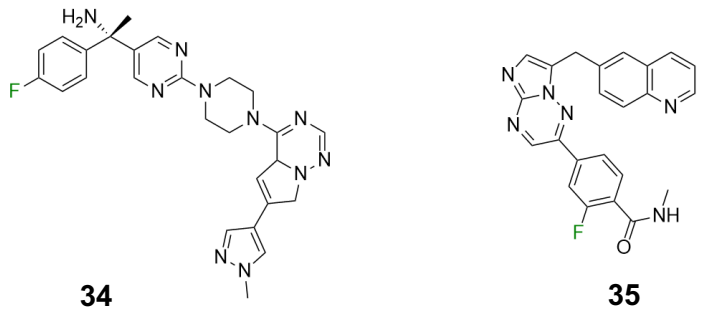

34 **35**

Figure 1.29: Chemical structures of Ayvakit (**34**) and Tabrecta (**35**) showing lipohphilicity enhancing fluorine atom in green.

1.2.2 Conformational Effects of the C-F Bond in Organic Compounds

Introduction of a C-F bond into an organic molecule can exert influence on the surrounding geometry, principally via electrostatic interactions. This can be harvested as a tool to supress or stabilise intramolecular conformations. Conversely, intermolecular associations are seldom observed as when fluorine acts as a hydrogen bond acceptor, the resulting interaction offers about a quarter of the strength exhibited by a 'normal' hydrogen bond.[37] Examples of conformational effects imparted by a C-F bond include:

A. Dipole-Dipole Interactions

Emanating a prevalent dipole, the carbon fluorine bond instinctively orientates in opposition to vicinal dipoles, such as carbonyl groups. For example, in α-fluoroamides C-F aligns antiparallel to C=O, an effect that diminishes with alternative α-fluorocarbonyl compounds that reduce the dipole, as seen in compounds **36** - **39** (**Figure 1.30**).[37]

36: R = NH_2, -7.5 kcal/mol
37: R = OMe, -4.5 kcal/mol
38: R = Me, -2.2 kcal/mol
39: R = H, -1.7 kcal/mol

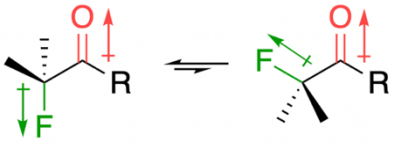

Figure 1.30: Depiction of dipole-dipole interactions in α-fluorocarbonyl compounds with corresponding energetic preferences. Values taken from L. Hunter 2010.[37]

B. Charge-Dipole Interactions

Electron dense, fluorine adopts conformations that minimise the distance to proximal substituents carrying a formal positive charge. This was first evidenced by fluorine's proclivity to be axial in 3-fluoropiperidinium ring systems but is also well pronounced in acyclic structures when a *gauche* conformation is favoured.[41] Snyder and co rationalised that in such piperidine based systems, fluorine's interaction with the formal positive charge is sufficient to counteract the di-axial steric compression brought about by the fluorine group.[42] As seen in **Figure 1.30**, equilibrium favours an axial placement of fluorine in an *N,N*-dimethyl-3-fluoro-4,4-diphenylpiperidinium salt (**40**), further evidenced by its solid state crystal structure.

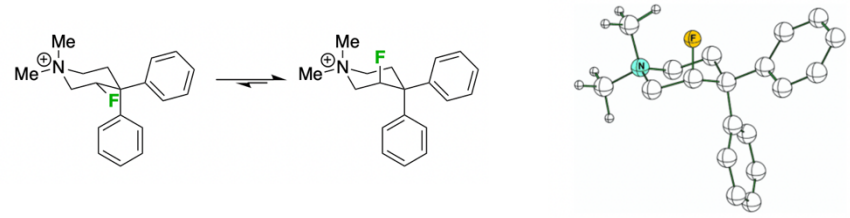

40a **40b** **40b**

Figure 1.31: Depictions of the equilibrium present in an *N,N*-dimethyl-3-fluoro-4,4-diphenylpiperidinium salt (**36**) which favours the axial placement of fluorine, alongside its solid state crystal structure taken from Snyder and Sun et al., 2005.[42]

C. The Fluorine *Gauche* Effect

A vacant, low energy antibonding $\sigma^*_{C\text{-}F}$ orbital is present in C-F comparable to that found in the C-O bond.[43] This affords opportunity for the donation of electron density from nearby orbitals. Oxygen and nitrogen lone pairs, electron-rich bonds and nucleophiles local to $\sigma^*_{C\text{-}F}$ can partake in hyperconjugative interactions to stabilise conformations.[43] Relatively subtle compared to dipole-dipole and charge-dipole interactions, the fluorine *gauche* effect exemplifies hyperconjugation to infer a conformational preference. Contrary to the intuitive 180° *anti*-conformation expected between two electronegative substituents, F atoms separate by 60° in a thermodynamically favourable *gauche* conformer. Subsequently, both $\sigma^*_{C\text{-}F}$ orbitals align to allow feeding of electron density from the two neighbouring $\sigma_{C\text{-}H}$. This effect is very general, apparent when fluorine is β to any electron withdrawing group, as seen in compounds **41** - **44** (**Figure 1.32**).

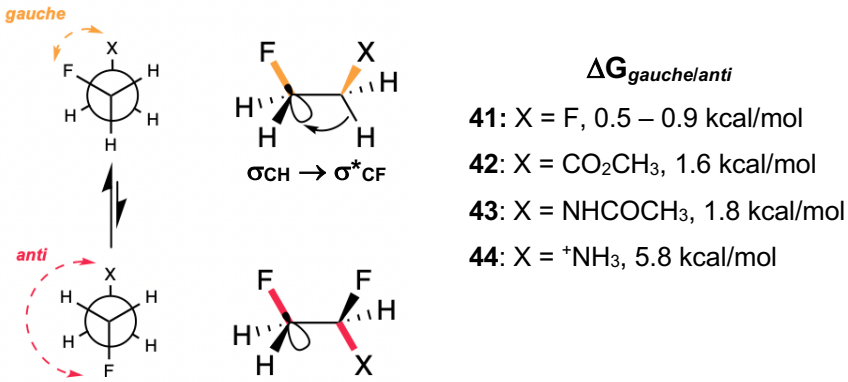

Figure 1.32: Example of hyperconjugation favouring the *gauche* conformation that allows electron density to be donated from C-H to $\sigma^*_{C\text{-}F}$. Values for $\Delta G_{gauche/anti}$ taken from Gilmour et al., 2017.[43]

1.2.3 Fluorine's Effect on Lipophilicity

Lipophilicity (log *P*) denotes an unionized compound's relative solubility between polar and non-polar mediums at equilibrium. Compounds exhibit decreased hydrophobic character with increased polarity i.e., the ability to interact with water molecules, yet become more hydrophobic with greater molecular weight. Generally, the introduction of halogens increases log *P*. Aforementioned, fluorine is reluctant to participate in hydrogen bonding and other halogens lack the required electronegativity, yet all introduce greater molecular weight therefore disfavouring dissolution into the aqueous phase. The C-F bond can also disturb the hydrophilic tendencies of nearby H-bond acceptors through the inductive effect. However, fluorination is not synonymous with increased lipophilic character.

The introduction of terminal fluorine to a saturated alkyl group reduces log *P*, being most pronounced for monofluorination and trifluoromethylation which have the strongest dipolar moments. For example, in octanol/water 1-fluoropentane has log *P* = 2.33 compared to 3.11 in its unsubstituted parent molecule.[44] Hydrophilicity is enhanced by the ionic character of the strong C–F dipole yet hindered by the increase in hydrophobic surface area. When another functional group is present in linear chains, such as OH or NH, lipophilicity can be increased by means of a CF_3 group, decreasing its basicity via inductive effects. Proximity to this substituent is crucial to an increased log *P*, as migration further along the chain can again lead to a decreased hydrophobicity.[45]

Linclau et al. investigated the effects of aliphatic fluorination on lipophilicity in detail (**Figure 1.33**),[46] finding monofluorinated aliphatic alcohol **51** to be significantly less lipophilic than its non-fluorinated parent alcohol **46**. However, this effect is dependent on the fluorine atoms position relative to the alcohol group, as seen by the 13% increase in log *P* for **50** and the 31% reduction for **54**. Geminal difluorination in alcohol **49**, though still less lipophilic than parent compound **46**, did increase log *P* relative to its mono fluorinated counterpart **51**. The organisation of the fluorine atoms also displayed influence over lipophilicity, with the more even distribution of F along the terminal carbons in **48** proving to be a less lipophilic arrangement than in **47**. Increasing the fluorine content of an already fluorinated alcohol increased the log *P* of the compound, as with **52** and **53**, with the CF_2-CF_3 terminus of **45** enhancing lipophilicity to greater than that of the unsubstituted **46**.

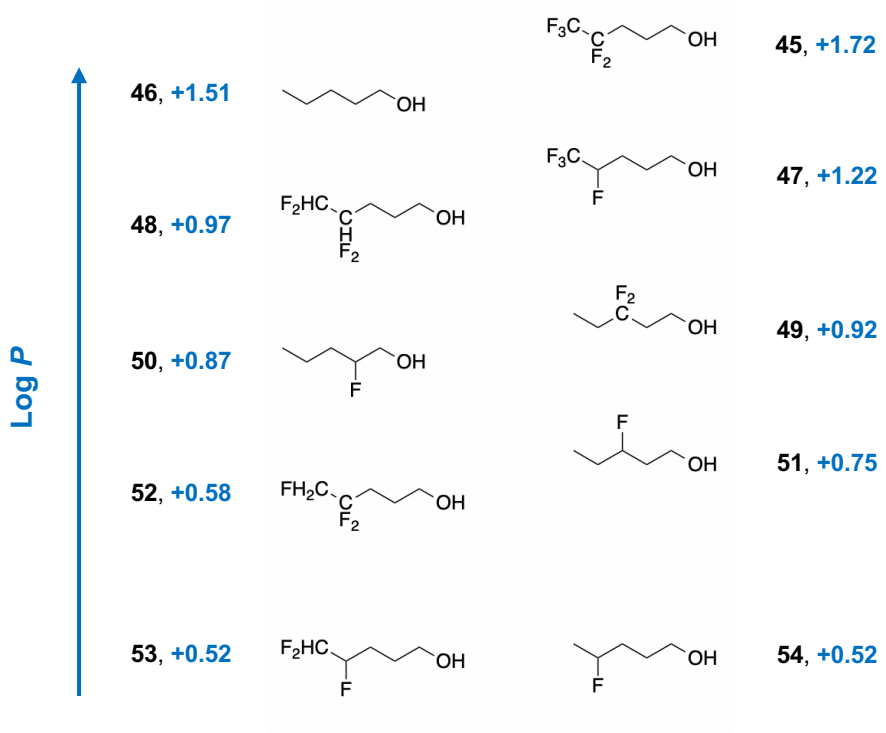

Figure 1.33: Log *P* values of various fluorinated aliphatic alcohols compared to the non-fluorinated parent molecule pentan-1-ol. Values taken from Linclau et al., 2020.[46]

An intrinsic property of a molecule, lipophilicity is a weighted average of the values that arise from individual conformers (**Figure 1.34a**). Linclau et al. utilized ^{19}F-NMR to isolate the individual log *p* values of compounds with multiple conformations,[47] obtaining an average measurement of lipophilicity based on both the distribution between octanol and water and the conformer equilibrium in both solvents. For example, Linclau found compound **55**, which exists in either the *cis* or *trans* conformation, to have $\Delta\log p = 0.09$ whereby the *cis* conformation is more lipophilic than the *trans* (**Figure 1.34b**). However, as the *trans* conformation was more prevalent, **55** gave an average log *P* value of -0.60.[47]

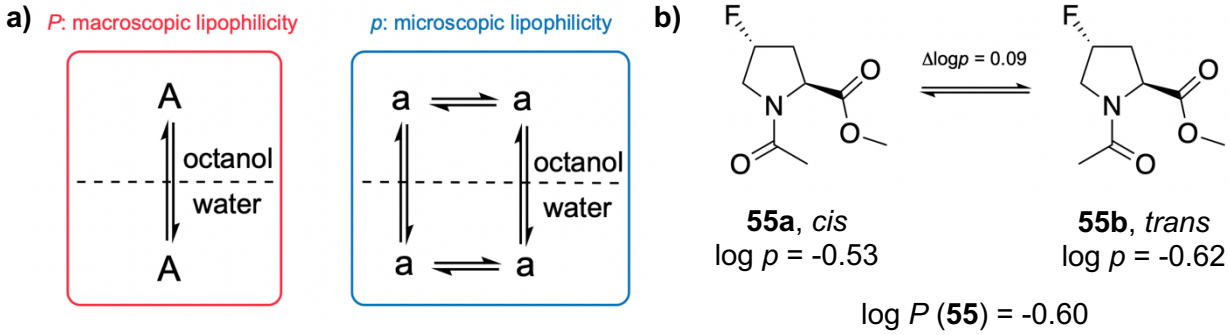

Figure 1.34: a) Depiction of the macroscopic log *P* of a compound as well as the microscopic equilibria of which this value is composite of. **b)** individual log *p* values of compound **55** with its weighted average log *P* value. Figures adapted and values taken from Linclau et al. 2021.[47]

Probed and quantified by Hansch et al.,[48] fluorination on an aromatic ring ensures an increased lipophilicity. Taken as the difference in log *P* for a parent molecule and it's derivates, Hansch hydrophobicity parameters (π_x) for benzene clearly show the hydrophobic properties of halogens, and how substituents capable of hydrogen bonding increase hydrophilicity (**Table 1.2**).

Table 1.2: Hansch Parameters of Benzene Substituents.[a] Values taken from Hansch et al., 1973.[48]

C_6H_5-X	π_x	C_6H_5-X	π_x	C_6H_5-X	π_x
F	0.14	I	1.12	NO_2	-0.28
Cl	0.71	CH_3	0.56	OH	-0.67
Br	0.86	CF_3	0.88	NH_2	-1.23

[a] π_x = log P_x – log P_H (octanol/water)

1.2.4 Fluorine as a Tool for the Conformational Control of Peptoids

As discussed in **Section 1.1.5**, quantum mechanical modelling at the HF/6-31G level for *N*-methylacetanilide displayed an overwhelming disposition towards the *trans* conformation, which was subsequently supressed by introduction of electron withdrawing groups to the phenyl ring. In this study, fluorine's -I properties surfaced in a sequential diminishment of energetic preference for *trans* upon increasing fluorination. Pentafluorophenyl, though still inclined towards the *trans* rotamer, reduced this preference by 2.38 kcal/mol relative to the unsubstituted acetamide **24**,[30] the greatest reduction of the models studied.

Gorske and Blackwell harnessed the pentafluorophenyl motif to aid in commanding a *cis* amide geometry, with *N*α-branched model peptoid *N*sfe (**56**) displaying a $K_{cis/trans}$ value of 3.84 in MeCN (**Figure 1.35**),[23] 88% larger than that of *N*spe (**3**) in the same solvent. Fluorination draws electron density from the phenyl ring, making n → π^*_{Ar} interactions even more favourable.

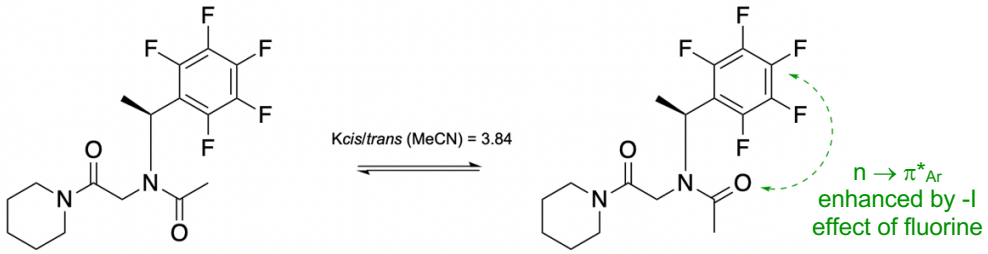

56a, *trans* **56b**, *cis*

Figure 1.35: Structure of the *N*sfe model peptoid studied by Gorske et al, 2009.[23]

Fluorinated aromatic peptoid monomers were investigated by Gimenez and Cobb,[49] to further promote the donation of electron density from oxygen to the sidechain in an n $\rightarrow \pi^*_{Ar}$ association. To circumvent the need for sidechain chirality, the electron deficiency of the non-fluorinated aromatic moiety was first addressed. In a model peptoid system, substitution of *N*pm (**57**) for a pyridine group (**58**) elevated $K_{cis/trans}$ from 1.20 to 1.66 in MeCN, as nitrogen draws electron density from the ring (**Figure 1.36**). Though successful in further promoting the *cis* geometry, **58** falls short of the *N*α-branched *N*spe ($K_{cis/trans}$ = 2.07 in MeCN). Channelling the success of the *N*sfe monomer (**56**), the pyridine ring was fluorinated to give N^{4f}pym (**59**). ^{1}H-NMR experiments revealed this model peptoid to have a $K_{cis/trans}$ of 3.22 in acetonitrile, exceeding that of *N*spe without employing chirality.

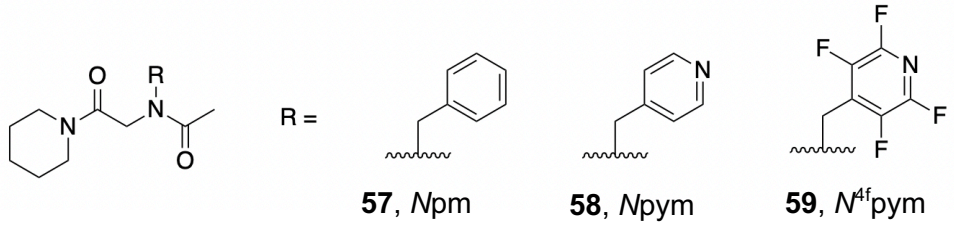

Figure 1.36: Structures of the *N*pm, *N*pym and N^{4f}pym model peptoids probed by Gimenez et al., 2019.[49]

Having been successful in bypassing the need for branching at the *N*α position, Gimenez then sought eliminate the need for aromaticity.[50] With the N^tBu and *N*s1tbe monomers (**18** and **19** respectively) being the only strongly *cis*-favouring alkyl units at the time, it was proposed that terminal fluorination of an *N*-ethyl sidechain could install a *gauche* conformation, translating to a *cis* peptoid backbone (**Figure 1.37**). Using *N*Et (**60**) as a reference, installation of a single fluorine atom to form *N*1fEt (**61**) saw a remarkable increase towards the *cis* rotamer in all three solvents (**Table 1.3**). When analysed in acetonitrile, mono-fluorination nearly matched that of the aromatic *N*pm monomer **57** ($K_{cis/trans}$ = 1.20). Incorporation of further fluorine atoms in *N*2fEt (**62**) and *N*3fEt (**62**) saw further increase towards the *cis* rotamer for both CD_3CN and CD_3OD, with the greatest result being 2.24 for the trifluorinated *N*3fEt monomer.[50] This was quite unprecedented, given that this value is greater than the widely used, chiral and aromatic *N*spe monomer. However, experiments performed in $CDCl_3$ saw an out of trend shift towards the *trans* rotamer moving from *N*2fEt to *N*3fEt. The energetic penalty experienced by the CF_3 group in the *cis* conformation may arise from an increased solvation barrier due to the large dipolar moment which will naturally be disfavoured by a non-polar solvent.

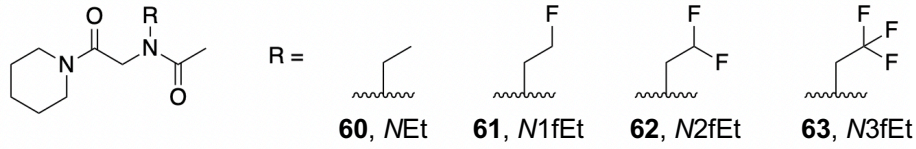

Figure 1.37: Structure of the model peptoids used to investigate non-chiral fluoroalkyl peptoid monomers by Gimenez et al.[50]

Table 1.3: $K_{cis/trans}$ values of fluoroalkyl monomers taken from Gimenez et al., 2018.[50]

Side Chain	Kcis/trans		
	CDCl3	CD_3CN	CD_3OD
***N*Et**	0.19 ± 0.01	0.66 ± 0.07	0.51 ± 0.04
***N1f*Et**	0.76 ± 0.03	1.15 ± 0.09	0.74 ± 0.07
***N2f*Et**	1.28 ± 0.08	2.05 ± 0.12	1.17 ± 0.04
***N3f*Et**	0.54 ± 0.06	2.24 ± 0.12	1.23 ± 0.03

A value of 20.0 Hz was determined by theoretical calculations to be an ideal coupling constant for a fluorine/amide *gauche* conformation in **61** (**Figure 1.38**). The predominant *cis* isomer of **61** had $^3J_{HF,obs}$ = 25.7 Hz (CD_3CN), strongly suggesting a *gauche* orientation to be present. However, in studying two staggered conformations of **62** a value of $^3J_{HF,obs}$ = 14.9 Hz (CD_3CN) indicated an *anti*/*gauche* conformation ($^3J_{HF,calc}$ = 14.0 Hz (CD_3CN)), rather than a +*g*/-*g*. This means only one of the fluorine atoms in **62** may be *gauche* to the amide. Fast rotation about CF_3 in **63** meant a $^3J_{HF,obs}$ = 9.8 (CD_3CN) significantly deviated from the calculated coupling constant for an all *gauche* composition ($^3J_{HF,calc}$ = 16.0 Hz (CD_3CN)) which assumes the arrangement between the amide and CF_3 to be static.[50] These vicinal $^3J_{HF}$ coupling constants do not support the hypothesis that the fluorine *gauche* effect is solely responsible for the *cis* amide geometry adopted. However, the solid-state crystal structure of **63** (**Figure 1.39**) did support an inductive effect between the amide oxygen and electron deficient carbon atom to be a driving force in the experimentally determined *cis* preference of these monomers, similar to that of the n $\rightarrow \pi^*_{Ar}$ interactions in aromatic sidechains.

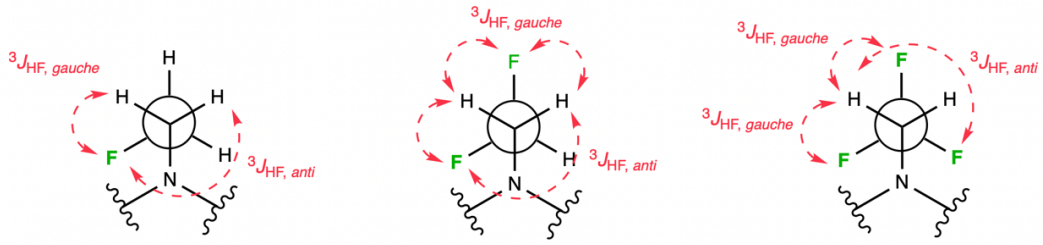

61, (*gauche*)
$^3J_{HF,calc}$ = 20.0 Hz
$^3J_{HF,obs}$ = 25.7 Hz

62, (*anti*, ± *gauche*)
$^3J_{HF,calc}$ = 14.0 Hz
$^3J_{HF,obs}$ = 14.9 Hz

63, (all *gauche*)
$^3J_{HF,calc}$ = 16.0 Hz
$^3J_{HF,obs}$ = 9.8 Hz

Figure 1.38: Theoretical and experimental vicinal $^3J_{HF}$ coupling constants for the cis conformation of model peptoids **61**, **62** and **63** in acetonitrile. Values taken from Gimenez et al., 2018.[50]

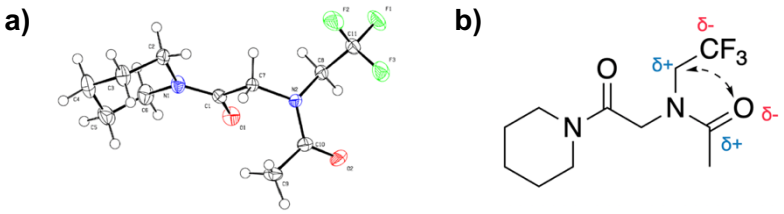

Figure 1.39: a) Solid state crystal structure of **63** taken from Gimenez et al., 2018.[50] **b)** Depiction of the electrostatic interaction between oxygen and electron deficient carbon responsible for the *cis* isomer preference in **63**.

Gimenez et al. then went on to incorporate these novel, fluoroalkyl monomer into 15-mer peptoids (**Figure 1.40a**), with three residues per turn.[50] As these fluorine containing sidechains are inherently hydrophobic, a lysine type *N*Lys monomer was incorporated every third residue to aid dissolution into aqueous solvents. This further created a facially amphipathic design, with all the positively charged lysine residues being stacked on a single face of the peptoid. As characterization by CD spectroscopy necessitates a chiral centre to be present, a single *N*spe monomer was incorporated two positions from the *N*-terminus of the peptoid, already found to be sufficient in "locking" the helicity of the peptoid by Shin et al.[29]

Using the *N*et sidechain (**60**) as a control, CD spectroscopy revealed peptoids **64** – **67** to all display stable helical spectra in water. The minimum at 218 nm ($M_{\theta,\ 218}$), one of the characteristic bands of an alpha helix,[25,27] was chosen to quantify the difference in helicity imparted by incorporation of non, mono, di, and tri-fluorinated sidechains.

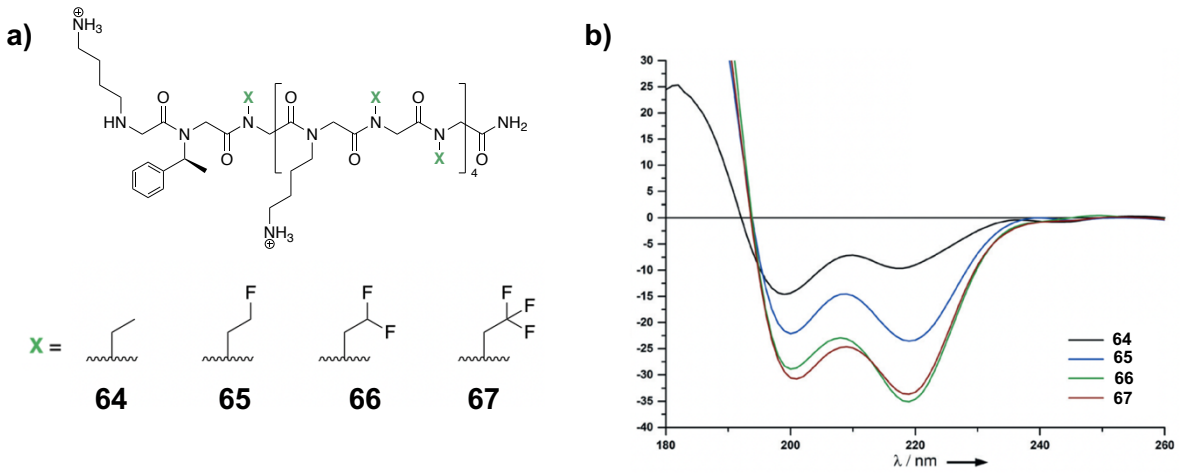

Figure 1.40: a) Structure of the peptoid oligomer scaffold used by Gimenez et al.[50] to study the novel fluoroalkyl sidechains. **b)** Comparison of CD traces for oligomers **64** – **67**, recorded in H_2O at room temp. Figure taken from Gimenez et al., 2018.[50]

As seen in **Figure 1.40b**, $M_{\theta,\ 218}$ for each of the fluorinated peptoids **65** – **67** drastically increases relative to the non-fluorinated **64**, confirming the inductive effects found through the study of model peptoids to translate into the formation of a stable secondary structure. The increase from **64** to **65** and from **65** to **66** is intuitive given the introduction of a fluorine atom. However, this increase is not so apparent on moving from peptoid **66** to **67**. This may be due to water being the chosen solvent for the CD study. As seen in **Table 1.3**, $K_{cis/trans}$ for the *N*2fEt and *N*3fEt sidechains in polar protic solvent MeOD are 1.17 and 1.23 respectively. Being so close together, it is possible that H_2O sees the *N*2fEt sidechain become more *cis* inducing, and hence more strongly helical, than *N*3fEt.

Inspired by the success of the *N*3fEt monomer, Gimenez et al envisioned that incorporation of a CF_3 group into the well-established, *cis* inducing *N*spe monomer may allow electronic dipolar interactions and steric influences to work in tandem.[49] The N^{CF3}rpe monomer (**68**) (**Figure 1.41**) displayed overwhelming preference for a single rotamer in solution. Quantum mechanical modelling revealed a *cis*-amide energy minimum 1.26 kcal/mol lower than the trans conformation, verifying the NMR-calculated $K_{cis/trans}$ value of 5.82 in MeCN.[49] The model peptoid almost exclusively populated the *cis* conformation, further evinced by CD spectroscopy of an N^{CF3}Rpe containing oligomer.

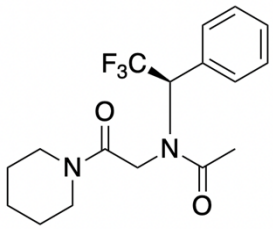

68, N^{CF3}rpe

Figure 1.41: Structure of the model peptoid containing the N^{CF3}rpe monomer reported by Gimenez et al., 2019.[49]

It is clear that fluorine's unique characteristics find value as a conformational tool and are particularly well suited for use in foldamer chemistry. The 'toolbox' of monomers available for the rational design peptoids remains reliant on aromatic moieties, with alkyl groups being neglected. The use of a CF_3 group has built the foundations to a new class of *N*-alkyl peptoids, circumventing previous requisites for the design of a rigid amide backbone. The potential of this trifluoromethyl group requires further inspection, in anticipation of unlocking novel peptoid sidechains capable of controlling the rotamer equilibrium.

1.3 Therapeutic Peptoids

1.3.1 Peptoids and Proteolysis

As with many other peptidomimetics, peptoids are resistant to proteolysis making them ideal alternatives for peptide structures suffering from such issues. The susceptibility of peptoids to enzymatic degradation was analysed by Miller et al.[51] L-peptide, D-peptide, parallel (all N) peptoid and anti-parallel (retro all N) peptoid sequences were subject to treatment with several known classes of relevant proteases: chymotrypsin, elastase, trypsin, papain, pepsin, and carboxypeptidase A (**Figure 1.42**).

All L-peptides were clearly substrates of their respective enzyme, exhibiting significant conversion by 20 minutes of treatment. Two of the D-peptides showed minimal cleavage, and no convincing proteolysis was observed for either of the peptoid sequences in all 6 enzymes. To remove the possibility that peptoids were acting as irreversible enzyme inhibitors (which would also be characterised by no conversion), equimolar concentrations of L-peptide and peptoid sequences were monitored under treatment with the enzymes. Conversion of the L-peptide was diminished by a maximum of 5%, confirming the peptoids to be resistant to proteolysis and not irreversible inhibitors.[51]

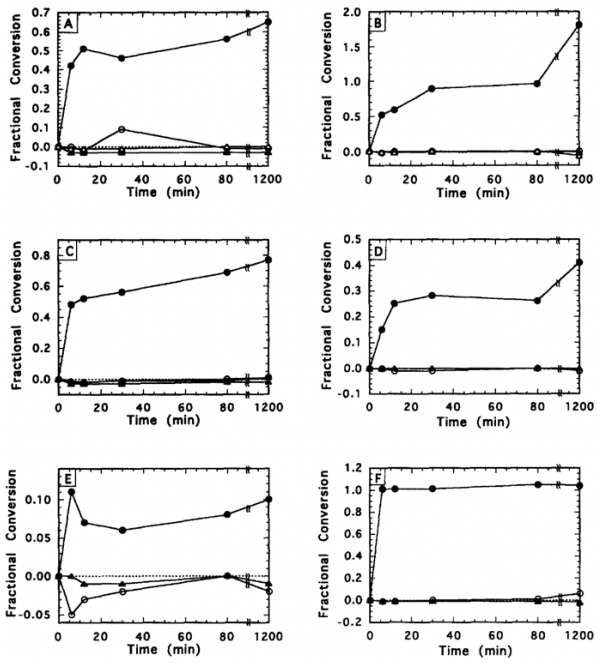

Figure 1.42: Fractional conversion over twenty hours of L-peptides (●), D-peptides (○) all N-peptoid (▲) and retro all N-peptoid (△) when treated with (A) chymotrypsin, (B) elastase, (C) trypsin, (D) papain, (E) pepsin and (F) carboxypeptidase A. Figure taken from S. M. Miller 1994.[51]

Misalignment of the sidechains and carbonyl groups leaves the cleavable C-N bond out of range for the nucleophilic sites present at the active site, rendering peptoids uncleavable by protease enzymes.

1.3.2 Cell Permeability

Delivery of therapeutic agents into the cell proves challenging. Internalization is policed by a biological barrier that deters large and hydrophilic molecules: the cell membrane. Highly lipophilic and low molecular weight compounds are all that stand a chance at passing this threshold, which of course imposes great limitations on the rational design of drugs.

Peptides are excellent protein ligands, having the ability to access binding sites less recognized by small molecules. Unfortunately, peptides are known for their lack of cell permeability. Conradi et al. formed a library of five peptide tetramers (**69** – **73**),[52] largely identical but with an increasing number of backbone nitrogen atoms methylated. Transport of the tetramers across confluent monolayers of Caco-2 cells increased parallel with the number of additional nitrogen atoms methylated. Log *P* coefficients varied very little between each analogue, pointing the rationale away from lipophilicity. The linear increase in permeability is consistent with the removal of hydrogen bonding protons, which has been assigned as the principal detriment to transport. The all-methylated backbone **73** gave an effective permeability coefficient (P_{eff}) over 36 times larger than its peptide tetramer parent scaffold **69**.[52] Further studies by Y. Kwon and Kodadek as well as Tan et al. mirrored the conclusion that a nitrogen bound sidechain increases cell permeability relative to a structurally isomeric peptide.[53,54]

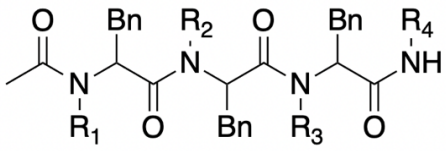

Compound	R_1	R_2	R_3	R_4	P_{eff}
69	H	H	H	H	0.66
70	H	H	CH_3	H	2.78
71	H	CH_3	CH_3	H	5.68
72	CH_3	CH_3	CH_3	H	13.80
73	CH_3	CH_3	CH_3	CH_3	23.80

Figure 1.43: Structure of the tetramers studied by Conradi and their corresponding P_{eff} values. Bn = benzyl group. Taken from Conradi et al., 1991.[52]

1.3.3 Antimicrobial Peptoids

As with peptides, peptoids have found a variety of applications in the biomedical field, including as cancer diagnostics[55] and anticancer agents,[56] as antiviral agents against SARS-CoV-2,[57] as drug carriers[58–60] and as inhibitors of protein-protein interactions.[61,62]

Pioneering work by the Barron group led to the development of peptoid **74** (**Figure 1.44**), a mimic of magainin-2 amide with 12 residues in a facially amphipathic distribution.[63] Both water soluble and evidenced as helical by CD spectroscopy, peptoid **74** was the first reported bioactive peptoid of defined structure. Since, the majority of antimicrobial peptoids have been designed with a scaffold reminiscent of Barron's.

Further antimicrobial screening from Barron found peptoid **74** to have a minimum inhibitory concentration (MIC) of 3.5 μM for *E. coli*,[64] compared to 20 μM in magainin-2 amide.[65] Peptoid **75**, which is identical to **74** but containing *N*rpe residues, exhibited an identical HPLC retention time and MIC against both *E. coli* and *B. subtilis* meaning backbone handedness does not contribute to antimicrobial activity, also observed in many AMPs. However, the selectivity ratio was reduced compared to **74**, meaning that for this sequence the *N*rpe enantiomer is more toxic than the *N*spe. Increasing chain length made the peptoid more potent, with shorter chains displaying larger MIC values as seen in peptoid **76** (**Table 1.4**). However, increasing the number of residues past 12 had a negative effect on MIC. Haemolysis increased linearly with chain length, with the optimum number of residues to balance potency and selectivity being the 12-mer **74**.

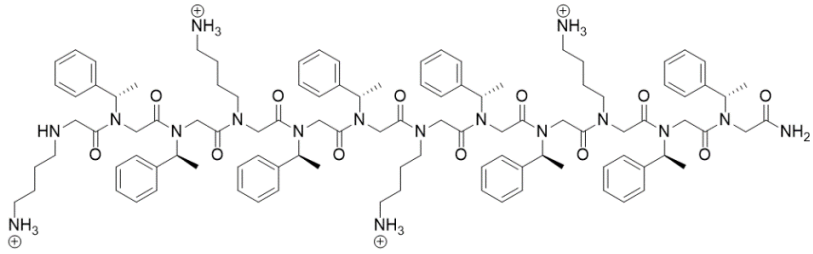

74

Figure 1.44: Structure of peptoid **74** pioneered by the Barron group,[63] showing a net charge of +4.

Table 1.4: Sequences of peptoids **74** – **77** alongside MIC values against *E. coli* and *B. subtilis* as well as selectivity ratios. Value taken from Cobb et al., 2020.[66]

Sequence	*E. coli* (MIC, μM)	*B. subtilis* (MIC, μM)	Selectivity Ratio
H-(*N*Lys-*N*spe-*N*spe)$_4$-NH$_2$ (**74**)	3.55	0.88	6.0
H-(*N*Lys-*N*rpe-*N*rpe)$_4$-NH$_2$ (**75**)	3.55	0.88	4.6
H-(*N*Lys-*N*spe-*N*spe)$_2$-NH$_2$ (**76**)	27.0	27.0	>8.1
H-(*N*Lys-*N*spe-*N*spe)$_5$-NH$_2$ (**77**)	5.50	1.40	0.55

Cobb and Bolt investigated a large library of peptoid oligomers for trends in antimicrobial activity.[67,68] Reiterating Barron's work, the 12-mer was found to be the optimum length though 9-mers also displayed broad activity. Interestingly, the introduction of fluorine increased antimicrobial activity, and chains displaying potent activity as well as little to no toxicity contained achiral monomers. Of the peptoids studied by Bolt, five structures tied for the lowest MIC against *E. coli* at 6 μM,[68] including the fluorine containing oligomer **78** shown in **Figure 1.45**. Molchanova et al. found limited aromatic fluorination to increase the activity of peptoid oligomers against both gram-positive and gram-negative bacteria, as well as increasing hydrophobicity and having no effect on toxicity.[69] However, extensive aromatic fluorination in the chain was shown to reduce cell selectivity, resulting in a more toxic compound.

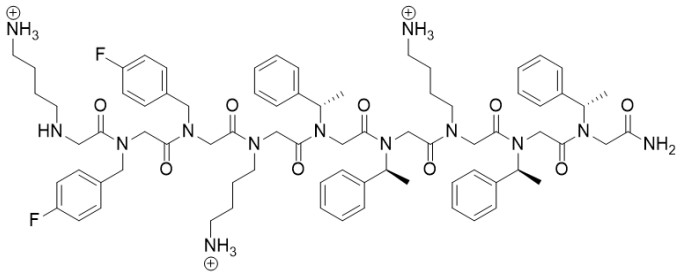

78

Figure 1.45: Structure of an antimicrobial peptoid **78** synthesised by Cobb and Bolt which displayed an MIC of 6 μM against *E. coli*.[68]

To understand the mode of action responsible for the antimicrobial properties of peptoids, Chongsiriwatana et al. used transmission electron microscopy to study the effects on bacteria upon treatment with **74**.[70] *E. coli* was treated with this peptoid for 5, 15, 30 and 60 minutes, with significant intracellular morphological changes occurring at the 5-minute mark (**Figure 1.46**). In fact, the extreme similarity between the four samples reveals that the effects of the peptoid are occurring within the first 5 minutes of treatment and are not a post-mortem artifact.

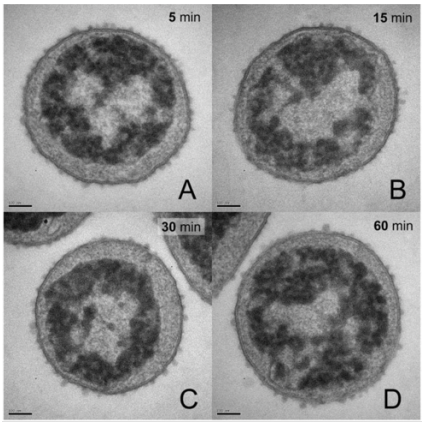

Figure 1.46: Transmission electron micrographs of *E. coli* after treatment with peptoid **74** for 5 (A), 15 (B), 30 (C) and 60 minutes (D). All bacteria killed at each time point. Scale bar represents 100 nm. Figure taken from Chongsiriwatana et al., 2017.[70]

Mojsoska et al. found peptoid **79** (**Figure 1.47a**) to operate via a different mode of action.[71] Using scanning electron microscopy, untreated *E. coli* displayed smooth surfaces whereas those treated with 1x and 4x the MIC of **79**, found to be 16 μg/mL,[72] exhibited significant roughening and leakage of the cytoplasmic content at 1 and 4 hours (**Figure 1.47b**). This mode of membrane lysis is common amongst AMPs, though the mechanism by which disruption of the membrane occurs is likely to vary with peptoid structure.[73]

a)

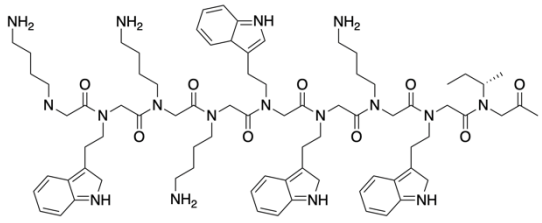

79

b)

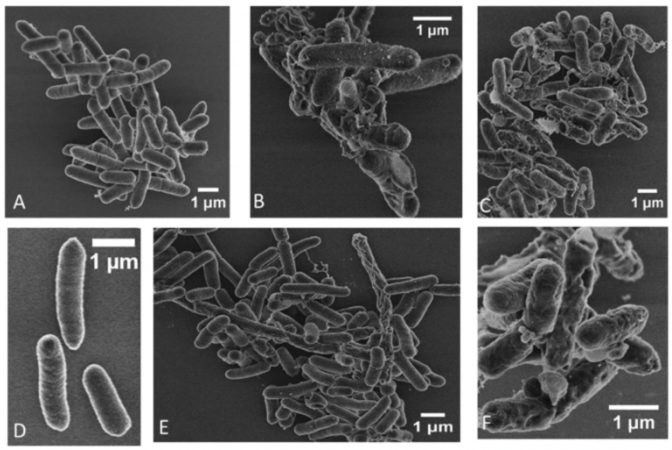

Figure 1.47: a) Structure of peptoid **79**. **b)** Scanning electron micrographs of untreated E. coli at 1 hour (A), E. coli treated with 1x MIC at 1 hour (B), E. coli treated with 4x MIC at 1 hour (C), untreated E. coli at 4 hours (D), E. coli treated with 1x MIC at 4 hours (E) and E. coli treated with 4x MIC at 4 hours (F). Image taken from Mojsoska et al., 2017.[71]

1.4 Project Aims

Peptoids offer a novel route to designing therapeutic compounds against a range of diseases, yet progress is hindered by an inherent flexibility that in many cases renders secondary structures undefined. In summary, three key considerations can be used to predict a side chain's ability to induce the *cis* rotamer in a peptoid:

1. **Steric effects:** Increased steric bulk proximal to the amide bond induces a *cis* peptide conformation, as larger substituents prefer not to be adjacent.

2. **$n \rightarrow \pi^*_{Ar}$:** Exclusively stabilises the *cis* conformation by donation of electron density from a carbonyl to an aryl side chain. Can be enhanced by the inductive effects of substituents.

3. **Intramolecular hydrogen bonding**: Hydrogen bonding is a secondary consideration as associations between a H donor and a carbonyl would interfere with said carbonyl's ability to partake in more favourable $n \rightarrow \pi^*$ interactions.

As with peptides, a peptoid's structure often directly correlates to its function. Currently, the design of oligomers capable of self-assembly into a peptoid helix relies on limited methods of rigid backbone regulation. Incorporating large amounts of bulky aryl side chains, such as *N*spe (**3**) and *N*s1npe (**9**), drastically increases the hydrophobic character of the peptoid, making them unsuitable for use in aqueous media. The *N*^{t}Bu monomer (**Figure 1.18**) pioneered by Roy's group, though extremely *cis* inducing with $K_{cis/trans}$ >19 in MeCN,[26] required solution phase techniques for monomer incorporation due to its acid lability, making it unfeasible for the growth of long chains. Though the charged triazolium (**Figure 1.26**) offer excellent jurisdiction over the backbone, two post modification steps are required after the oligomer is synthesized.[33] The library of monomers capable of controlling *cis*/*trans* isomerization requires much greater expansion, allowing diverse units to be available for the rational design of peptoid oligomers.

The fluoroalkyl *N*3fEt side chain, reported by Cobb and Gimenez,[50] has opened the door for a new class of *cis* isomer favouring monomers. Fluorine's inductive effects have already been utilized in the design of aromatic peptoid sidechains as a neutral backbone influence. The

activity of antimicrobial peptoids has been shown to increase upon fluorination, and toxicity diminishes by the removal of chiral monomers from the chain.[68]

As well as influencing the tertiary amide backbone, available monomers should ideally offer favourable characteristics to oligomers. Fluorine is widely utilized in therapeutic drugs, such as Ayvakit (**34**) and Tabrecta (**35**), to enhance lipophilicity. Log *P* tends to increase upon fluorination but is known to vary depending on its position relative to other heteroatoms and its distribution along the chain (**Figure 1.33**).[46]

The aims of this project are:

- To explore the influence of fluoralkyl side chains further, accessing new moieties capable of exerting a *cis* preference in the amide backbone that are achiral, uncharged and aliphatic.

- To measure the effect on lipophilicity by increasing the distance of fluorine from the amide functionality, as well increasing the fluorine content of the side chain.

- To incorporate new fluoroalkyl monomers into peptoid oligomers that show a defined secondary structure in solution.

1.5 References

1) A. C.-L. Lee, J. L. Harris, K. K. Khanna and J.-H. Hong, *Int J Mol Sci*, 2019, **20**, 2383.
2) B. J. Evans, A. T. King, A. Katsifis, L. Matesic and J. F. Jamie, *Molecules*, 2020, **25**, 2314.
3) A. Patel, K. Cholkar and A. K. Mitra, *Ther Deliv*, 2014, **5**, 337–365.
4) G. Li Petri, S. di Martino and M. de Rosa, *J Med Chem*, 2022, **65**, 7438–7475.
5) M. Pelay-Gimeno, A. Glas, O. Koch and T. N. Grossmann, *Angew Chem Int Edit*, 2015, **54**, 8896–8927.
6) I. W. Hamley, *Chem. Commun.*, 2015, **51**, 8574–8583.
7) I. W. Hamley, *Biomacromolecules*, 2014, **15**, 1543–1559.
8) C. M. Goodman, S. Choi, S. Shandler and W. F. DeGrado, *Nat Chem Biol*, 2007, **3**, 252–262.
9) R. J. Simon, R. S. Kania, R. N. Zuckermann, V. D. Huebner, D. A. Jewell, S. Banville, S. Ng, L. Wang, S. Rosenberg and C. K. Marlowe, *Proc Natl Acad Sci*, 1992, **89**, 9367–9371.
10) G. Fischer, *Chem Soc Rev*, 2000, **29**, 119–127.
11) A. P. Joseph, N. Srinivasan and A. G. de Brevern, *Amino Acids*, 2012, **43**, 1369–81.
12) J. Zhang and M. W. Germann, *Biopolymers*, 2011, **95**, 755–62.
13) H.-C. Tang and Y.-C. Chen, *RSC Adv*, 2015, **5**, 20623–20633.
14) S. A. Fowler and H. E. Blackwell, *Org Biomol Chem*, 2009, **7**, 1508.
15) J. S. Laursen, J. Engel-Andreasen, P. Fristrup, P. Harris and C. A. Olsen, *J Am Chem Soc*, 2013, **135**, 2835–2844.
16) J. A. Crapster, J. R. Stringer, I. A. Guzei and H. E. Blackwell, *Biopolymers*, 2011, **96**, 604–616.
17) J. A. Crapster, I. A. Guzei and H. E. Blackwell, *Angew Chem Int Edit*, 2013, **52**, 5079–5084.
18) K. Kirshenbaum, A. E. Barron, R. A. Goldsmith, P. Armand, E. K. Bradley, K. T. v. Truong, K. A. Dill, F. E. Cohen and R. N. Zuckermann, *Proc Natll Acad Sci*, 1998, **95**, 4303–4308.
19) P. Armand, K. Kirshenbaum, A. Falicov, R. L. Dunbrack, K. A. Dill, R. N. Zuckermann and F. E. Cohen, *Fold Des*, 1997, **2**, 369–375.
20) S. A. Fowler and H. E. Blackwell, *Org Biomol Chem*, 2009, **7**, 1508.
21) P. Armand, K. Kirshenbaum, R. A. Goldsmith, S. Farr-Jones, A. E. Barron, K. T. v. Truong, K. A. Dill, D. F. Mierke, F. E. Cohen, R. N. Zuckermann and E. K. Bradley, *Proc Natl Acad Sci*, 1998, **95**, 4309–4314.
22) J. R. Stringer, J. A. Crapster, I. A. Guzei and H. E. Blackwell, *J Am Chem Soc*, 2011, **133**, 15559–15567.
23) B. C. Gorske, J. R. Stringer, B. L. Bastian, S. A. Fowler and H. E. Blackwell, *J Am Chem Soc*, 2009, **131**, 16555–16567.
24) C. W. Wu, T. J. Sanborn, K. Huang, R. N. Zuckermann and A. E. Barron, *J Am Chem Soc*, 2001, **123**, 6778–6784.
25) C. W. Wu, K. Kirshenbaum, T. J. Sanborn, J. A. Patch, K. Huang, K. A. Dill, R. N. Zuckermann and A. E. Barron, *J Am Chem Soc*, 2003, **125**, 13525–13530.
26) O. Roy, C. Caumes, Y. Esvan, C. Didierjean, S. Faure and C. Taillefumier, *Org Lett*, 2013, **15**, 2246–2249.
27) O. Roy, G. Dumonteil, S. Faure, L. Jouffret, A. Kriznik and C. Taillefumier, *J Am Chem Soc*, 2017, **139**, 13533–13540.
28) M. Rzeigui, M. Traikia, L. Jouffret, A. Kriznik, J. Khiari, O. Roy and C. Taillefumier, *J Org Chem*, 2020, **85**, 2190–2201.
29) H.-M. Shin, C.-M. Kang, M.-H. Yoon and J. Seo, *Chem. Commun.*, 2014, **50**, 4465–4468.
30) N. H. Shah, G. L. Butterfoss, K. Nguyen, B. Yoo, R. Bonneau, D. L. Rabenstein and K. Kirshenbaum, *J Am Chem Soc*, 2008, **130**, 16622–16632.
31) B. F. Pedersen, W. Hälg, P. Fischer, E. Stoll, G. Eriksson, R. Blinc, S. Paušak, L. Ehrenberg and J. Dumanović, *Acta Chem Scand*, 1967, **21**, 1415–1424.
32) B. C. Gorske, B. L. Bastian, G. D. Geske and H. E. Blackwell, *J Am Chem Soc*, 2007, **129**, 8928–8929.
33) C. Caumes, O. Roy, S. Faure and C. Taillefumier, *J Am Chem Soc*, 2012, **134**, 9553–9556.
34) J. R. Stringer, J. A. Crapster, I. A. Guzei and H. E. Blackwell, *J Org Chem*, 2010, **75**, 6068–6078.
35) D. O'Hagan, *Chem. Soc. Rev.*, 2008, **37**, 308–319.
36) P. W. Y. Chan, A. F. Yakunin, E. A. Edwards and E. F. Pai, *J Am Chem Soc*, 2011, **133**, 7461–7468.
37) L. Hunter, *Beilstein J. Org. Chem.*, 2010, **6**, No. 38
38) M. Inoue, Y. Sumii and N. Shibata, *ACS Omega*, 2020, **5**, 10633–10640.

39) E. P. Gillis, K. J. Eastman, M. D. Hill, D. J. Donnelly and N. A. Meanwell, *J Med Chem*, 2015, **58**, 8315–8359.
40) Y. Yu, A. Liu, G. Dhawan, H. Mei, W. Zhang, K. Izawa, V. A. Soloshonok and J. Han, *Chin. Chem. Lett.*, 2021, **32**, 3342–3354.
41) Z. Nairoukh, F. Strieth-Kalthoff, K. Bergander and F. Glorius, *Chem. Eur. J.*, 2020, **26**, 6141–6146.
42) A. Sun, D. C. Lankin, K. Hardcastle and J. P. Snyder, *Chem. Eur. J.*, 2005, **11**, 1579–1591.
43) C. Thiehoff, Y. P. Rey and R. Gilmour, *Isr J Chem*, 2017, **57**, 92–100.
44) B. E. Smart, *J Fluor Chem*, 2001, **109**, 3–11.
45) N. Muller, *J Pharm Sci*, 1986, **75**, 987–991.
46) B. Jeffries, Z. Wang, H. R. Felstead, J.-Y. le Questel, J. S. Scott, E. Chiarparin, J. Graton and B. Linclau, *J Med Chem*, 2020, **63**, 1002–1031.
47) B. Linclau, Z. Wang, B. Jeffries, J. Graton, R. J. Carbajo, D. Sinnaeve, J. le Questel, J. S. Scott and E. Chiarparin, *Angew Chem Int Edit*, 2021, **61**, *7*.
48) C. Hansch, A. Leo, S. H. Unger, K. H. Kim, D. Nikaitani and E. J. Lien, *J Med Chem*, 1973, **16**, 1207–1216.
49) D. Gimenez, G. Zhou, M. F. D. Hurley, J. A. Aguilar, V. A. Voelz and S. L. Cobb, *J Am Chem Soc*, 2019, **141**, 3430–3434.
50) D. Gimenez, J. A. Aguilar, E. H. C. Bromley and S. L. Cobb, *Angew Chem Int Edit*, 2018, **57**, 10549–10553.
51) S. M. Miller, R. J. Simon, S. Ng, R. N. Zuckermann, J. M. Kerr and W. H. Moos, *Bioorg Med Chem Lett*, 1994, **4**, 2657–2662.
52) R. A. Conradi, A. R. Hilgers, N. F. H. Ho and P. S. Burton, *Pharm Res*, 1992, **09**, 435–439.
53) Y.-U. Kwon and T. Kodadek, *J Am Chem Soc*, 2007, **129**, 1508–1509.
54) N. C. Tan, P. Yu, Y.-U. Kwon and T. Kodadek, *Bioorg Med Chem*, 2008, **16**, 5853–5861.
55) M. K. Ghosh, *Front Biosci*, 2017, **9**, 789.
56) W. Huang, J. Seo, S. B. Willingham, A. M. Czyzewski, M. L. Gonzalgo, I. L. Weissman and A. E. Barron, *PLoS One*, 2014, **9**, e90397.
57) G. Diamond, N. Molchanova, C. Herlan, J. Fortkort, J. Lin, E. Figgins, N. Bopp, L. Ryan, D. Chung, R. Adcock, M. Sherman and A. Barron, *Pharmaceuticals*, 2021, **14**, 304.
58) Schröder T, Quintilla A, Setzler J, Birtalan E, Wenzel W and Bräse S, *WSEAS Trans. Biol. Biomed.*, 2007, **4**, 145–148.
59) D. Kölmel, D. Fürniss, S. Susanto, A. Lauer, C. Grabher, S. Bräse and U. Schepers, *Pharmaceuticals*, 2012, **5**, 1265–1281.
60) H.-S. Kim, Y. Lee, M. H. Shin and H.-S. Lim, *Chem. Commun.*, 2021, **57**, 6800–6803.
61) B. Liu, P. G. Alluri, P. Yu and T. Kodadek, *J Am Chem Soc*, 2005, **127**, 8254–8255.
62) P. Alluri, B. Liu, P. Yu, X. Xiao and T. Kodadek, *Mol Biosyst*, 2006, **2**, 568.
63) J. A. Patch and A. E. Barron, *J Am Chem Soc*, 2003, **125**, 12092–12093.
64) N. P. Chongsiriwatana, J. A. Patch, A. M. Czyzewski, M. T. Dohm, A. Ivankin, D. Gidalevitz, R. N. Zuckermann and A. E. Barron, *Proc. Natl. Acad. Sci.*, 2008, **105**, 2794–2799.
65) K. T. Nguyen, S. v. le Clair, S. Ye and Z. Chen, *J Phys Chem B*, 2009, **113**, 12358–12363.
66) K. L. Bicker and S. L. Cobb, *Chem. Commun.*, 2020, **56**, 11158–11168.
67) Z. Wang, B. F. Jeffries, H. R. Felstead, N. J. Wells, E. Chiarparin and B. Linclau, *J. Vis. Exp.*, 2019, 143, e58567
68) H. L. Bolt, G. A. Eggimann, C. A. B. Jahoda, R. N. Zuckermann, G. J. Sharples and S. L. Cobb, *Medchemcomm*, 2017, **8**, 886–896.
69) N. Molchanova, P. R. Hansen, P. Damborg, H. M. Nielsen and H. Franzyk, *ChemMedChem*, 2017, **12**, 312–318.
70) N. P. Chongsiriwatana, J. S. Lin, R. Kapoor, M. Wetzler, J. A. C. Rea, M. K. Didwania, C. H. Contag and A. E. Barron, *Sci Rep*, 2017, **7**, 16718.
71) B. Mojsoska, G. Carretero, S. Larsen, R. V. Mateiu and H. Jenssen, *Sci Rep*, 2017, **7**, 42332.
72) B. Mojsoska, R. N. Zuckermann and H. Jenssen, *Antimicrob Agents Chemother*, 2015, **59**, 4112–4120.
73) K. L. Bicker and S. L. Cobb, *Chem. Comm.*, 2020, **56**, 11158–11168.

Chapter 2: Evaluating the *Cis* Inducing Effects of Fluoroalkyl Sidechains

2.1 Introduction

2.1.1 Dipeptoid Model Systems

Previously, the propensity of peptoid monomers to induce helix-like secondary structures was evaluated through Circular Dichroism (CD) spectroscopy.[1–3] However, the synthesis of homogeneous sequences naturally brings about issues with solubility, making the direct comparison of individual monomers much more complicated. Molecular modelling of extended peptoid sequences has also been widely utilized.[4,5]

One of the first attempts to quantify the influence of individual *N*-appended side chains was by the Rabstein group in 2007.[6] Rotation around the tertiary amide bond is relatively slow on the NMR timescale, meaning the ^{1}H-NMR spectra of peptoids are composite of the spectra arising from each isomer. Rabstein et al. formed a small library of N-acetylated monomers, dipeptoids and tripeptoids to study the equilibrium about the tertiary amide, using 2D NOESY experiments to assign rotamer peaks in the ^{1}H-NMR (**Figure 2.1**).[6]

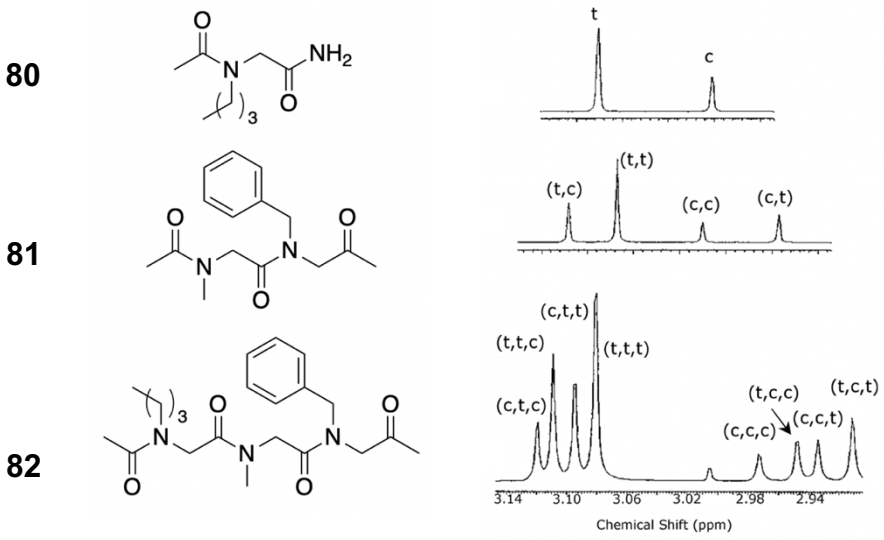

Figure 2.1: Examples of peptoid monomer (**80**), dipeptoid (**81**) and tripeptoid (**82**) studied by the Rabstein group, with corresponding ^{1}H-NMR spectra and assigned rotamer peaks for the acetyl methyl protons. Figure adapted from Rabstein et al. 2007.[6]

Evident from **Figure 2.1**, resolution between rotamer peaks suffers with increased chain length, giving rise to peak crowding and ambiguous assignment. To facilitate spectral resolution and assignment, *N*-α-chiral residues were excluded from the study. Evaluating $K_{cis/trans}$ in dimers and trimers gave rise to 4 and 8 unique rates of rotation respectively,[6] which would make direct comparison throughout large libraries of sidechains laborious and inefficient. The acetylated monomer provided the clearest, quantifiable measurement of the *cis/trans* isomerization. However, it's structure does not best represent the local environment of most *N*-substituted glycines in oligomers.

Pioneering work by Blackwell et al, saw the development of model *N*,*N*-disubstituted acetamides,[7] capable of evaluating $K_{cis/trans}$ with similar 1D and 2D NMR experiments utilized by Rabstein. The design of these models closely mimics the isolated environment of individual sidechains and allows for the evaluation of short range i to i and i to i ± 1 interactions (**Figure 2.2**).

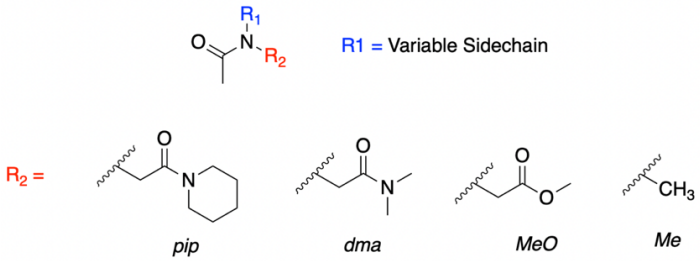

Figure 2.2: General structure *N*,*N*-disubstituted acetamide models along with various C-terminal capping groups.

Unlike Rabstein, Blackwell's study heavily represented *N*-α-chiral residues as these had been extensively studied and found to induce the peptoid helix secondary structure. Of the C-terminal capping groups, R_2 = *pip* has been the most widely adopted amongst the peptoid community. R_2 = Me and R_2 = MeO are less representative of the amide backbone, making *pip* and *dma* the most viable options.

As discussed in **Section 1.2.4**, two electronic effects compete in the peptoid backbone: n → π^*_{Ar} (*cis* stabilizing) and n → π^*_{Am} (*trans* stabilizing). The dimethylamide (*dma*) capping group is less effective at stabilising a positive charge on nitrogen compared to the relatively larger, more electron rich piperidinyl group (*pip*). This means the amide nitrogen in *dma* is less likely to donate electron density into the carbonyl, making the corresponding carbon atom a better electrophile than in a piperidinyl terminus.[7] Subsequently, n → π^*_{Am} interactions are more favourable in the dimethylated models (**Figure 2.3**). Blackwell's studies revealed up to a 50%

reduction in $K_{cis/trans}$ throughout a series of *dma* capped models in comparison to their piperidinyl equivalents (**Table 2.1**).[8] The terminal piperidinyl group closely resembles the chemical composition of a peptoid, retains a simple synthesis and provides a more realistic electronic environment in which tautomerization of the amide is better tolerated and $n \rightarrow \pi^*_{Am}$ interactions are less favoured.

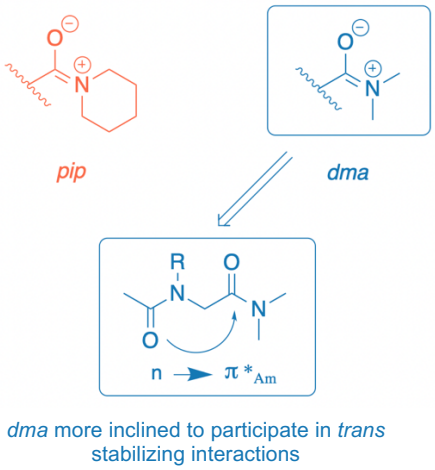

Figure 2.3: Structure of *pip* and *dma* capping amide tautomers showing the $n \rightarrow \pi^*_{Am}$ interaction better favoured by *dma*.

Table 2.1: $K_{cis/trans}$ values in MeCN of various *N*-sidechains with either the *pip* or *dma* C-terminal amide capping group. Values taken from Blackwell et al. 2007.[8]

C-Terminal Capping Group	*N*-Appended Variable Sidechain	$K_{cis/trans}$ (MeCN)
pip	*np*	3.43 ± 0.19
dma	*np*	3.06 ± 0.01
pip	*pe*	2.04 ± 0.27
dma	*pe*	1.69 ± 0.14
pip	*ch*	1.22 ± 0.01
dma	*ch*	0.58 ± 0.06

Another major benefit of Blackwell's model dipeptoids is a relatively simple numerical evaluation of $K_{cis/trans}$ by ^{1}H-NMR. Characteristic diastereotopic behaviour exhibited by the terminal acetal group gives rise to distinguishable chemical shifts for both the *cis* and *trans* rotamers. Like in Rabsteins work, these peaks show defined ^{1}H-^{1}H Nuclear Overhauser Effect correlation patterns (NOE's), allowing peaks arising from each isomer to be assigned unequivocally.

2.1.2 *N*-Alkyl Sidechains in Peptoids

As previously discussed in **Section 1.1.4**, the bulky *tert*-butyl group reported by Roy et al. offers high levels of *cis* enforcement in the peptoid amide backbone.[9] Further, the same group introduced a stereogenic centre to this monomer creating the α-chiral *N*s1tbe unit, albeit less *cis* inducing than its *N*^{t}Bu predecessor.[2,9] The *tert*-butyl sidechain required solution phase synthesis techniques, with any attempts at solid phase growth resulting in mixtures of truncated *N*^{t}Bu oligomers. For this reason, *N*s1tbe (**19**) monomers were also incorporated in solution which is arduous and time consuming compared to an on-resin approach. These two sidechains, along with the mildly *cis* inducing *N*sch monomer (**5**) ($K_{cis/trans}$ = 1.22 in MeCN),[7] were the first non-aromatic, alkyl sidechains reported for the formation of PP1 type helices. Unfortunately, a lack of functionalization means they offer no beneficial characteristics for the rational design of therapeutic peptoids, aside from their *cis* preference.

Building from the foundations of the ^{t}Bu group, Roy et al., proposed to functionalise this *cis* inducing monomer with *N*cα-*gem*-dimethylated sidechains that mimic proteinogenic amino acids.[10] Examples of the alkyl groups suggested are shown in **Figure 2.4**.

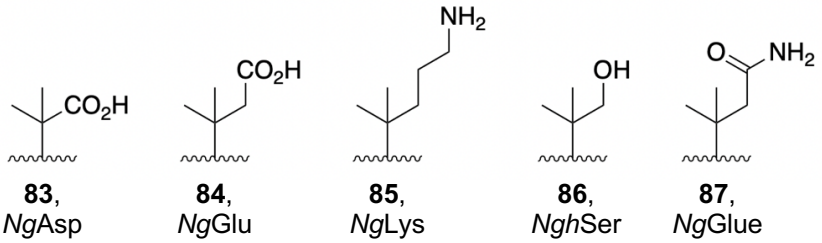

Figure 2.4: Structures of *N*cα-*gem*-dimethylated alkyl sidechains mimicking proteinogenic amino acids.

Of the proposed structures, the group investigated the *Ng*Lys and *Ngh*Ser sidechains (**85** and **86** respectively) for their impact on the amide equilibrium. Model piperidyl systems of each gave $K_{cis/trans}$ > 19 in both polar and non-polar solvents.[10] Trimers were also synthesised incorporating these monomers, yielding a defined *cis* backbone. These groups offer structural diversity whilst retaining a high degree of conformational control. Closely mimicking a natural peptide sequence can be crucial to allow for peptoid-protein recognition, making proteinogenic based sidechains a useful tool in structure-activity relationship studies.[10] However, it must be noted that such monomers again required solution phase synthesis techniques in order to grow oligomers.

Zuckermann et al. further probed lysine-like sidechains to stabilize the *cis* conformation via intramolecular hydrogen bonding.[11] A library of cationic, alkyl monomers were evaluated, examples of which are shown in **Figure 2.5** alongside their ^{1}H-NMR determined $K_{cis/trans}$ values in piperidinyl model systems.

Proof of an intramolecular hydrogen bonding interaction was evidenced by a reduced $K_{cis/trans}$ in polar protic solvents and sensitivity to temperature for the *N*ap monomer (**88**). For the quaternary ammonium type monomers, the observed strong *cis* preference is due to attraction between the cationic group and the carbonyl oxygen's lone pair. It is important to note that the positive charge in a quaternary ammonium is delocalised about surrounding hydrogens, not fully realised in the Lewis structure.[11] Depictions of the interactions mentioned can be seen in **Figure 2.6**.

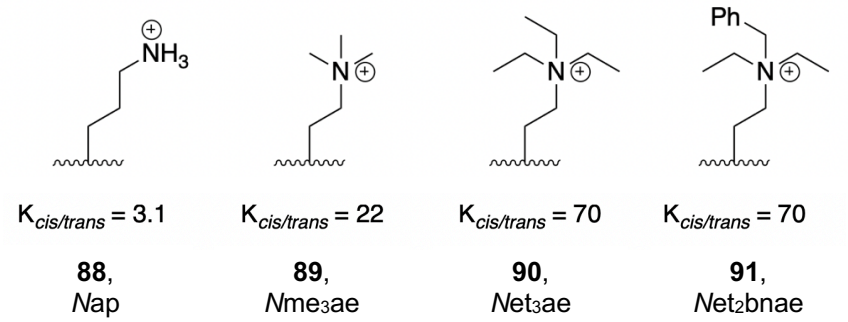

Figure 2.5: Selection of cationic, alkyl monomers designed by Zuckermann et al. alongside experimentally determined $K_{cis/trans}$ in $CDCl_3$. Values taken from Zuckermann et al. 2019.[11]

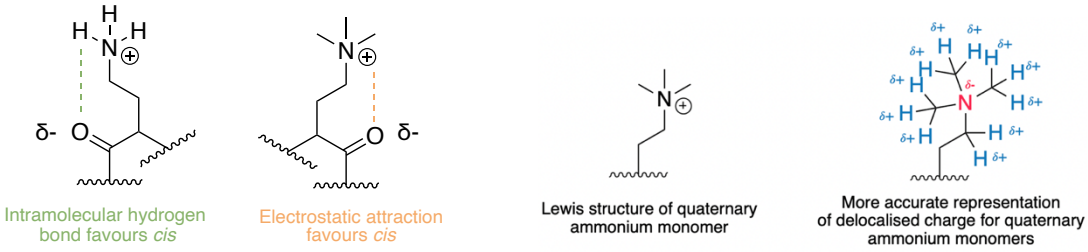

Figure 2.6: Depictions of electronic interactions stabilizing the *cis* conformation in Zuckermann et al. monomers as well as a realistic depiction of the charge delocalization in quaternary ammonium sidechains.

These cationic alkyl sidechains are structurally diverse, cheap to obtain, hydrophilic and compatible with solid phase synthesis, with excellent *cis* enforcement in the amide backbone.[11]

Of the handful of functionalized *N*-alkyl sidechains reported in the literature, only the cationic monomers from Zuckermann's research offer a strong *cis* preference whilst remaining compatible with solid phase chain growth, which is crucial to produce large peptoid libraries. The available alkyl side chains for helix formation require diversification, with a gap in the peptoid market for a *cis* enforcing, lipophilic alkyl series.

Mentioned in **Section 1.3.5**, the *N*3fEt monomer (**Figure 2.7**), first published in 2018 by D. Gimenez of the Cobb group at Durham,[12] offers a *cis* amide preference in model systems and has been shown to form extended sequences that self-assemble into PPI type helices in solution. The further potential of fluorinated alkyl side chains has remained unexplored, with the possibility of identifying new *cis* inducing, lipophilic moieties compatible with on-resin synthesis.

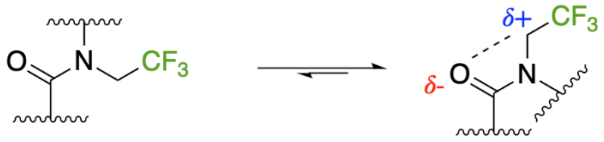

Figure 2.7: Depiction of the *cis* amide preference of the *N*3fEt group driven by electronic interactions between the carbonyl oxygen and electron deficient carbon adjacent to CF_3 in the sidechain.

2.1.3 Chapter 2 Objectives

As a continuation of Gimenez' work, the structural effects of fluoroalkyl side chains will be explored further and quantified by use of piperidinyl model systems. The aim of this chapter is to uncover novel peptoid monomers to add to the 'toolbox' of sidechains available for the design of structurally defined oligomers. Further, it is hoped that these monomers will offer suitable alternatives to the charged, chiral and aromatic monomers already in use. The three main objectives of this chapter are:

- To create a library of fluorinated model peptoids for $K_{cis/trans}$ evaluation by established NMR methods.

- To study the effects of controlling $K_{cis/trans}$ in these novel sidechains through solvent studies and X-ray crystallography.

- To further understand fluorine's effect on lipophilicity when present in an alkyl peptoid sidechain.

2.2 Results and Discussion

2.2.1 Design and Synthesis of Model Systems

In order for the $K_{cis/trans}$ values determined in our model dipeptoids to be comparable with those reported in literature, the widely adopted piperidinyl system was chosen for this study. Models were synthesized by adapting an established method outlined by Blackwell,[8] shown in **Scheme 2.1**.

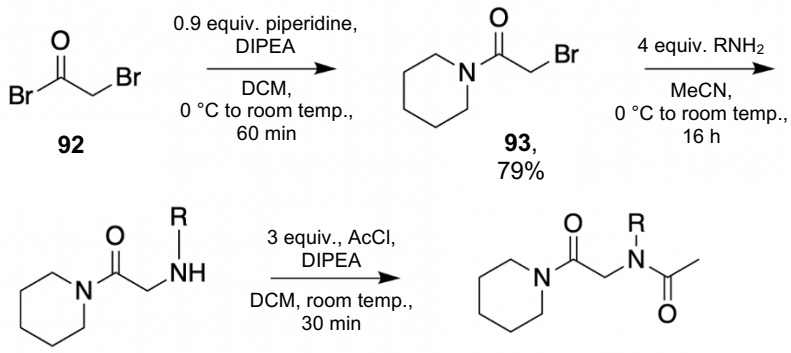

Scheme 2.1: General synthesis employed for model piperidinyl peptoid systems.

1-(2-bromoacetyl)piperidine (**93**) was synthesized in good yield from bromoacetyl bromide (**92**) and did not require purification before use in the next reaction. Acetylation in the final step also proceeded smoothly, with 100% conversion by TLC observed for all models. The nucleophilic substitution of primary amine monomers with **93** proved challenging. The slow, dropwise addition of 1-(2-bromoacetyl)piperidine (**93**) into a stirred solution of amine at 0 °C was outlined in the literature to minimize di-substitutions. Blackwell reported the use of 1.2 molar equivalents of primary amine to 1 equivalent of **93** which, when utilized in our synthesis, resulted in product mixtures with significant amounts of di-substituted amine, ultimately reducing the overall yield of the models. Instead, 4 equivalents of the primary amine were employed, and this substantially reduced the presence of over-alkylated side-products. **Figure 2.8** demonstrates this improvement by comparison of crude LCMS analysis following nucleophilic substitution in the presence of 1.2 vs 4 molar equivalents of amine.

Isolation of the final models also proved challenging. Purification was performed by flash column chromatography. When choosing a solvent system with thin layer chromatography, almost all model systems were unable to leave the baseline in 100 % EtOAc. MeOH/DCM offered considerably less control over the gradient and model peptoids eluted with various

impurities. Multiple repurifications ensued, resulting in much lower yields than anticipated. This was resolved by first loading the crude with and subsequently passing through two to three column volumes of 100% EtOAc until no further eluents were observed by spotting on TLC. 1 to 3% MeOH in DCM was then pumped through the column, efficiently isolating the model peptoid.

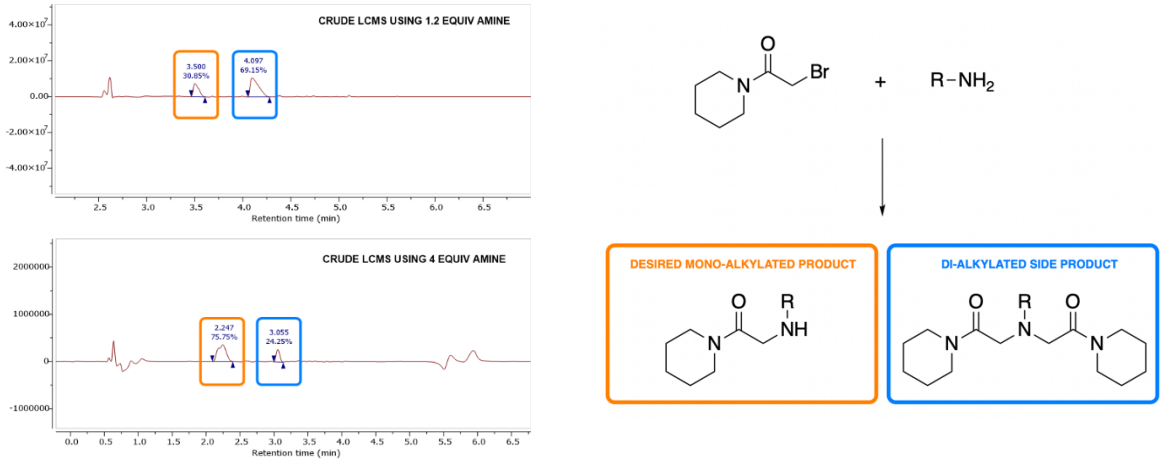

Figure 2.8: Comparison of crude LCMS traces following alkylation of a model peptoid with 1.2 vs 4 equivalents of primary amine (*n*-butylamine). Desired mono-alkylated product makes up significantly greater fraction of the crude composition when 4 equivalents of amine are employed.

To understand the electronic effects found to impose the *cis* conformation in Gimenez' *N*3fEt model, we first investigated the effects of increasing the distance of CF_3 from the peptoid backbone. This was done by increasing the number of CH_2 spacers in the alkyl sidechain under the hypothesis that $K_{cis/trans}$ would decrease. Equivalent non-fluorinated monomers were also incorporated into our library, as this would allow for direct judgement on the effect of terminal fluorination as well as revealing if increasing the size of the alkyl chain enforced any steric influence on the amide isomerism.

Next, we sought to explore the impact on $K_{cis/trans}$ by increasing the amount of fluorine in the alkyl sidechain. This was carried out under the assumption that increased fluorination could further favour the *cis* rotamer. Two approaches were employed: by directly substituting hydrogen for fluorine in the sidechain and by branching the sidechain to add another CF_3 group.

The structure of all models synthesized for this chapter can be seen in **Figure 2.9**. All fluorine-containing sidechains yielded less product in comparison to the non-fluorinated. This is a result of the primary amine being deactivated by the electron withdrawing fluorine groups.

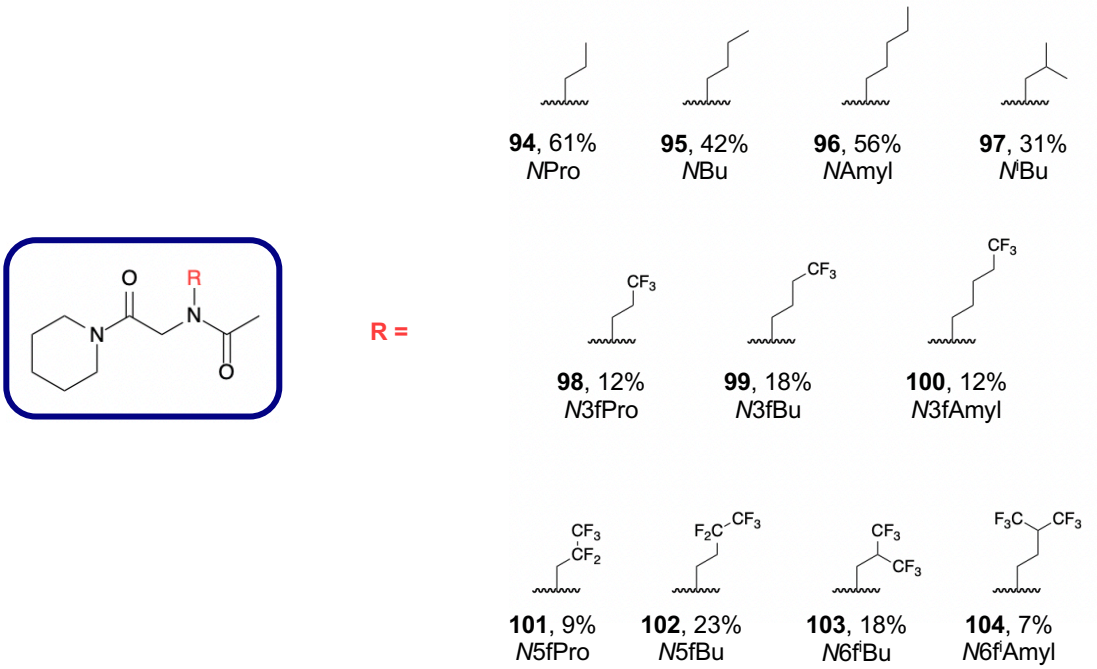

Figure 2.9: Structures of all monomers incorporated into model piperidinyl systems for this chapter, showing their name and corresponding overall yields following purification.

The corresponding primary amines required to synthesize compounds **100**, **103** and **104** were unfortunately not commercially available or unaffordable. Therefore, these three models required an alternative synthesis to be developed. Assessing suitable alternatives, primary alkyl halides were found to be readily available and inexpensive. Modelled on **Scheme 2.1**, a method was designed in which 2-amino-1-(piperidin-1-yl)ethan-1-one (**107**) was used as the reaction's nucleophile instead of a primary amine monomer. Synthesis of **107** was adapted from Wen and Li 2020,[13] whereby Boc-Gly-OH (**105**) undergoes an amide coupling with piperidine before deprotection of the Boc group with TFA. The synthesis of **107** and its use to construct model peptoids are outlined and **Scheme 2.2** and **Scheme 2.3** respectively.

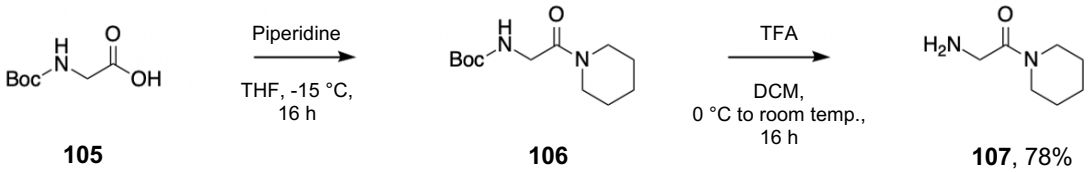

Scheme 2.2: Synthesis of 2-amino-1-(piperidin-1-yl)ethan-1-one adapted from Wen and Li 2020.[13]

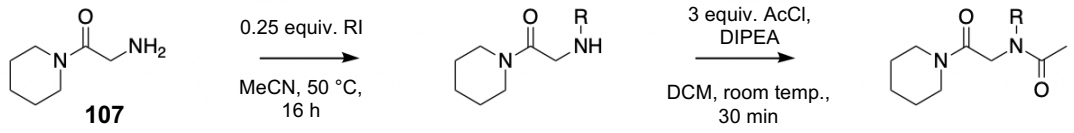

Scheme 2.3: Synthesis of model peptoids with iodoalkanes.

In addition to iodoalkanes being cheaper in comparison to primary amines, less monomer was required from commercial suppliers as the sidechain was not used in excess, unlike in **Scheme 2.1**. Higher temperatures were required for alkylation, but yields tended to match or exceed the literature method of synthesizing models. Although the synthesis of precursor **107** is relatively less simple than **103**, and requires purification by flash column chromatography, this new method could allow for large libraries of sidechains to be evaluated at a fraction of the cost.

2.2.2 NMR Determination of $K_{cis/trans}$ Values

Once the model peptoids (**Figure 2.9**) were isolated, they were subject to a series of 1D and 2D NMR experiments to determine the rate constant of backbone isomerization ($K_{cis/trans}$). ^{1}H-NMR, ^{1}H-*psyche*, ^{13}C-NMR, ^{1}H-^{1}H COSY, ^{1}H-^{1}H NOESY, ^{1}H-^{13}C HSQC and ^{1}H-^{13}C HMBC spectra were obtained for all models, with the addition of fluorine decoupled ^{19}F-NMR for models **98** – **104**. This allowed all peaks to be independently assigned.

In line with previous methods of $K_{cis/trans}$ determination reported in the literature,[8] the three main proton peaks directly involved in the amide equilibrium were used to determine the equilibrium constant. These are the terminal acetyl protons, the backbone CH_2 protons, and the protons appended to the sidechain carbon atom directly bonded to the amide nitrogen (**Figure 2.10**).

The diastereotopic behaviour of the acetyl group gives rise to characteristic NOE's in 2D NMR, allowing the unequivocal assignment of the *cis* and *trans* rotamers. The *cis* conformation gives rise to a NOE between the terminal acetyl protons and the backbone CH_2 protons. The *trans* conformation gives a NOE between the terminal acetyl protons and the sidechain CH_2 protons directly bonded to nitrogen.

Once both rotamers were identified for each of the three main proton groups, peaks were directly integrated to give three independent ratios between the *cis* and *trans* conformations. Two proton spectra were analysed for each monomer and, where possible, an average of the

six values gave $K_{cis/trans}$. **Figure 2.11** shows an example of how $K_{cis/trans}$ was derived for model peptoids from characteristic NOEs.

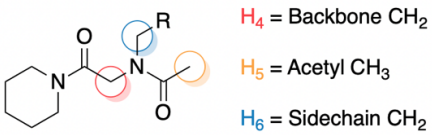

Figure 2.10: Depiction of H_4, H_5 and H_6, the three groups of protons integrated to calculate $K_{cis/trans}$.

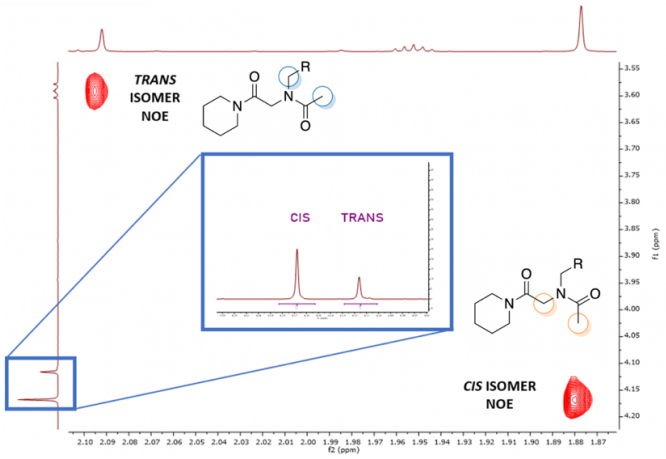

Figure 2.11: Example of how $K_{cis/trans}$ was determined for model peptoids from characteristic NOEs.

Each model peptoid was characterised in three different solvents to identify the forces giving rise to the preferred rotamer. All $K_{cis/trans}$ values for model peptoids **94** to **104** are reported in **Table 2.3** along with ΔG and standard deviations (see **Section 5.4** for more information on how standard deviation was calculated). The table includes values for the *N*Et and *N*3fEt model peptoids developed by Gimenez.[12] For fluorinated monomers **98** to **104**, $K_{cis/trans}$ values from ^{19}F-NMR have been included under a separate column for comparison but note that these have not been included in the overall $K_{cis/trans}$ for the monomer.

Inversion recovery experiments were performed on model peptoids **94** and **98**. T1 was determined for the three main proton groups used in calculating $K_{cis/trans}$. To ensure integration is quantitative for all model systems, the relaxation time of the NMR experiment should be at least 5 times greater than the longest T1. Experiments were carried out in $CDCl_3$, CD_3OD and CD_3CN as were all $K_{cis/trans}$ calculations. All $K_{cis/trans}$ values were calculated from ^{1}H-NMR experiments on a 599 MHz instrument with a 13.9 second relaxation time (d1 = 10 s, acquisition time = 3.9 s), therefore the longest T1 for the protons of interest should be 2.78 seconds or less. T1 data for both **94** and **98** are summarised in **Table 2.2**. Little difference in T1 relaxation was observed between the two models, nor between the *cis* and *trans* rotamers for each peak. T1 times also differed very little in $CDCl_3$ and CD_3OD for each of the models,

whereas all proton signals gave a larger T1 in CD_3CN. This is consistent with the observation that relaxation times are shorter in more viscous solvents, with chloroform and methanol having similar viscosities and acetonitrile being considerably less viscous.[14] The protons with the fastest motion in the whole molecule were at the terminal acetyl position, unsurprising given its diastereotopic nature. This rapid motion between the *cis* and *trans* isomers gives a relatively less efficient mechanism for relaxation compared to the other protons in the model. Nevertheless, the acetyl CH_3 group in acetonitrile gave a T1 less than 2.78 seconds for both rotamers, making the NMR experimental setup appropriate for quantitative integration (**Figure 2.12**).

Table 2.2: T1 values (s) for the three main sets of $K_{cis/trans}$ protons in compounds **3** and **7.**

Model Peptoid	NMR Solvent	T1 (s)					
		H_4 *cis*	H_4 *trans*	H_5 *cis*	H_5 *trans*	H_6 *cis*	H_6 *trans*
94	$CDCl_3$	0.74	0.93	1.74	1.72	-*	0.95
	CD_3OD	0.75	0.90	1.87	1.77	-*	0.93
	CD_3CN	1.45	1.63	2.68	2.74	1.77	1.64
98	$CDCl_3$	0.79	0.91	1.78	1.73	-*	0.93
	CD_3OD	0.76	0.87	1.86	1.77	-*	0.91
	CD_3CN	1.35	1.48	2.75	2.62	-*	1.53

*Peak overlapping with other signals in the ^{1}H-NMR

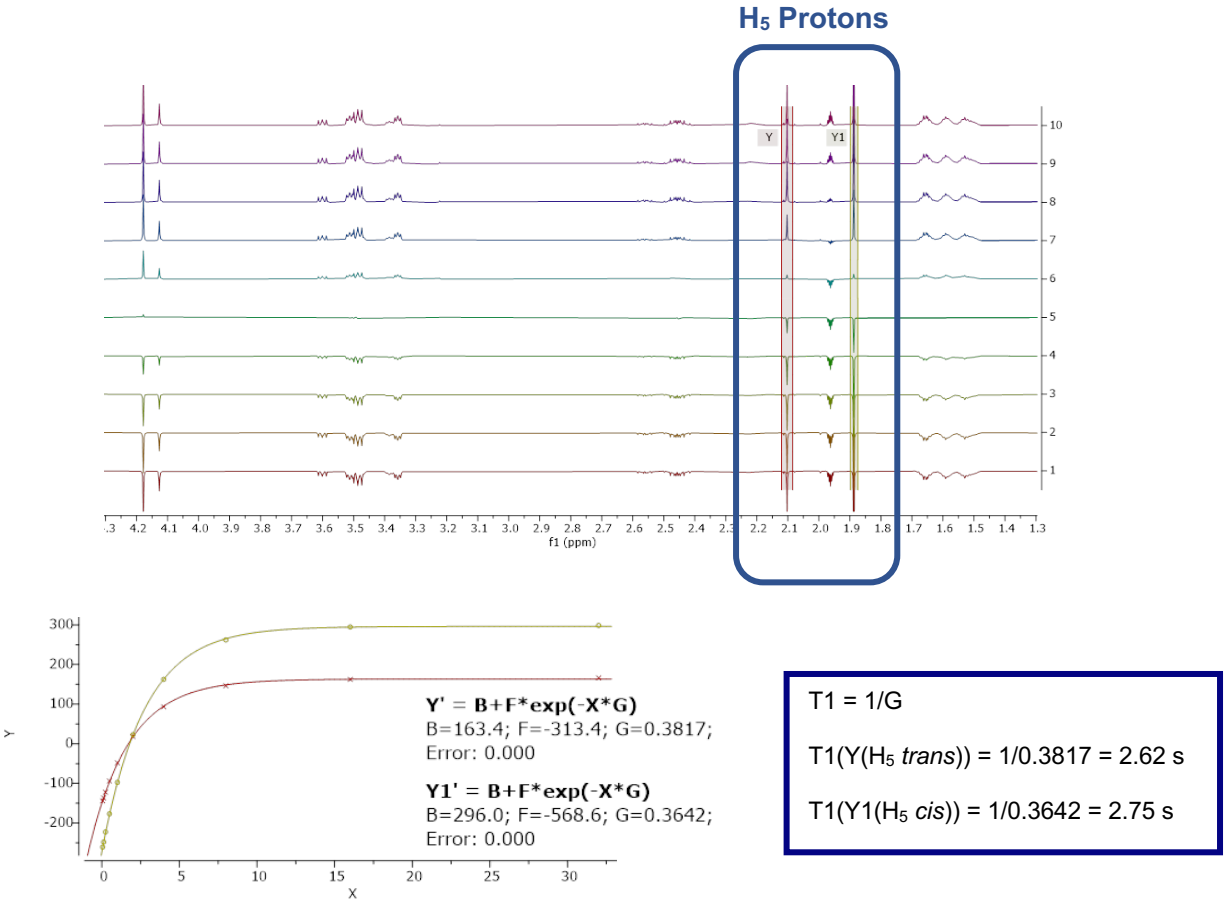

Figure 2.12: Example of inversion experiment for compound **98** in CD_3CN showing how T1 was calculated for the terminal acetal protons.

Table 2.3: $K_{cis/trans}$ and ΔG values for all model peptoids synthesized for chapter 2 in $CDCl_3$, CD_3OD and CD_3CN.

Model Peptoid	Monomer	$CDCl_3$			CD_3OD			CD_3CN		
		$K_{cis/trans}$ (^{1}H-NMR)	$\Delta G_{cis/trans}$ [b] (kcal/mol)	$K_{cis/trans}$ (^{19}F-NMR) [c]	$K_{cis/trans}$ (^{1}H-NMR)	$\Delta G_{cis/trans}$ [b] (kcal/mol)	$K_{cis/trans}$ (^{19}F-NMR) [c]	$K_{cis/trans}$ (^{1}H-NMR)	$\Delta G_{cis/trans}$ [b] (kcal/mol)	$K_{cis/trans}$ (^{19}F-NMR) [c]
-	*N*Et [a]	0.19 ± 0.01	0.97 ± 0.01	-	0.51 ± 0.04	0.43 ± 0.05	-	0.66 ± 0.07	0.28 ± 0.08	-
94	*N*Pro	0.18 ± 0.01 [d]	1.00 ± 0.02	-	0.50 ± 0.01 [d]	0.41 ± 0.01	-	0.70 ± 0.01	0.21 ± 0.01	-
95	*N*Bu	0.17 ± 0.01 [d]	1.04 ± 0.02	-	0.52 ± 0.02 [d]	0.39 ± 0.02	-	0.74 ± 0.01	0.18 ± 0.01	-
96	*N*Amyl	0.18 ± 0.02 [d]	1.01 ± 0.05	-	0.50 ± 0.03 [d]	0.41 ± 0.03	-	0.76 ± 0.03 [d]	0.16 ± 0.01	-
97	*N*^{i}Bu	0.19 ± 0.01 [d]	0.99 ± 0.02	-	0.57 ± 0.01	0.33 ± 0.01	-	0.85 ± 0.02	0.10 ± 0.01	-
-	*N*3fEt [a]	0.54 ± 0.06	0.35 ± 0.01	-	1.23 ± 0.03	-0.13 ± 0.01	-	2.24 ± 0.12	-0.48 ± 0.03	-
98	*N*3fPro	0.83 ± 0.06 [d]	0.12 ± 0.04	0.88	1.34 ± 0.02 [d]	-0.17 ± 0.01	1.25	2.01 ± 0.10 [d]	-0.41 ± 0.03	1.67
99	*N*3fBu	0.52 ± 0.02 [d]	0.38 ± 0.02	0.62	0.97 ± 0.07 [d]	0.02 ± 0.04	~1.00 [f]	1.35 ± 0.03 [d]	-0.18 ± 0.01	1.48
100	*N*3fAmyl	0.39 ± 0.02 [d]	0.56 ± 0.03	- [h]	0.77 ± 0.03	0.15 ± 0.02	- [h]	1.11 ± 0.06 [d]	-0.06 ± 0.03	- [h]
101	*N*5fPro	0.65 ± 0.01	0.26 ± 0.01	0.92 ± 0.04	2.12 ± 0.11	-0.44 ± 0.03	2.17 ± 0.01	4.01 ± 0.01 [e]	-0.82 ± 0.00	3.93 ± 0.11
102	*N*5fBu	0.95 ± 0.03 [d]	0.03 ± 0.02	0.94 ± 0.02	1.60 ± 0.03	-0.28 ± 0.01	1.60 ± 0.05	2.17 ± 0.05 [d]	-0.91 ± 0.01	2.02 [g]
103	*N*6f^{i}Bu	3.23 ± 0.14	-0.69 ± 0.02	3.23	3.28 ± 0.09	-0.70 ± 0.02	3.60	6.22 ± 0.03 [d]	-1.08 ± 0.00	6.09
104	*N*6f^{i}Amyl	0.79 ± 0.03 [d]	0.14 ± 0.02	0.79	1.46 ± 0.01 [e]	-0.22 ± 0.01	1.51	2.26 ± 0.03 [d]	-0.48 ± 0.01	2.29

[a] Values taken from Gimenez 2018.[12]

[b] ΔG calculated as -RTln($K_{cis/trans}$) at 25 °C for each replica.

[c] $K_{cis/trans}$ from ^{19}F-NMR calculated as a ratio of *cis* to *trans* from a single spectrum. Standard deviation is given only for models **101** and **102** as two fluorine environments are present, giving two *cis* rotamer peaks and two *trans*.

[d] $K_{cis/trans}$ (and subsequently ΔG and std dev.) calculated from 2 main sets of protons (4 independent ratios) instead of 3 due to peak overlap in ^{1}H-NMR.

[e] $K_{cis/trans}$ (and subsequently ΔG and std dev.) calculated from 1 main set of protons (2 independent ratios) instead of 3 due to peak overlap in ^{1}H-NMR.

[f] $K_{cis/trans}$ from ^{19}F-NMR approximated to 1.00 as *cis* and *trans* peaks cannot be distinguished by integration alone.

[g] $K_{cis/trans}$ from ^{19}F-NMR calculated from one set of peaks due to overlap in the spectra, hence no standard deviation reported.

[h] Overlap in ^{19}F-NMR prevents $K_{cis/trans}$ being calculated.

The main limitation of this work is that of the models synthesised, $K_{cis/trans}$ was determined from all three major proton groups in only 30% of cases. Most were calculated from two sets of protons due to peak overlap in ^{1}H-NMR that made integration not possible. In the overwhelming number of cases, one of the H_6 rotamer peaks was overlapping with signals arising from the piperidine ring. Additionally, H_6 showed overlap with the solvent peak in CD_3OD. In two instances, **101** and **104**, only a single set of protons could be accurately integrated for a *cis*/*trans* ratio, though the $K_{cis/trans}$ value still closely mirrored those determined from the corresponding ^{19}F-NMR experiment.

Collectively, all compounds gave lower $K_{cis/trans}$ values in $CDCl_3$ which is in line with previous model peptoid solvent studies.[7,8,15] $K_{cis/trans}$ was also lower in protic CD_3OD relative to CD_3CN, though previous studies by D. Gimenez found the *cis* isomer preference to still increase upon going from monofluorinated to trifluorinated monomers, indicating that hydrogen bonding is not involved.[12] CD_3CN gave the greatest values of $K_{cis/trans}$ in all models, being particularly apparent for fluorinated monomers. This supports an electrostatic fluorine effect being responsible for the *cis* rotamer preference.

The non-fluorinated models **94** – **96**, along with Gimenez's *N*Et monomer, displayed little to no change in $K_{cis/trans}$ with increasing chain length, retaining their strong *trans* influence. This is true across all three solvents. Compound **97** was chosen for the study as assessment of its bioisosterism found it to be rather similar to the ethyl group and "smaller" than the isopropyl group.[16] This makes **97** sterically bulkier than Gimenez's *N*3fEt group, yet it still displayed similar $K_{cis/trans}$ values to the other non-fluorinated chains, including *N*Et. A slight increase towards the *cis* rotamer was seen in polar solvents but not enough to convince that steric effects are imparting additional control over the amide backbone.

Models **98** – **100** were chosen to evaluate the effect of moving the CF_3 group further from the backbone relative to Gimenez's *N*3fEt monomer. All three displayed increased *cis* preference relative to their non-fluorinated counterparts even in non-polar $CDCl_3$, perhaps implying the CF_3 group is enhancing the lipophilicity of the alkyl chain. Moving from two CH_2 spacers in **58** to four CH_2 spacers in **100**, $K_{cis/trans}$ decreased linearly in all solvents as predicted, due to an increased distance between the carbonyl oxygen lone pair and electrophilic carbon adjacent to CF_3. $\Delta G_{cis/trans}$ showed the greatest increase in non-polar $CDCl_3$, further confirming an electronic *cis* inducing effect to be at play. Interestingly, an out of trend shift in *cis* preference was observed in $CDCl_3$ moving from *N*3fEt to *N*3fPro. $\Delta G_{cis/trans}$ was lower in **98**, which has been attributed to a reduction in the overall dipole moment of the model, shown in **Figure**

2.13. Model **98**'s $K_{cis/trans}$ values closely match the widely used, α-helix inducing *N*pe monomer, differing by -0.09 kcal/mol ($CDCl_3$), -0.03 kcal/mol (CD_3OD) and +0.01 kcal/mol (CD_3CN).[7] Though less *cis* inducing than the *N*3fEt sidechain in polar solvents, the additional CH_2 spacer makes the corresponding 3,3,3-trifluoropropylamine less deactivated, leading to shorter coupling steps in the submonomer synthesis of oligomers.

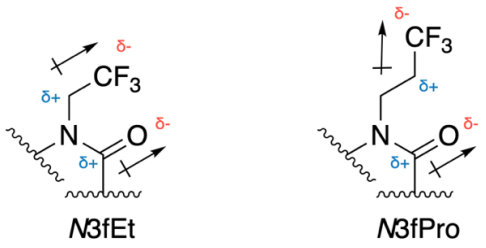

Figure 2.13: Depiction of the relative overall dipole moments conferred in the *N*3fEt and *N*3fPro monomers.

Next, we sought to find fluoroalkyl monomers capable of increasing $K_{cis/trans}$ relative to Gimenez's *N*3fEt sidechain. We postulated this could be accomplished by incorporating more fluorine atoms into the alkyl chain. This hypothesis was first tested by modifying monomers **98** and **99**, substituting the CH_2 adjacent to the terminal trifluoromethyl group with CF_2. $K_{cis/trans}$ was calculated as 0.65 and 0.95 in $CDCl_3$ for models **98** and **99** respectively. This greater *cis* preference arising from an additional CH_2 spacer can again in part be attributed to the overall dipole moment of the model system being reduced, as was the case for *N*3fEt and *N*3fPro.

When dissolved in acetonitrile, $K_{cis/trans}$ = 4.01 and 2.17 values were found with respect to *N*5fPro (**101**) and *N*5fBu (**102**). Mirroring previous observations, **102** was relatively less *cis* inducing than **101** owing the greater distance over which the electronic interaction occurs. However, quite unprecedented was the $K_{cis/trans}$ value of 4.01 for *N*5fPro. Although not substantially out of error, this monomer exceeds reported values for fluorinated aromatic sidechains N^{4f}pym (**105**) and *N*fe (**106**) (**Figure 2.14**).

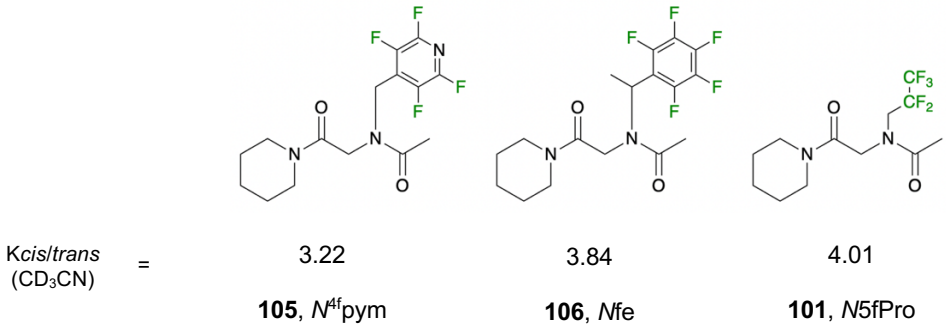

Figure 2.14: Comparison of $K_{cis/trans}$ in CD_3CN of monomer **101** with fluorinated, aromatic monomers from literature. Value for N^{4f}pym taken from Gimenez et al. 2019[17] and value for *N*fe taken from Blackewell et al. 2009.[7]

Despite success in controlling the amide isomerization in CD_3CN, the $K_{cis/trans}$ of **101** was 54% and 59% less in $CDCl_3$ than literature monomers N^{4f}pym and *N*fe respectively.[7,17] It could be inferred that **101** is less lipophilic than these established monomers, perhaps due to its relatively large overall dipole. Additionally, aromatic fluorination is already well established as a tool to increase the lipophilicity of a molecule, where fluorinated alkyl groups have less predictable effects.

Fuelled by our success in promoting the *cis* geometry, we next explored the consequences of appending another trifluoromethyl group to the electrophilic carbon, in order to further promote the electronic interactions with oxygen. We were pleased to discover that *N*6f^{t}Bu (**103**) imparted great preference towards the *cis* isomer, giving the largest values of $K_{cis/trans}$ in each solvent for all our models. A $K_{cis/trans}$ of 6.22 in acetonitrile is one of the highest reported for an uncharged sidechain, falling just short of *N*s1npe (**9**) at 6.27. This is quite extraordinary given **103** is neither chiral nor aromatic. This ranking purposely does not encompass the bulky *tert*-butyl (**18**) or *N*cα-*gem*-dimethylated (**83** – **87**) sidechains which almost exclusively populate the *cis* conformation, as these are incompatible with solid phase synthesis, restricting their applications.

Despite being almost isoenergetic in CD_3CN, **103** has a $K_{cis/trans}$ 24% greater in $CDCl_3$ than *N*s1npe (**9**) (**Figure 2.15**). Further, *N*s1npe shows a 41% increase in $K_{cis/trans}$ in CD_3OD relative to **103.**[18] These two observations combined imply **103** is more lipophilic than this literature monomer.

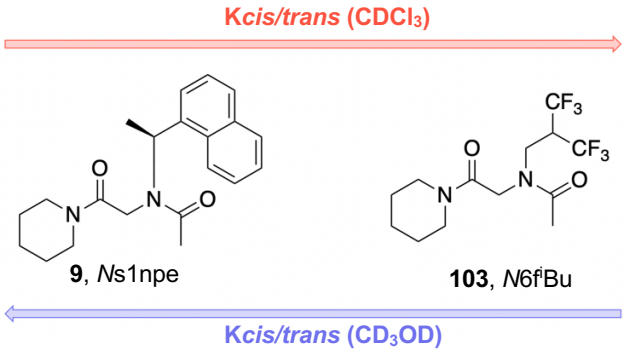

Figure 2.15: Depiction of the solvent influences on $K_{cis/trans}$ for the **9** compared to **103**.

Unlike *N*3fEt and **98** or **101** and **102**, addition of a CH_2 spacer going from **103** to **104** saw a drop in $K_{cis/trans}$ in $CDCl_3$ as well as the two polar solvents. We theorize that this may not be heavily attributable to the overall dipole of the molecule as with previous observations. These branched monomers differ in that our monomer with fluorinated carbons most proximal to the peptoid backbone (**103**) is already distanced from the amide nitrogen by two other carbon

atoms as opposed to one. Our dipole explanation only holds true on going from one carbon spacer to two, after which $K_{cis/trans}$ reduces in all three solvents (**Figure 2.16**). For example, you might expect *N*3fAmyl (**100**) to show an increased $K_{cis/trans}$ in $CDCl_3$ relative to *N*3fBu (**99**), as the progression in dipolar moment is like that shown in **Figure 2.13**. Of course, this does not occur as our model systems are not planar.

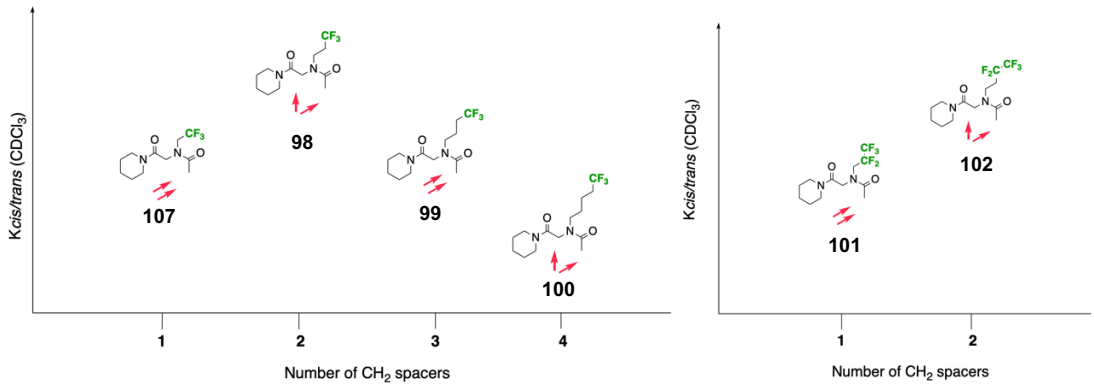

Figure 2.16: Graphs showing predicted relative dipole orientations of C=O and CH_2-CF_X (red arrows) displaying an increase in $K_{cis/trans}$ ($CDCl_3$) only from one to two CH_2 spacers in fluorinated model peptoid systems.

It is therefore reasonable to suggest that an isopropyl-like derivative of our branched monomers (**Figure 2.17**) would show a lower $K_{cis/trans}$ in $CDCl_3$ than *N*6f^{i}Bu (**103**) but an increased $K_{cis/trans}$ in both CD_3OD and CD_3CN. However, similar to *N*-aryl sidechains, the presence of such an electronegative group with relatively less conformational flexibility than *N*3fEt could repel the amide oxygen, promoting a *trans* preference. This would require further investigation. Regardless, monomer **104** still displays increased influence over the backbone equilibrium relative to Gimenez's *N*3fEt sidechain in all solvents studied. This is impressive given its structural similarity to *N*3fBu, showing how powerful the addition of another CF_3 group is at influencing this isomerization.

Figure 2.17: Possible electronic interactions that could occur in an *N*6f^{i}Pro model peptoid either favouring the *cis* or *trans* conformation.

2.2.3 Single Crystal X-Ray Studies

In an effort to further ratify our proposed mechanisms of *cis*-induction, further structural data was acquired by crystallisation of our fluorinated compounds. Models were dissolved in a

minimal amount of ethyl acetate, dichloromethane or chloroform to form a saturated solution. Hexane was then added dropwise until the model precipitated, then the solution re-cleared with minimal polar solvent and finally left for slow evaporation. Diffraction quality crystals were obtained for models **98** and **100** – **103**, which were then analysed by single crystal X-ray crystallography. All determined structures are given in **Figure 2.18**, with torsional angles listed in **Table 2.4**.

Unfortunately, no crystal growth could be induced for model peptoids **99** and **104**. Though unsure of the effects limiting the ability of **99** to crystalise, **104** yielded the smallest amount of material of all the models synthesised. This is perhaps a contributing factor preventing the formation of the supersaturated solution needed for crystal growth.

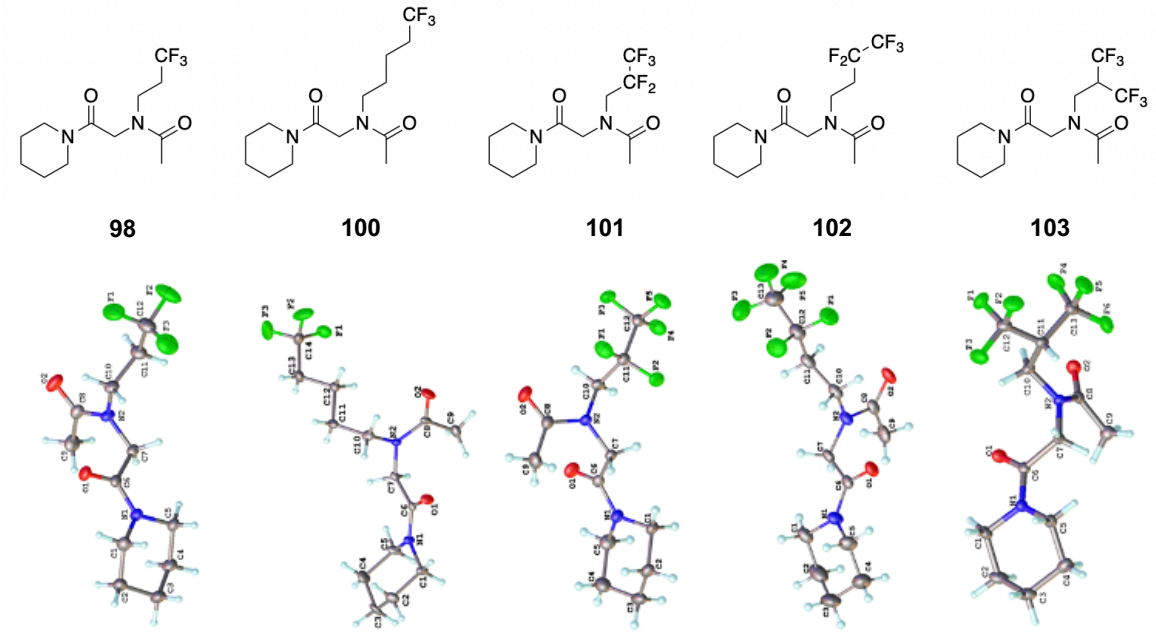

Figure 2.18: X-ray crystal structures of model peptoids **98** and **100** – **103** shown as ball and stick representations. Colour code: carbon atoms in grey, nitrogen atoms in blue, oxygen atoms in red, hydrogen atoms in white and fluorine atoms in green. All structures were generated with Olex2 software[19]. Crystal structures are reported with a 50% thermal ellipsoid probability.

Reinforcing the *cis* directing nature of our novel fluorinated monomers, all models gave dihedral angles within the region of an idealized *cis* peptoid conformation (ω = 0°, ψ = 180°, ϕ = 90°).[20,21] The independent part of model **98**'s unit cell revealed two unique structures. Seen in **Table 2.4** these are nearly identical, as shown in their overlayed structures in **Figure 2.19**. The χ_1 angles of each model show the fluorinated sidechains to be sitting orthogonal to the peptoid backbone, also observed in the crystal structures of Gimenez's fluoroalkyl models.[12] We hypothesise this arrangement minimises electronic repulsion between the fluorine groups and the amide nitrogen. Further, this orientation leaves the amide oxygen and *N*Cα eclipsed

as seen in the C10-N2-C8-O2 torsional angles (**Table 2.4**), which allows for the favourable inductive interaction to occur. Notably, this structural analysis gave no convincing evidence that any steric clashes were occurring to influence the *cis* conformation.

Table 2.4: Torsional angles of model peptoids **98** and **100** – **103** in their solid state from X-ray crystallography

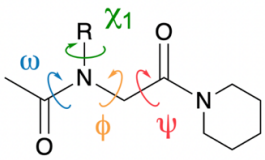

Model Peptoid	ω C7-N2-C8-C9	ψ N1-C6-C7-N2	ϕ C8-N2-C7-C6	χ1 C7-N2-C10-C11	C10-N2-C8-O2
98[a]	-7.42 (15) / 3.09 (15)	-179.71 (8) / -176.96 (8)	-90.08 (11) / 101.35 (11)	98.05 (11) / -96.94 (11)	5.13 (15) / -0.15 (15)
100	9.0 (4)	173.4 (2)	82.9 (3)	-80.1 (3)	-6.3 (4)
101	13.5 (2)	-174.42 (13)	72.70 (18)	-91.35 (16)	-5.2 (2)
102	5.7 (4)	-176.4 (2)	98.1 (3)	-104.2 (3)	0.5 (4)
103	-12.0 (2)	176.58 (13)	-83.72 (17)	81.13 (17)	4.4 (2)

[a] Values given for each individual structure in the unit cell.

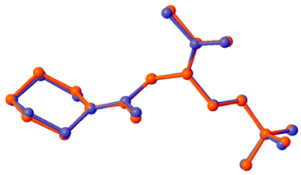

Figure 2.19: Overlayed structures of the two nearly identical independent structures in the unit cell of model peptoid **98**. Crystal structures are reported with a 50% thermal ellipsoid probability.

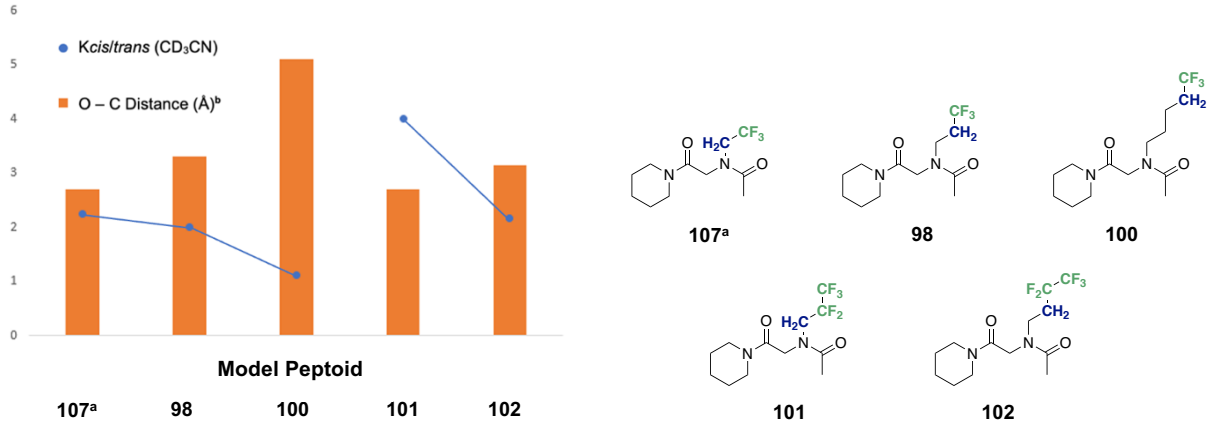

[a]Crystal structure information obtained by D. Gimenez
[b]O – C distance reported for **98** taken as the average between the two individual structures found in the cell

Figure 2.20: Plot of through space distance between the carbonyl oxygen and sidechain carbon (blue) responsible for the inductive interaction in model peptoid systems, calculated using Olex2 software, as well as experimentally determined K*cis*/*trans* values in CD_3CN.

Using Olex2 software, the distance through space between the carbonyl oxygen and electron deficient sidechain carbon was calculated for the models. This shows $K_{cis/trans}$ (CD_3CN) to

reduce linearly with increased distance of C(δ+) from the peptoid backbone, in perfect agreement with our proposed inductive effect mechanism (**Figure 2.20**).

2.2.4 Log P Lipophilicity Studies

Aforementioned in **Section 2.2.2**, $K_{cis/trans}$ NMR studies gave unpredicted, out of trend observations for some models in the non-polar solvent chloroform. Expecting the *cis* influence to diminish linearly, models **98** (3fPro) and **102** (5fBu) instead show increased values in $CDCl_3$ relative to a model peptoid of *N*3fEt and **101** respectively. Shown in **Figure 2.13**, the overall dipole moment of the molecule gives rise to this effect. Knowing **98** and **102** to be more favoured in non-polar solvents, it was also hypothesized that modulation of sidechains individual dipole moment could affect the lipophilicity of the peptoid.

Compounds **98**, **99**, **101** and a model peptoid with the *N*3fEt sidechain (**108**) (**Figure 2.21**) were partitioned between layers of octan-1-ol and water, alongside 2,2,2-trifluoroethanol (TFE) as a reference, to experimentally determine their log *P* values. Using an established ^{19}F-NMR protocol developed by Linclau et al.,[22,23] the peaks arising from the *cis* and *trans* rotamers were integrated relative to the reference compound TFE with known log *P* (+0.36)[23] (**Figure 2.22**). Two spectra were recorded for each partitioned layer.

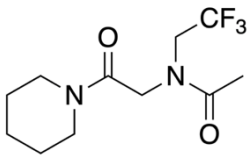

108, 13.7%

Figure 2.21: Structure of the model peptoid **108** containing the *N*3fEt sidechain used in the log *P* study.

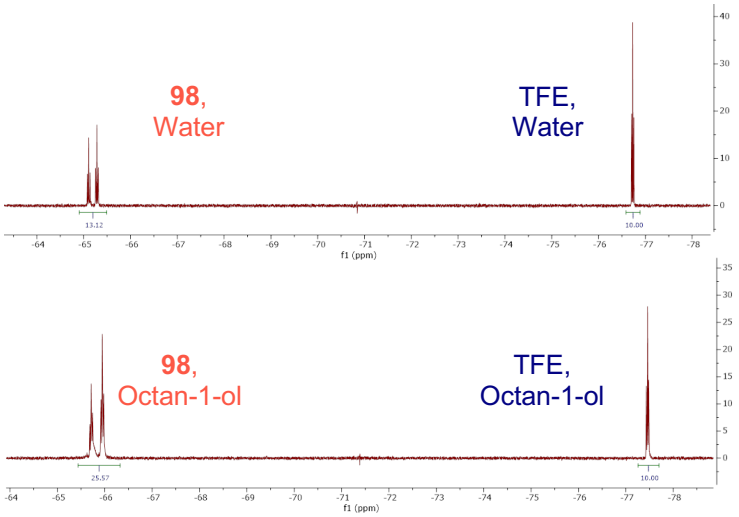

Figure 2.22: ^{19}F-NMR experiment used to determine the log *P* value of model peptoid **98**.

The Log P of the model was subsequently calculated using **Equation 2.1**, the results of which can be seen in **Table 2.5** alongside standard deviation.

$$Log\ P^{x} = Log\ P^{ref} + Log^{p(oct)}/_{p(aq)}$$

Equation 2.1

Table 2.5: Experimentally determined values of log *P* for models **108**, **98**, **99** and **101**.

Model	Sidechain	Model Peptoid Integrated Area Relative to TFE Reference Peak (^{19}F-NMR)				Log *P*
		Water (1)	Water (2)	Octan-1-ol (1)	Octan-1-ol (2)	
108	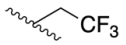	23.78	24.32	33.45	33.02	0.500 ± 0.011
98	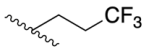	13.12	12.99	25.57	25.55	0.652 ± 0.003
99	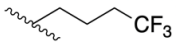	4.84	5.03	10.94	11.55	0.718 ± 0.005
101	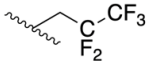	11.23	11.10	58.29	57.28	1.074 ± 0.002

The lipophilicity of the models is a composite average of each individual rotamer. Though literature methodology has been published for the log *p* determination of each conformation,[23] this study aimed to review the overall effects of the sidechains. It must be noted that changes in log *P* are also attributable to the increased presence of hydrophobic CH_2 residues, as well as the influence of dipolar moments.

Interestingly, though a decrease in log *P* is not observed going from model **98** to **99** the increase was 57% less pronounced than that going from **108** to **98**. It would be expected for log *P* to increase linearly with the addition of a further CH_2 spacer, though these observations indicate another force to be at play. This is consistent with the hypothesis based on the observations of $K_{cis/trans}$ in $CDCl_3$, in which a reduced overall dipolar moment increases the lipophilicity of the sidechain. Though extension of the carbon chain seems to ensure an increase in log *P*, these results suggest that modulation of the spatial orientation of the trifluoromethyl group can significantly influence lipophilicity.

Further, the effect of increasing the fluorine content of the sidechain was evaluated under the assumption that log *P* would also increase. Model peptoid **101** is identical in structure to **98** bar the substitution of a CH_2 for CF_2. ^{19}F-NMR experiments showed **101** to be 1.65 times more lipophilic than **98**, evidencing the incorporation of fluorine to be a useful tool in influencing the intrinsic properties of a peptoid. As an increased fluorine content has also already been shown

to increase $K_{cis/trans}$, it can be deduced that the driving force in these observed log *P* values is the greater propensity of the sidechain to draw electron density from the carbonyl oxygen, reducing its capacity to interact with water molecules in hydrogen bonding interactions.

2.3 Chapter 2 Summary and Key Findings

Model peptoids offer insight into the structural properties induced by a particular sidechain. Moreover, being widely reported in literature allows for the direct comparison of such effects from various studies. A novel route to synthesising model peptoids **100**, **103** and **104** was developed using haloalkanes as opposed to primary amines (**Scheme 2.3**). This has proved relatively inexpensive in comparison to the literature synthesis, potentially allowing for greater numbers of monomers to be evaluated at a significantly reduced cost.

The 'toolbox' of peptoid monomers requires expansion, with alkyl groups being relatively underdeveloped in comparison to aromatic sidechains. Bulky *tert*-butyl type groups suffer from an inability to be coupled via solid phase methods, drastically reducing their scope in the synthesis of peptoid oligomers. Charged ammonium type monomers offer excellent jurisdiction over the *cis*/*trans* isomerization, being an ideal choice as a hydrophilic component in the design of facially amphipathic peptoids: an extremely important element to ensure antimicrobial activity.

Gimenez first published fluoroalkyl sidechains capable of exuding a *cis* preference.[12] In this chapter, this structural effect has been explored further to understand the relationship between fluorine and $K_{cis/trans}$. The inductive effect of fluorine has been further ratified by increasing the distance of CF_3 from the peptoid backbone, predictably reducing the sidechains capacity to promote the *cis* orientation. Interestingly, solvent studies unveiled a relationship between the orientation of the C-CF_3 dipole and the peptoids ability to orientate itself in non-polar solvents (**Table 2.3**). This effect was further scrutinized in log *P* studies (**Table 2.5**), which found the lipophilicity of the model to not only increase with further CH_2 residues but to also be dependent on the relative overall dipolar moment of the system.

By increasing the presence of fluorine in the sidechain, novel peptoid monomers have been developed with $K_{cis/trans}$ values exceeding those of published aromatic moieties also possessing chiral centres. This is quite unprecedented given their aliphatic nature. Models **101** and **103** (*N*5fPro and *N*6f^{i}Bu respectively) gave the largest $K_{cis/trans}$ values in this study,

being some of the highest amongst uncharged sidechains in literature, whilst still being compatible with solid phase synthesis. Further, the substitution of CH_2 for CF_2 increased the log *P* value of the model peptoid system by 65% (**Table 2.5**). Not only are these fluorinated sidechains capable of pre-organizing the structural environment of the peptoid, but they also provide an excellent choice in the selection of a hydrophobic component for peptoid oligomers.

2.4 References

1) C. W. Wu, T. J. Sanborn, K. Huang, R. N. Zuckermann and A. E. Barron, *J Am Chem Soc*, 2001, **123**, 6778–6784.
2) O. Roy, G. Dumonteil, S. Faure, L. Jouffret, A. Kriznik and C. Taillefumier, *J Am Chem Soc*, 2017, **139**, 13533–13540.
3) K. Kirshenbaum, A. E. Barron, R. A. Goldsmith, P. Armand, E. K. Bradley, K. T. v. Truong, K. A. Dill, F. E. Cohen and R. N. Zuckermann, *Proc. Natl. Acad. Sci.*, 1998, **95**, 4303–4308.
4) P. Armand, K. Kirshenbaum, A. Falicov, R. L. Dunbrack, K. A. Dill, R. N. Zuckermann and F. E. Cohen, *Fold Des*, 1997, **2**, 369–375.
5) N. H. Shah, G. L. Butterfoss, K. Nguyen, B. Yoo, R. Bonneau, D. L. Rabenstein and K. Kirshenbaum, *J Am Chem Soc*, 2008, **130**, 16622–16632.
6) Q. Sui, D. Borchardt and D. L. Rabenstein, *J Am Chem Soc*, 2007, **129**, 12042–12048.
7) B. C. Gorske, J. R. Stringer, B. L. Bastian, S. A. Fowler and H. E. Blackwell, *J Am Chem Soc*, 2009, **131**, 16555–16567.
8) B. C. Gorske, B. L. Bastian, G. D. Geske and H. E. Blackwell, *J Am Chem Soc*, 2007, **129**, 8928–8929.
9) O. Roy, C. Caumes, Y. Esvan, C. Didierjean, S. Faure and C. Taillefumier, *Org Lett*, 2013, **15**, 2246–2249.
10) R. Shyam, L. Nauton, G. Angelici, O. Roy, C. Taillefumier and S. Faure, *Biopolymers*, 2019, **110** (6), e23273
11) A. W. Wijaya, A. I. Nguyen, L. T. Roe, G. L. Butterfoss, R. K. Spencer, N. K. Li and R. N. Zuckermann, *J Am Chem Soc*, 2019, **141**, 19436–19447.
12) D. Gimenez, J. A. Aguilar, E. H. C. Bromley and S. L. Cobb, *Angew. Chem. Int. Ed.*, 2018, **57**, 10549–10553.
13) F. Wen and Z. Li, *Synth Commun*, 2020, **50**, 3462–3474.
14) K.-J. Liu and J. E. Anderson, *Macromolecules*, 1970, **3**, 163–164.
15) J. R. Stringer, J. A. Crapster, I. A. Guzei and H. E. Blackwell, *J Am Chem Soc*, 2011, **133**, 15559–15567.
16) M. Jagodzinska, F. Huguenot, G. Candiani and M. Zanda, *ChemMedChem*, 2009, **4**, 49–51.
17) D. Gimenez, G. Zhou, M. F. D. Hurley, J. A. Aguilar, V. A. Voelz and S. L. Cobb, *J Am Chem Soc*, 2019, **141**, 3430–3434.
18) D. Kalita, B. Sahariah, S. Pravo Mookerjee and B. Kanta Sarma, *Chem Asian J*, 2022, **17** (11), e202200149.
19) O. v. Dolomanov, L. J. Bourhis, R. J. Gildea, J. A. K. Howard and H. Puschmann, *J Appl Crystallogr*, 2009, **42**, 339–341.
20) S. H. Park and I. Szleifer, *J Phys Chem B*, 2011, **115**, 10967–10975.
21) R. K. Spencer, G. L. Butterfoss, J. R. Edison, J. R. Eastwood, S. Whitelam, K. Kirshenbaum and R. N. Zuckermann, *Biopolymers*, 2019, **110** (6), e23266.
22) Z. Wang, B. F. Jeffries, H. R. Felstead, N. J. Wells, E. Chiarparin and B. Linclau, *J. Vis. Exp.*, 2019.
23) B. Linclau, Z. Wang, B. Jeffries, J. Graton, R. J. Carbajo, D. Sinnaeve, J. le Questel, J. S. Scott and E. Chiarparin, *Angew. Chem. Int. Ed.*, 2021, **61** (7), e202114862.

Chapter 3: Self-Assembling Peptoid Helices with Novel Fluorinated Monomers

3.1 Introduction

3.1.1 Solid Phase Peptoid Synthesis

Peptoids benefit from a simple "submonomer" synthesis (**Scheme 3.1**), coined by Zuckermann in 1992, with some reported oligomer yields exceeding 90%.[1] Oligomers grow on a solid-phase support as alternating condensation copolymers between two submonomers: bromoacetic acid and a primary amine. The synthesis is fast, efficient, and diverse owing the commercial availability of a wide range of amines. There is no need for backbone protecting groups, as is the case with peptides, and the process can be fully automated.[2,3]

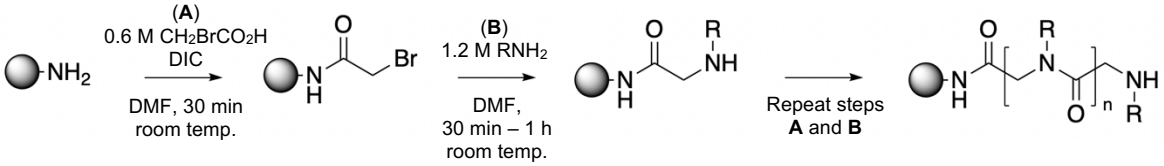

Scheme 3.1: General solid phase synthesis of peptoid oligomers via the submonomer method.[1]

Olivos and co-workers demonstrated that microwave irradiation accelerates both steps of the submonomer process such that reaction times of as little as 1 minute can be used, with yields and purity matching or exceeding standard techniques.[4] Microwave assistance has been shown to aid a 'monomer' strategy of *N*-(triethylene glycol)glycine synthesis, in which the conventional submonomer approach is not suitable.[5] Further, Rasmussen and co-workers demonstrated the synthesis of an arylopeptoid nonamer (**109**), shown in **Figure 3.1**, with challenging sidechains could be completed in less than half the reaction time previously required when the sequence was constructed at room temperature.[6]

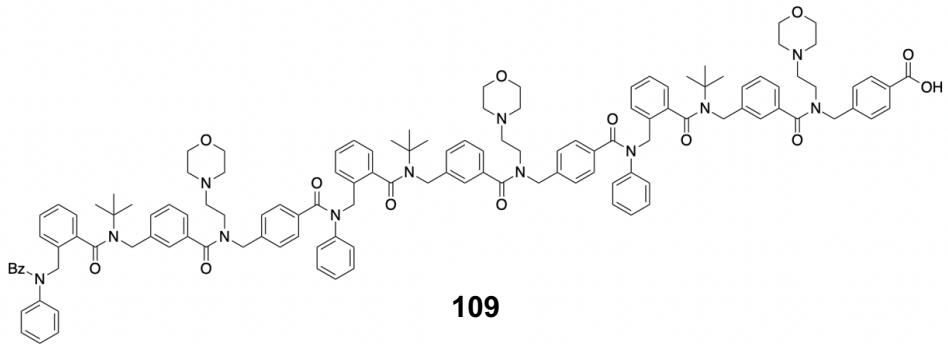

109

Figure 3.1: Arylopeptoid synthesised by Rasmussen et al[6] under accelerated microwave conditions.

More recently, Zuckermann and co-workers reported a revised submonomer process to aid in the incorporation of weakly nucleophilic amines (**Scheme 3.2**). The S_N2 displacement of bromine can take up to 16 hours for *N*-aryl substituents,[7] with shorter times prompting poorer yields. Addition of silver perchlorate ($AgClO_4$) to the displacement complexes bromine, increasing electrophilicity at the alpha carbon. Additionally driven by the formation of an extremely stable leaving group (AgBr), reaction times were shortened by up to 76-fold,[7] offering an improved synthesis for any submonomer amine with diminished nucleophilicity (e.g., anilines).

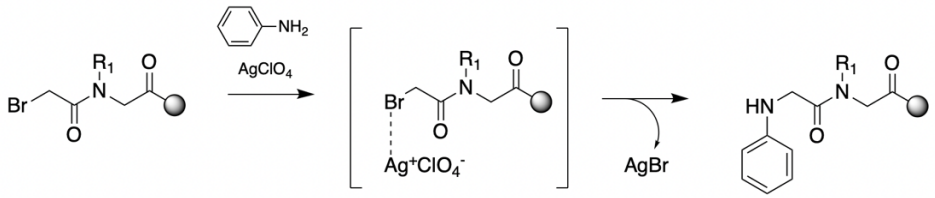

Scheme 3.2: Accelerated synthesis of peptoids using silver perchlorate.

3.1.2 Circular Dichroism for Peptoid Structural Analysis

Circular dichroism (CD) is a valuable phenomenon which can be exploited to unveil the structural properties of biomolecules in solution. Such systems are comprised of optically active chiral subunits which interact with left and right-handed circularly polarized light to different extents.

Peptoid studies can take advantage of CD to probe their secondary structures, as amide bonds are the main chromophore in the far-UV region. **Figure 3.2** depicts the electronic transitions responsible for the molecular orbitals in an amide moiety. The conformation adopted by a molecule affects these transitions, altering the shape and intensity of the CD spectra.[8] **Figure 3.3** shows typical traces associated with different secondary structures in solution.

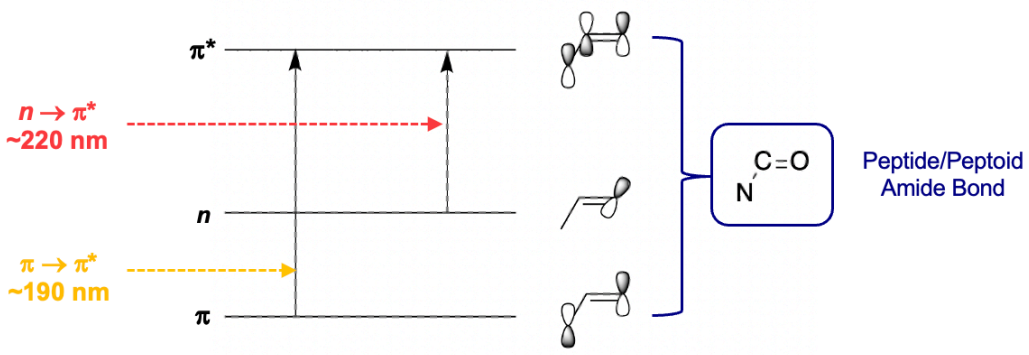

Figure 3.2: Electronic transitions occurring in the far-UV region allowing for characterization of peptides and peptoids by circular dichroism.

CD spectroscopy has several advantages over other conformational analysis techniques. Unlike X-ray crystallography, samples can be analysed in solution. This circumvents the need to crystalise products, which can be extremely difficult for extended peptoid sequences. NMR spectroscopy has previously been established in assigning the structures of peptides, particularly by identification of the amide proton peaks.[9] This not possible for peptoids due to their tertiary amide structure, making CD spectroscopy an excellent alternative. CD also requires very little sample to accrue good spectra due to its high levels of sensitivity. Circular dichroism has found applications in thermal denaturization assays,[10] the study of protein-ligand interactions,[11] the study of conformational transitions,[12] the formation of conformational intermediates,[13] kinetic interrogation[14] and the interaction of proteins with cell membranes.[15]

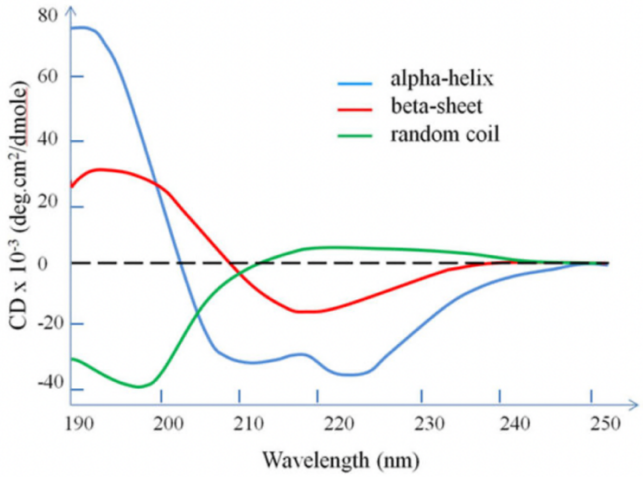

Figure 3.3: Typical CD traces associated with different secondary structures in solution. Figure taken from Y.Wei et al., 2014.[16]

One of the major limitations of CD spectroscopy, and consequently the main source of error, is accurately recording sample concentration prior to analysis. Calculating the degree of helicity from a CD spectrum requires the true concentration of the sample to be known before allowing comparison with other samples. Often, peptides and peptoids are synthesised on a milligram scale which makes weighing out product, even on a microbalance, inaccurate enough to bring error to CD measurements. In addition, cleaving oligomers from resin under acidic conditions often leaves TFA counter-ions with charged residues, such as *N*Lys, again making the weighed-measurement inaccurate.

3.1.3 Chapter 3 Objectives

Inspired by the success of the novel sidechains synthesised in **Chapter 2** to impart a localised *cis* isomer preference, the ability of these monomers to form defined, extended sequences in solution was to be evaluated. Owing to fluorine's electron withdrawing properties, adaptations to standard submonomer protocols may be required to incorporate the weakly nucleophilic amines. CD spectroscopy offers a valuable tool to measure the form of folding adopted by these peptoids, which would either confirm or reject the *cis* inducing properties discovered through the model systems reported in **Chapter 2**. The three main objectives of this chapter are:

- To create a library of oligomers using the peptoid monomers studied under **Chapter 2**, employing the submonomer approach.

- To use HPLC retention times as an indication of fluorine's effect on lipophilicity.

- To study these peptoids by CD in order to evaluate the secondary structure adopted by these molecules in solution.

3.2 Results and Discussion

3.2.1 Design and Synthesis of Peptoid Oligomers

To allow for comparison with previously documented fluoroalkyl sidechains, oligomers were synthesised based on the scaffold utilised and reported by Gimenez et al.[17] (**Figure 3.4**). The peptoid is a 15-mer, with three residues per turn in a facially amphipathic sequence. Due to the achiral nature of the integrated sidechains, one *N*spe residue is specifically incorporated two residues from the *N*-terminus. In line with studies by Shin et al.,[18] this placement is sufficient to 'lock' the helicity of the peptoid, allowing it to be interrogated via CD spectroscopy.

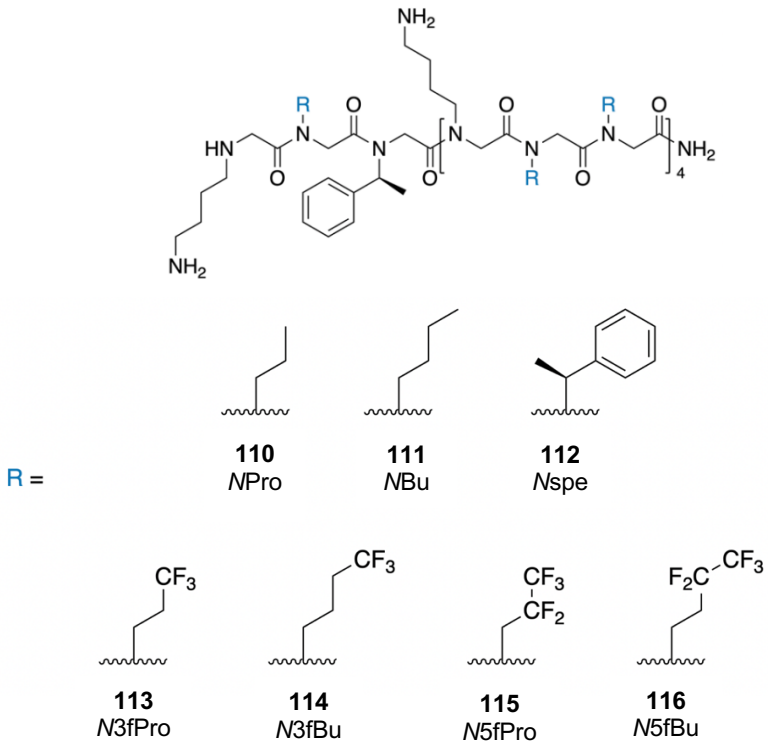

Figure 3.4: General 15-mer scaffold employed in this chapter alongside the sidechains used to create the peptoid library.

Non-fluorinated peptoids **110** and **111** were chosen for direct structural scrutinization with their fluorinated counterparts. The well-reported *N*spe residue in peptoid **112** was incorporated to act as a reference oligomer, as sequences reported in literature have already been shown to exhibit a helical spectrum.[19] Additionally, non-fluorinated sidechains were chosen to compare HPLC retention times with peptoids **113 - 116**, as a preliminary indication of fluorine's influence on hydrophobicity.

All peptoids were synthesised using the well-established submonomer method.[17,20] Peptoids **110 - 112** were synthesised at room temperature, incorporating sidechains as primary amines in a bromine displacement step 45 minutes long. This same strategy was applied to fluorinated peptoid **113**; however, the crude yield was significantly reduced relative to the non-fluorinated (e.g., 116% vs 50% for peptoids **112** and **113** respectively). The crude HPLC traces for these peptoids can be seen in **Figure 3.5**. The electron-withdrawing nature of fluorine deactivates the primary amine, diminishing its ability to act as a nucleophile in the S_N2 displacement of bromine.

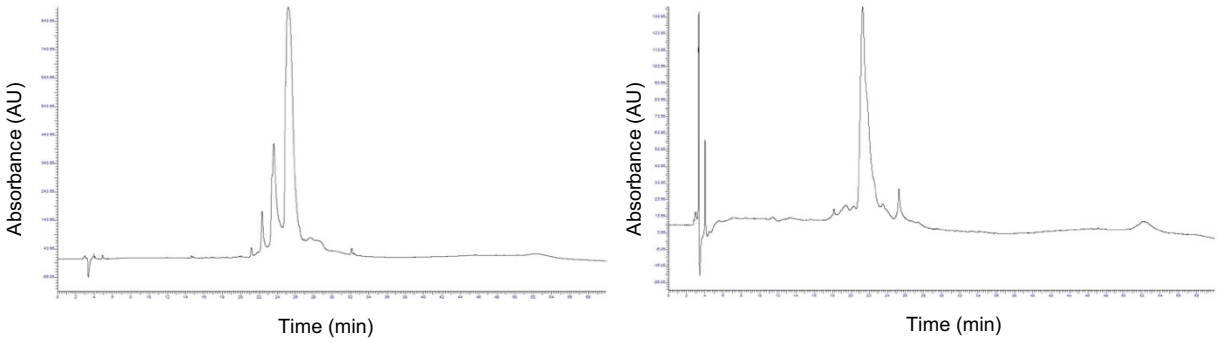

Figure 3.5: Crude HPLC traces of peptoids **112** (left) and **113** (right).

In order to synthesize the other fluorinated peptoids **114** – **116**, without drastically increasing coupling steps relative to those used for peptoid **113**, silver perchlorate ($AgClO_4$) was added into the displacement step in line with previously documented methods.[7] This was first tested for the most deactivated amine of the study: in oligomer **115**. Using 5 molar equivalents of $AgClO_4$ and a coupling time of 45 minutes, a test cleave of the resin did not show the desired mass in LCMS. Further, the associated UV trace was crowded with peaks of multiple different *m/z* values, far more impure than test cleaves performed in the synthesis of non-fluorinated peptoids **110 - 112**.

Next, microwave irradiation was utilised in an attempt to reduce the length of the bromine displacement step. Following the bromoacetylation, the resin was washed and drained before being transferred into a 5 mL microwave vial. Excess DMF was employed to transfer the resin, which was then removed from the microwave vial using a clean syringe. The weakly nucleophilic 4,4,4-trifluorobutylamine (used to make peptoid **114**) was added at standard concentrations and the resin stirred at 80 °C for just 15 minutes. Gratifyingly, test cleaves confirmed the chain to be growing as expected. Microwave irradiation was subsequently employed in the synthesis of model peptoids **114** - **116**, for all bromine displacement steps using a fluorinated amine. *N*Lys and *N*spe were still coupled under regular procedures as though great care was taken during transfer of the resin between the microwave vial and reaction cartridge, some resin was lost.

Once synthesised, the peptoids were isolated from the resin using a cleavage cocktail primarily composed of trifluoracetic acid (TFA/H_2O/TIPS 95:2.5:2.5 v/v/v). Boc-protected amine **117** (**Figure 3.6**) was utilised to incorporate *N*Lys residues into the chain, which was subsequently deprotected in tandem with peptoid cleavage from the resin under acidic conditions.

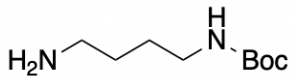

117

Figure 3.6: Chemical structure of *N*-Boc-1,4-butanediamine used to incorporate *N*Lys monomers into peptoids **110 – 116**.

Disappointingly, the most *cis* inducing sidechain (*N*6f^{i}Bu) could not be incorporated into this library of oligomers as an iodoalkane was used to synthesize model peptoid **103** in **Chapter 2**. A primary amine is an essential requirement for peptoid oligomer synthesis. Two strategies were attempted to form peptoid monomers from iodoalkane **118** (which possesses the 6f^{i}Bu sidechain) capable of being incorporated into oligomers. **Scheme 3.3** outlines these methods but unfortunately neither were successful.

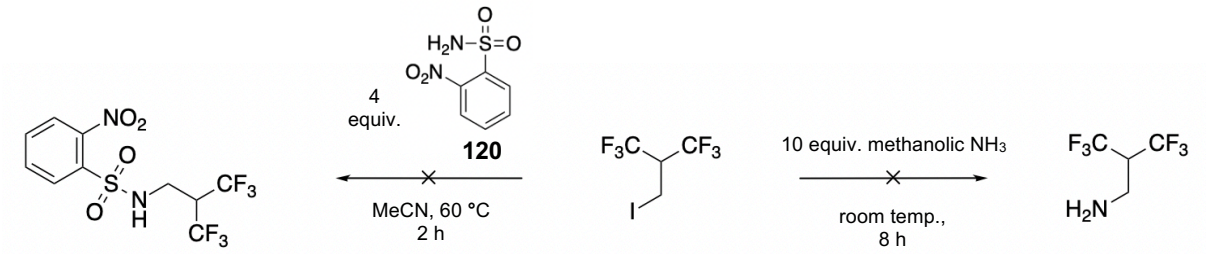

121 **118** **119**

Scheme 3.3: Summary of attempts to incorporate the 6f^{i}Bu sidechain into a monomer building block from iodoalkane **118**.

Firstly, iodoalkane **118** was added dropwise to a large excess of methanolic ammonia in an attempt to convert it to the corresponding primary amine **119** through direct alkylation. The preparation of primary amines by alkylation of ammonia employs such an excess to reduce the formation unwanted secondary and tertiary amine side products. Unfortunately, due to limitations in the size of apparatus, the reaction needed to be carried out on a small scale which, combined with the poor yield of the reaction due to the formation of over-alkylated products, made the prospect of synthesising suitable quantities of **119** for an oligomer arduous. Further, extracting any of the reaction's products from the solution was immensely difficult owing their volatility. The primary amine **119** could not be successfully isolated from the complex mixture of products.

In another effort to make use of iodoalkane **118**, an adaptation of the nosyl protecting group was employed. Similar to the alkylation of **107** in **Scheme 2.3**, 2-nitrobenzenesulfonamide (**120**) in a fourfold excess was heated by microwave irradiation with **118** in an attempt to form a secondary amine submonomer. If successful, **121** would have been added to the growing

chain following bromoacetylation and subsequently deprotected of it's nosyl group using previously published reagents: PhSH and base.[21] However, monitoring of the reaction by LCMS showed no conversion of the starting amine (**120**), even when temperatures of above 60 °C were employed. Therefore, it was decided that it was not worth pursuing the synthesis of **119** further due to time constraints in the laboratory.

3.2.2 Purification and Analysis of Peptoid Oligomers

Once oligomers **110 - 116** were synthesised and cleaved from the resin on which they were grown, they were dissolved in a 50:50 mixture of H_2O:MeCN and lyophilized to give the peptoids as white solids. 100 mg of the crude peptoid was then dissolved in 10 mL of a mixture of 50:50 H_2O:MeCN ready for purification by reverse-phase HPLC. Difficulty was observed in getting fluorinated peptoids **113 - 116** to dissolve, therefore 2 – 3% TFA by volume was added in order to aid dissolution.

Of the library synthesised, the fluorinated peptoids proved the most difficult to purify. As seen in **Figure 3.7**, analytical HPLC traces of the crude fluorine containing oligomers were significantly more impure than the corresponding non-fluorinated, particularly with the presence of small baseline peaks surrounding the product. This outcome is rather predictable, given the diminishment of nucleophilicity upon fluorination of an amine, allowing for the formation of more side-products during submonomer synthesis. All peptoids were subsequently purified and isolated in at least 95% purity, as can be seen in **Table 3.1**.

Table 3.1: Yield, purity and HPLC retention times of peptoids **110** - **116**

Peptoid	Crude Mass (mg)	Yields Following Purification*		Purity (%)	HPLC Retention time (min)
		Mass (mg)	Yield (%)		
110 (*N*Pro)	172	45	26.3	≥95	16.47
111 (*N*Bu)	206	38	20.7	≥95	21.25
112 (*N*spe)	263	10	4.4	≥95	25.38
113 (*N*3fPro)	109	12	5.5	≥95	20.86
114 (*N*3fBu)	175	21	9.0	≥95	23.37
115 (*N*5fPro)	232	6	2.4	≥95	24.91
116 (*N*5fBu)	212	12	4.5	≥98	27.48

*Note only 100 mg of crude peptoid was purified for each compound. Yield is given for the mass of pure peptoid obtained from 100 mg of crude compound.

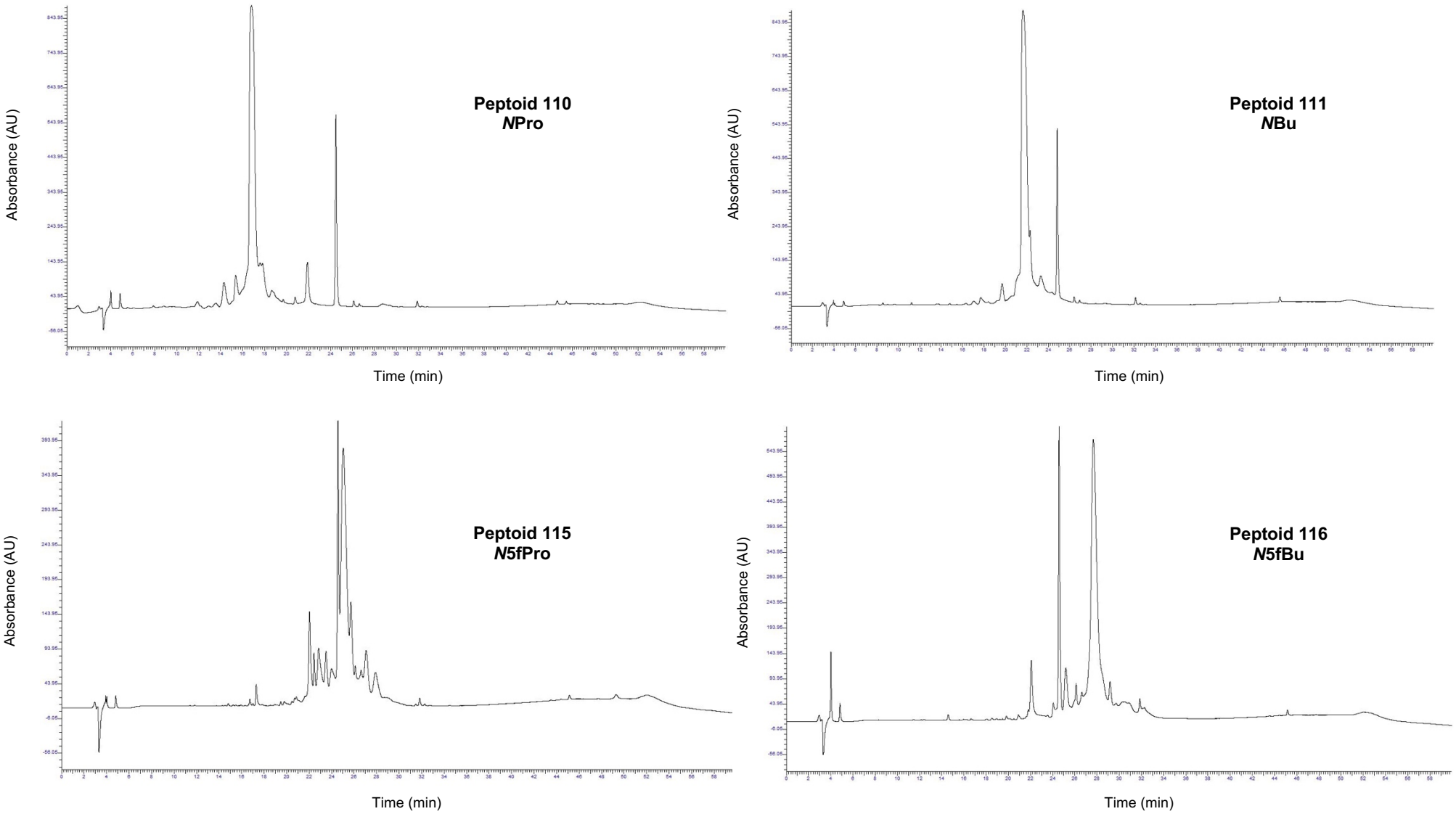

Figure 3.7: Comparison of crude analytical HPLC traces for non-fluorinated (**110** and **111**) and fluorinated peptoid oligomers (**115** and **116**).

Pure yields obtained were by far greatest for the non-fluorinated, aliphatic peptoids **110** (*N*pro) and **111** (*N*Bu). The remaining fluorinated peptoids **112** – **116** all yielded relatively similar amounts of pure product, though **115** was considerably lower. This peptoid contains the *N*5fPro monomer, the most deactivated primary amine utilised in the submonomer strategy.

As with any reverse-phase separation technique, the least polar compounds of the sample will exhibit the longest retention times on the stationary phase. For the peptoids synthesised in this study, this can be used as a rough indication of their hydrophobicity. This comparison of retention times is only a crude measurement, as studies have found discrepancies between peptoid HPLC retention times and experimentally determined log D values.[22] Factors such as the solution phase folding of the oligomers and the presence of ionizable sidechains all contribute to unpredictable differences between retention time and log D.[22]

Nevertheless, peptoid **111** (*N*Bu) predictably gave a longer retention time than **110** (*N*Pro) owing to the presence of an additional hydrophobic CH_2 residue in the alkyl sidechain. Peptoids **110** (*N*Pro), **113** (*N*3fPro) and **115** (*N*5fPro) gave retention times of 16.47, 20.86 and 24.91 minutes respectively. This gradual increase in RT is parallel with the incorporation of more fluorine atoms in the sidechain, suggesting substitution of hydrogen for fluorine increases the hydrophobicity of these compounds. This mirrors the findings in **Section 2.2.4**, in which increased fluorination gave greater log P values for the model piperidinyl systems. This pattern is repeated in peptoids **111** (*N*Bu), **114** (*N*3fBu) and **116** (*N*5fBu), albeit with longer retention times due to the additional CH_2. This observed change also mirrors the general trend for incorporation of fluorine atoms into the side chains of hydrophobic amino acids, which in general is seen to increases their hydrophobicity.[23]

Peptoid **116**, which contains the *N*5fBu monomer, displayed the longest retention time of all the sequences prepared, eluting at 27.48 minutes. Based on the model system log *P* studies of **Chapter 2**, this is unsurprising given that the *N*5fBu monomer contains five fluorine atoms as well as a chain comprised of four carbons. This RT is even greater than that of peptoid **112** which contains the hydrophobic *N*spe residue, perhaps inferring this oligomer is more hydrophobic. With an RT of 24.91 mins, **115** gives a retention almost identical to reference peptoid **112** (*N*spe), differing only by 0.47 minutes. This goes to show that high degrees of hydrophobicity can be efficiently incorporated with fluorine atoms as well as with aromatic sidechains. However, experimental log D studies are required to ratify these crude conclusions.

3.2.3 Preliminary CD Studies

As previously discussed in **Section 3.1.2**, sample concentration is one of the main sources of error in CD spectroscopy. In peptides, the presence of tryptophan or tyrosine residues allows for concentration to be determined relatively easily by UV spectroscopy. Ultraviolet absorbance of the sample is measured at 280 nm, as at this wavelength the molar absorptivity can be predicted directly from the primary sequence.[24] Concentration is then accurately calculated using the Beer-Lambert law. This methodology has also been previously applied to peptoids.[25] Only containing one aromatic residue per chain, the library of oligomers in this study are not UV active enough for accurate concentration determination, this fact was also previously reported by Gimenez et al.[17] They overcame this by correcting the concentration of the peptoid stock solutions by evaluation of their relative TFA content by ^{19}F-NMR spectroscopy. This procedure calls for multiple freeze-thaw cycles in the freeze dryer. Due to time restraints in the laboratory, detailed TFA evaluation was not possible for this project. Hence, these preliminary CD studies cannot quantify the degree of helicity imposed by each of the novel sidechains. Instead, the spectra recorded act as a qualitative indication of the solution state folding of these oligomers.

Stock solutions of 2 mg/mL in water were prepared for each oligomer, and subsequently made to 250 μM by serial dilutions. CD spectra were taken as an average of three consecutive accumulations. Once recorded, the trace from the blank (H_2O) was subtracted and the curve smoothed. The CD spectra for peptoids **110**, **111** and **113** - **116** can be seen in **Figure 3.8**.

All peptoids gave a double minima which is indicative of backbone handedness, confirming the strategic incorporation of a single chiral *N*spe residue to be sufficient in 'locking' the handedness of the oligomer.[18] The sign in which the spectra was generated is consistent with the (*S*)-stereochemistry of the *N*spe monomer, giving traces implicative of a right-handed helix for peptoids **110** – **116.**[26] These minima at ~200 and ~218 nm mirror those produced in Gimenez et al.'s study of non-chiral fluoroalkyl peptoid monomers,[17] confirming these oligomers to fold into defined helical structures in solution.

Compounds **110** and **113** – **116** all displayed a maximum at ~185 nm correlating to the π to π^* electronic transition in the peptoid backbone, while **111** showed no well-defined maximum. This peak is blue-shifted relative to reference peptoid **112** (**Figure 3.9**) which showed a maximum at 190 nm, consistent with literature data of its corresponding 12-mer peptoid **38**.[27]

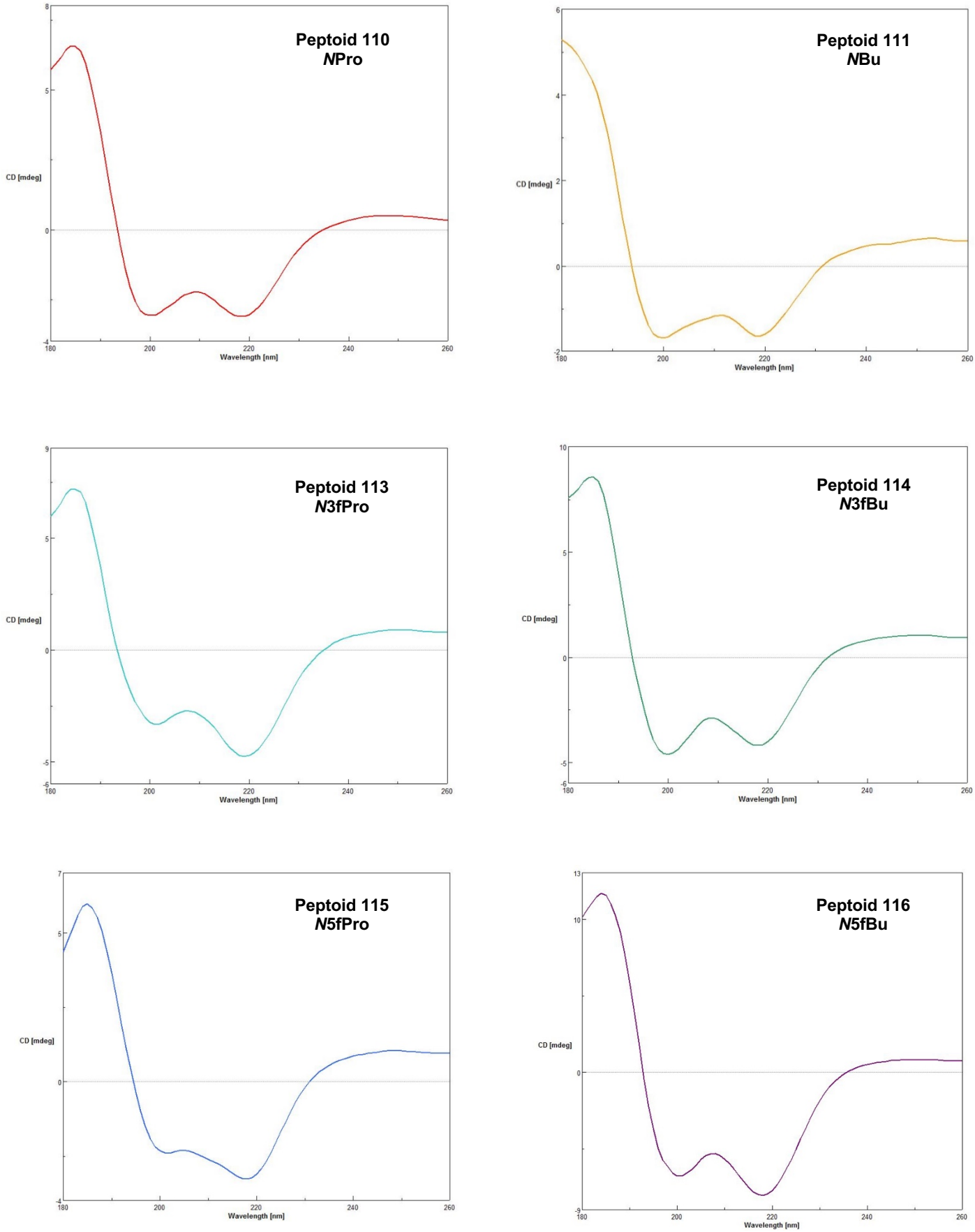

Figure 3.8: Preliminary CD spectra of peptoids **110**, **111** and **113** – **116**. All spectra recorded in H_2O at 20 °C as an average of three sequential accumulations. A blank trace (H_2O) was subtracted from each spectra before it was smoothed with Means-Movement smoothing on Spectral Manager II software (JASCO, UK).

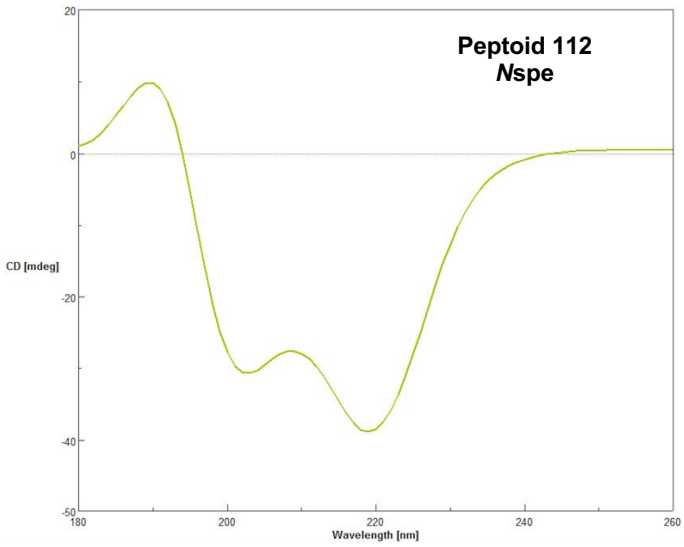

Figure 3.9: Preliminary CD spectra of peptoid **112**. Spectrum recorded in H_2O at 20 °C as an average of three sequential accumulations. A blank trace (H_2O) was subtracted from the spectrum before it was smoothed with Means-Movement smoothing on Spectral Manager II software (JASCO, UK).

Interestingly, the peptoids with non-fluorinated aliphatic chains (**110** and **111**) displayed characteristic minima despite their corresponding model peptoids (**94** and **95** respectively) favouring the *trans* rotamer by two-fold in polar protic solvent MeOD. The relative intensity of the peaks at ~218 nm require quantification by accurate concentration determination to evidence the magnitude of the *cis* directing nature of these novel fluorinated monomers. Still, it is clear by qualitative investigation that these peptoids are adopting an alpha helical secondary structure.

3.3 Chapter 3 Summary and Key Findings

The study of model peptoid systems in **Chapter 2** identified novel monomers with a preference to enforce a *cis* geometry in the amide backbone. These fluorinated motifs proved difficult to incorporate under ambient condition in the submonomer synthesis (**Scheme 3.1**), yet this work has shown them to be sufficiently coupled with assistance from microwave irradiation. The time allowed for the bromine displacement step under these elevated temperatures was in fact halved compared to the synthesis of non-fluorinated peptoids **110** – **112**.

Attempts were made to incorporate iodoalkane **118** into a suitable monomer compatible with submonomer peptoid oligomer synthesis, as its corresponding model peptoid (**103**) gave the highest $K_{cis/trans}$ values of the NMR experiments. Unfortunately, this was unsuccessful (**Scheme 3.3**), leaving scope for future work to analyse the folding conferred by this monomer.

By virtue of their analytical HPLC retention times (**Table 3.1**), conclusions made from the model peptoid log P studies in **Section 2.2.4** were mirrored, indicating an increase in hydrophobicity with an increased fluorine content of the peptoid oligomer.

Though further experiments are required to correct the concentrations of the peptoid stock solutions, this work has successfully incorporated novel fluorinated monomers into extended chains. Preliminary CD studies (**Figures 3.8** and **3.9**) have been used to show these sequences to adopt a right-handed, alpha-helical structure in solution, giving these compounds the potential to act as mimics of biopolymers such as antimicrobial peptides.

3.4 References

1 R. N. Zuckermann, J. M. Kerr, S. B. H. Kent and W. H. Moos, *J Am Chem Soc*, 1992, **114**, 10646–10647.
2 A. Lone, A. Arnous, P. R. Hansen, B. Mojsoska and H. Jenssen, *Front Chem*, 2020, **8**, 370.
3 S. C. Leguizamon and T. F. Scott, *Nat Commun*, 2020, **11**, 784.
4 H. J. Olivos, P. G. Alluri, M. M. Reddy, D. Salony and T. Kodadek, *Org Lett*, 2002, **4**, 4057–4059.
5 T. Jong, A. M. Pérez-López, E. M. v. Johansson, A. Lilienkampf and M. Bradley, *Bioconjug Chem*, 2015, **26**, 1759–1765.
6 J. E. Rasmussen, M. M. Boccia, J. Nielsen, C. Taillefumier, S. Faure and T. Hjelmgaard, *Tetrahedron Lett*, 2014, **55**, 5940–5943.
7 C. Proulx, S. Yoo, M. D. Connolly and R. N. Zuckermann, *J Org Chem*, 2015, **80**, 10490–10497.
8 N. J. Greenfield, *Trends Anal Chem*, 1999, **18**, 236–244.
9 A. J. Miles, R. W. Janes and B. A. Wallace, *Chem Soc Rev*, 2021, **50**, 8400–8413.
10 N. J. Greenfield, *Nat Protoc*, 2006, **1**, 2527–2535.
11 A. Rodger, R. Marrington, D. Roper and S. Windsor, in *Protein-Ligand Interactions*, Humana Press, New Jersey, pp. 343–364.
12 J. Safar, P. P. Roller, D. C. Gajdusek and C. J. Gibbs, *J. Biol. Chem.*, 1993, **268**, 20276–20284.
13 N. J. Greenfield and S. E. Hitchcock-Degregori, *Protein Sci*, 1993, **2**, 1263–1273.
14 N. J. Greenfield, *Nat Protoc*, 2006, **1**, 2891–2899.
15 A. J. Miles and B. A. Wallace, *Chem Soc Rev*, 2016, **45**, 4859–4872.
16 Y. Wei, A. A. Thyparambil and R. A. Latour, *Biochim Biophys Acta*, 2014, **1844**, 2331–2337.
17 D. Gimenez, J. A. Aguilar, E. H. C. Bromley and S. L. Cobb, *Angew Chem Int Ed*, 2018, **57**, 10549–10553.
18 H.-M. Shin, C.-M. Kang, M.-H. Yoon and J. Seo, *Chem. Commun.*, 2014, **50**, 4465–4468.
19 J. A. Patch and A. E. Barron, *J Am Chem Soc*, 2003, **125**, 12092–12093.
20 T. Kan and T. Fukuyama, *Chem. Comm.*, 2004, 353.
21 H. L. Bolt, C. E. J. Williams, R. v. Brooks, R. N. Zuckermann, S. L. Cobb and E. H. C. Bromley, *Pep Sci*, 2017, **108**, e23014.
22 J. R. Robalo, S. Huhmann, B. Koksch and A. Vila Verde, *Chem*, 2017, **3**, 881–897.
23 N. J. Anthis and G. M. Clore, *Protein Sci*, 2013, **22**, 851–858.
24 M. R. Landry, J. L. Rangel, V. P. Dao, M. A. MacKenzie, F. L. Gutierrez, K. M. Dowell, A. L. Calkins, A. A. Fuller and G. Y. Stokes, *J Phys Chem B*, 2019, **123**, 5822–5831.
25 K. Kirshenbaum, A. E. Barron, R. A. Goldsmith, P. Armand, E. K. Bradley, K. T. v. Truong, K. A. Dill, F. E. Cohen and R. N. Zuckermann, *Proc Natl Acad Sci*, 1998, **95**, 4303–4308.
N. P. Chongsiriwatana, J. A. Patch, A. M. Czyzewski, M. T. Dohm, A. Ivankin, D. Gidalevitz, R. N. Zuckermann and A. E. Barron, *Proc Natl Acad Sci*, 2008, **105**, 2794–279

Chapter 4: Conclusions and Future Work

Peptidomimetics have been shown to offer enhanced lipophilicity, diversity and proteolytic resistance compared to native peptides, whilst retaining promising levels of biological activity.[1] *N*-substituted glycines (peptoids) are a specific family of class B peptidomimetics that often exhibit conformational heterogeneity due to the presence of tertiary amides in their backbone, resulting in a lack of nitrogen bound protons for hydrogen bonding. Pioneering work by Kirshenbaum et al.[2] unveiled the ability of bulky, *N*α-chiral monomers to predictably direct the amide bond into an all *cis*, α-helix peptoid oligomer. Since this seminal work, various peptoid sidechains (peptoid monomers) have been developed to enable the formation of stable helical frameworks in oligomeric systems.

Various peptoid sequences have been screened for their antimicrobial activity,[3,4] with a facially amphipathic distribution of sidechains proven to be crucial in determining the potency of the peptoid.[5] Work reported by Cobb and Bolt found the introduction of fluorine into the peptoid sidechain could increase antimicrobial activity and the use of achiral monomers could help to minimise toxicity.[6]

In developing novel monomers to induce a *cis* conformation in the peptoid backbone, Cobb and Gimenez et al.[7] found the non-chiral, fluoroalkyl *N*3fEt to give a $K_{cis/trans}$ value greater than that of Kirshenbaum's[2] *N*spe sidechain in a model peptoid system. This was quite unprecedented given charge, chirality and aromaticity were not employed. The *N*3fEt fluorinated monomer was then incorporated into a series of 15-mers which upon analysis gave characteristic, alpha-helix CD spectra.[7]

In **Chapter 2**, as a continuation of Gimenez's work, a library of model peptoid systems, seen in **Figure 2.9**, were synthesized to further investigate the propensity of fluoroalkyl sidechains to stabilize a *cis* amide conformation. A literature method developed by Blackwell et al[8] was used for this synthesis, though an alternative route was developed in order to allow for more sidechains to be investigated using iodoalkanes as opposed to primary amines (**Scheme 2.3**). This new method of synthesizing model peptoid systems was found to be cheaper and less wasteful of externally procured reagents without affecting yields, though unlike the literature a purification step was required as well as overnight reaction steps.

1D and 2D NMR experiments were then used to quantify the ratio between the *cis* and *trans* conformations in three different solvents. Inversion recovery experiments showed the greatest

T1 value in the model systems to be 2.75 seconds (**Table 2.2**) which is under five times less than the NMR experiment of 13.9 seconds. This confirmed the NMR setup to have a sufficient relaxation time to ensure quantitative integration, improving the reliability of any comparisons between the monomers developed in the study. However, a major source of error in this study was overlap in the 1D NMR which prevented integration. Three sets of peaks were evaluated for each spectrum, but as seen in **Table 2.3** only two sets of peaks could be accurately integrated for the majority of the models due to either overlap with adjacent peaks or the peak arising from the solvent. In future studies, the acquisition time would be varied in order to find parameters that improve spectral resolution, followed by further inversion recovery experiments to confirm their suitability for quantitative NMR. Nevertheless, good agreement was seen between individual ratios with the standard deviation of $K_{cis/trans}$ never exceeding ± 0.1 (**Table 2.3**).

Fluorinated model peptoids **98** – **100** were chosen to study the effect of moving CF_3 further from the amide backbone. When compared to Gimenez's *N*3fEt monomer,[7] an out of trend shift towards the *cis* conformation was seen in $CDCl_3$ for model **98** (*N*3fPro), which has been associated with the reduction in the overall dipolar moment of the molecule (**Figure 4.1**). Highly fluorinated sidechains gave the greatest values of $K_{cis/trans}$, with *N*5fPro (**101**) and *N*6f^{i}Bu (**103**) being the greatest at 4.01 and 6.22 in CD_3CN respectively. Both values exceed those of already reported charged, chiral, aromatic, and other fluorinated sidechains,[8,9] including *N*3fEt.[7]

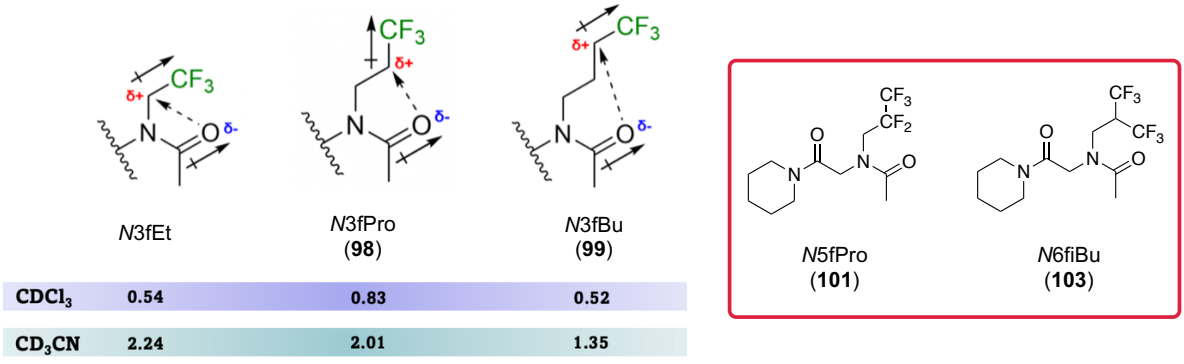

Figure 4.1: Reduction in overall dipolar moment of model peptoid **98** subsequently giving an out of trend shift towards the *cis* rotamer in $CDCl_3$ (values for *N*3fEt taken from Gimenez et al 2018[7]) as well as structures of model peptoids **101** and **103** which gave the greatest values of $K_{cis/trans}$ in the study.

Fluorinated models **98** and **100** – **103** were successfully crystalized by slow evaporation in various solvents, allowing for single crystal X-ray studies (**Figure 2.18**). Each model peptoid crystalised in the *cis* orientation (**Figure 4.2**), in agreement with the preference for *cis* observed in ^{1}H-NMR. Given more time in the laboratory, further crystallization methods, such as liquid and vapour diffusion, would be attempted to crystalize model peptoid **99**. Model **104**

(*N*6f^{i}Amyl) would be resynthesized for a greater yield, which was thought to be a contributing factor to the lack of crystal growth observed.

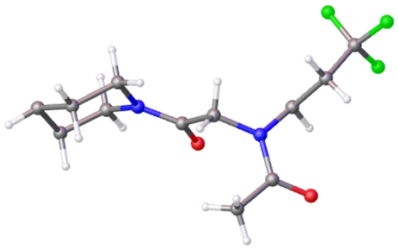

Figure 4.2: Crystal structure of model peptoid **98**. Reported at 50% thermal ellipsoid probability.

Log *P* studies evidenced that the orientation of dipoles in model peptoid **98** (*N*3fPro) increased the lipophilicity of the compound relative to **107** (*N*3fEt) and **99** (*N*3fBu). A reduced overall dipole moment led to a greater increase in log *P* than if the presence of an additional CH_2 group was singlehandedly modulating lipophilicity. Sidechains that form stronger affiliations with the carbonyl oxygen, and subsequently favour the *cis* orientation, reduce this oxygen's ability to interact with water molecules via hydrogen bonding. The study showed model **101** (*N*5fPro) to be 1.6 times more lipophilic than **98**, where they only differ by substitution of CH_2 for CF_2 (**Figure 4.3**). This implies that fluorination of an alkyl chain increases the lipophilicity of a peptoid, though a different model structure would be needed in future work to confirm a fluorinated monomer is more lipophilic than a completely non-fluorinated one if the ^{19}F-NMR experiment was to be used again.

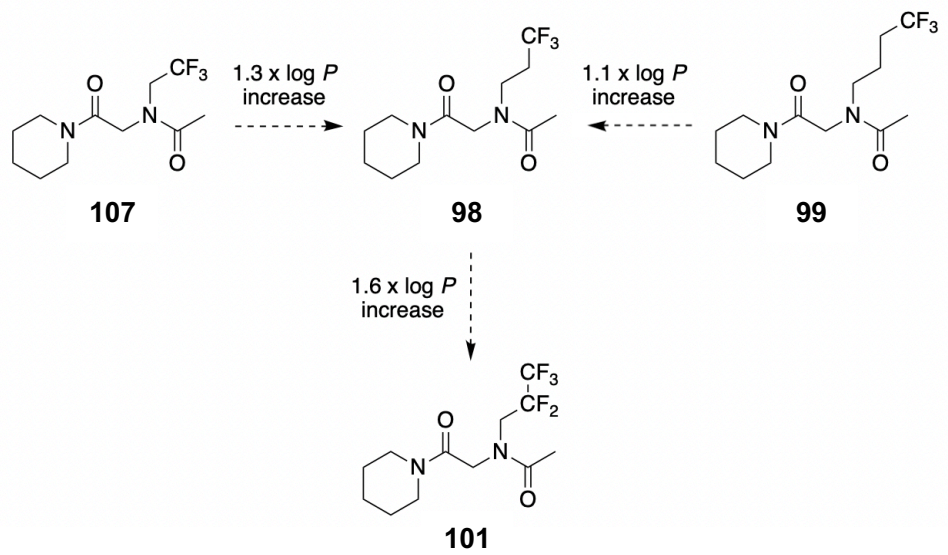

Figure 4.3: Differences in log *P* for the fluorinated model peptoid systems studied in **Chapter 2**.

In the future work, more fluoralkyl sidechains could be subjected to the same NMR, crystallography, and log *P* studies. Higher degrees of fluorination, as well as varying the distance between fluorine and the peptoid backbone, would be investigated. The structure of some proposed peptoid sidechains are shown in **Figure 4.4**. The ultimate aim here would be to have a range of monomers that could be installed into peptoid sequences to subtlety fine tune factors such as hydrophobicity and subsequently biological activity.

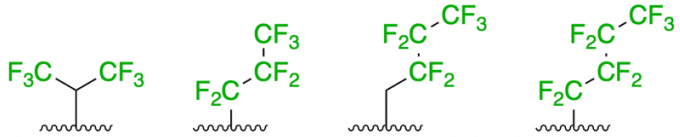

Figure 4.4: Selection of peptoid sidechains that would be investigated in future working which are potentially capable of being *cis* directing.

In **Chapter 3**, non-fluorinated and fluorinated monomers from the study of the peptoid models were incorporated into a series of 15-mer peptoids via the solid phase submonomer method. Attempts were made to incorporate sidechains which had been acquired as idoalkanes instead of as primary amines (**Scheme 3.3**), though neither of these strategies were successful. If the project were to be extended, the corresponding primary amines would be purchased to allow for compatibility with the submonomer process.

Microwave irradiation accelerated the bromine displacement step of the submonomer synthesis for the fluorinated primary amines, and peptoids **110** – **116** were successfully purified. Retention times on analytical HPLC gave a crude indication of each peptoid's relative hydrophobicity (**Table 3.1**). At 27.48 minutes, peptoid **116** gave the longest RT being comprised of highly fluorinated *N*5fBu monomers. This is in agreement with **Chapter 2**'s log *P* study, which found sidechains with the most carbon atoms and highest degree of fluorination to be the most lipophilic (**Table 2.5**). To fully evaluate log D in these peptoids, partitioning experiments would be performed using previously established methodology by Bolt et al.[10]

Gratifyingly, preliminary Circular Dichroism (CD) studies showed peptoids **110** – **116** to form stable alpha helix like secondary structures in water (**Figure 4.5**). This finding is significant, as it shows that fluorinated monomers *N*3fPro, *N*3fBu, *N*5fPro and *N*5fBu can all be added to the 'toolbox' of monomers for the rational design of peptoid alpha helices. Non-fluorinated alkyl sidechains **110** (*N*Pro) and **111** (*N*Bu) also gave characteristic alpha helix like spectra. Due to time restraints in the laboratory, it was not possible to accurately determine the concentration of the peptoid stock solutions that were used in the CD studies. In future work, ^{19}F-NMR techniques, previously established by Gimenez et al.,[7] would be utilized to calculate the true

concentration of these samples. This would allow for the quantification of the degree of helicity imparted by each of these individual sidechains/ monomers.

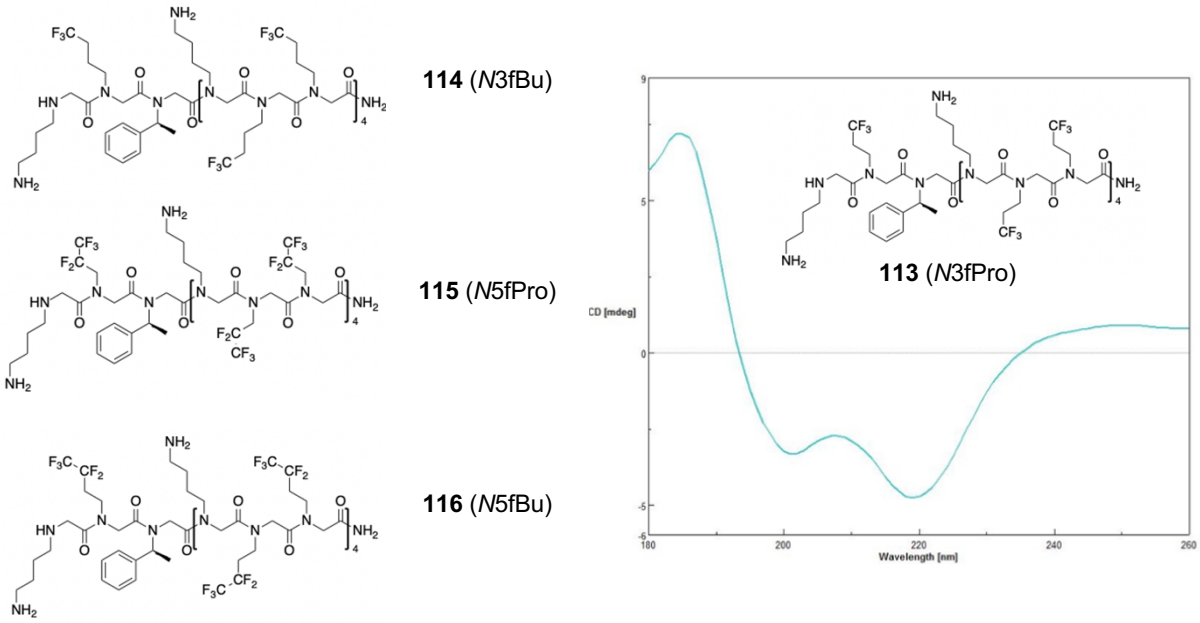

Figure 4.5: Structures of peptoids **113** – **116** alomng with the CD spectra of peptoid **113** recorded in H_2O at room temperature.

In future, the peptoid oligomers prepared (**110** to **116**) could be screened for their antimicrobial properties. Their cell permeability could also be evaluated which, coupled with log D experiments, would reveal if fluorine was increasing the lipophilicity of the peptoid as was seen in the model peptoid partitioning study.

As outlined in **Chapter 1**, the core aims of this project were:

- To explore the influence of fluoralkyl side chains further, accessing new moieties capable of exerting a *cis* preference in the amide backbone that are achiral, uncharged and aliphatic.

- To measure the effect on lipophilicity by increasing the distance of fluorine from the amide functionality, as well increasing the fluorine content of the side chain.

- To incorporate new fluoroalkyl monomers into peptoid oligomers that show a defined secondary structure in solution.

A library of novel fluoroalkyl peptoid sidechains have been identified, capable of directing the tertiary amide bond into the *cis* orientation. A dipolar effect was found to influence the amide

equilibrium in non-polar solvents, which further went on to influence trends in log *P*. The addition of fluorine was found to increase the lipophilicity of an alkyl peptoid sidechain, and these novel monomers were successfully incorporated into oligomers which gave characteristic alpha helix like CD spectra.

Chapter 4 References

1) E. Lenci and A. Trabocchi, *Chem Soc Rev*, 2020, **49**, 3262–3277.
2) P. Armand, K. Kirshenbaum, A. Falicov, R. L. Dunbrack, K. A. Dill, R. N. Zuckermann and F. E. Cohen, *Fold Des*, 1997, **2**, 369–375.
3) B. Mojsoska, R. N. Zuckermann and H. Jenssen, *Antimicrob Agents Chemother*, 2015, **59**, 4112–4120.
4) N. P. Chongsiriwatana, J. A. Patch, A. M. Czyzewski, M. T. Dohm, A. Ivankin, D. Gidalevitz, R. N. Zuckermann and A. E. Barron, *Proc. Natl. Acad. Sci.*, 2008, **105**, 2794–2799.
5) J. A. Patch and A. E. Barron, *J Am Chem Soc*, 2003, **125**, 12092–12093.
6) H. L. Bolt, G. A. Eggimann, C. A. B. Jahoda, R. N. Zuckermann, G. J. Sharples and S. L. Cobb, *Medchemcomm*, 2017, **8**, 886–896.
7) D. Gimenez, J. A. Aguilar, E. H. C. Bromley and S. L. Cobb, *Angew. Chem. Int. Ed.*, 2018, **57**, 10549–10553.
8) B. C. Gorske, J. R. Stringer, B. L. Bastian, S. A. Fowler and H. E. Blackwell, *J Am Chem Soc*, 2009, **131**, 16555–16567.
9) C. Caumes, O. Roy, S. Faure and C. Taillefumier, *J Am Chem Soc*, 2012, **134**, 9553–9556.
10) H. L. Bolt, C. E. J. Williams, R. v. Brooks, R. N. Zuckermann, S. L. Cobb and E. H. C. Bromley, *Peptide Science*, 2017, **108** (4)

Chapter 5: Experimental

5.1 Materials and Reagents

Reagents used for this project were purchased from commercial suppliers and subsequently employed without further purification. Amines used for the synthesis of model peptoids or peptoid oligomers were sourced from Sigma Aldrich (Gillingham, UK), Fluorochem Ltd (Glossop, UK), Manchester Organics Ltd (Runcorn, UK) and Alfa Aesar (Lancashire, UK). Iodalkanes used in model peptoid synthesis were purchased from Fluorochem Ltd. All solvents were supplied by Fisher Scientific (Loughborough, UK) and used without further purification. Rink amide resin for solid phase peptide synthesis was obtained from Novabiochem by Merck (Darmstadt, Germany), bromoacetic acid from Sigma Aldrich, *N*,*N*′-Diisopropylcarbodiimide (DIC) from Alfa Aesar and fritted polypropylene cartridges from Crawford Scientific Ltd (Strathaven, UK). Model peptoid purification was performed using Fluorochem Silicagel LC60A (40 – 63 micron) and thin layer chromatography (TLC) pre-coated silica plates from Macherey-Nagel (Duren, Germany). All deuterated solvents for NMR experiments were sourced from CK Isotopes Ltd (Newton Unthank, UK).

5.2 General Methods

5.2.1 Liquid Chromatography Electrospray Ionisation Mass Spectrometry

Liquid chromatography (LC)-mass spectrometry (ESI-MS) analysis was performed using an Acquity UPLC BEH C_{18} 1.7 µm (2.1 mm x 50 mm) column using a Waters Acquity UPLC system fitted with a photodiode array detector, providing absorbance data from 210 nm to 400 nm. A gradient with eluent A (0.1% HCOOH in water) and eluent B (acetonitrile) rising linearly from 5 to 95% of B in 3.8 min was applied at a flow rate of 0.6 mL/min. The continuous exit flow is then directed into the electrospray source of the mass spectrometer and analysed. For compounds **70**, **74** and **75** only, analysis was performed on an Acquity UPLC BEH C_{18} 1.7 µm (2.1 mm x 100 mm) column using a Waters Acquity UPLC system fitted with a photodiode array detector, providing absorbance data from 210 nm to 400 nm. A gradient with eluent A (0.1% HCOOH in water) and eluent B (acetonitrile) rising linearly from 5 to 35% of B in 13 min rising linearly again to 95% over 2 min was applied at a flow rate of 0.6 mL/min.

5.2.2 Quadrupole Time-of-Flight Mass Spectrometry

QToF-LC/MS analysis was performed on an Acquity UPLC BEH C_{18} 1.7µm (2.1 mm x 100 mm) column using a Waters Acquity UPLC system coupled to Micromass QToF Premier mass spectrometer, also equipped with a photodiode array detector providing absorbance data from 210 nm to 400 nm. A gradient with eluent A (0.1% HCOOH in water) and eluent B (acetonitrile) rising linearly from 0 to 99% of B was applied at a flow rate of 0.6 mL/min over 6 min. The solvent flow from the UPLC was injected into a flow of acetonitrile at 0.2 mL/min which was introduced into the electrospray ion source.

5.2.3 Nuclear Magnetic Resonance (NMR) Spectroscopy

NMR spectra were recorded on a Varian VNMRS-700 NMR spectrometer at 298 K. ^{1}H-NMR data was obtained at 599 MHz using 2 - 8 scans with a relaxation delay of 10 s between them. ^{13}C-NMR spectroscopic data was obtained at 151 MHz and bi-dimensional ^{1}H-^{1}H NOESY experiments were run with a minimum mixing time of 150 ms, a spectral width between 6,000 - 8,000 Hz in both dimensions and a minimum of 2 transients with 2 x 256 increments. ^{19}F-NMR spectra were recorded at 376 MHz using a Bruker Advance III spectrometer. Data was processed using Mestrenova 11® software, and chemical shifts are reported in ppm relative to residual solvent peaks as internal standards ($CDCl_3$: δ^{1}H = 7.26 ppm, δ^{13}C = 77.1 ppm; CD_3CN δ^{1}H = 1.94 ppm, δ^{13}C = 1.32 ppm; CD_3OD: δ^{1}H = 3.34 ppm, δ^{13}C = 49.00 ppm). J couplings are given in Hertz (Hz). Multiplicities: s = singlet, d =doublet, m = multiplet, t = triplet, q = quartet, quint = quintet.

5.3 Synthesis of Model Peptoid Systems

5.3.1 Synthesis of 2-Bromo-1-(piperidin-1-yl)ethenone (93)

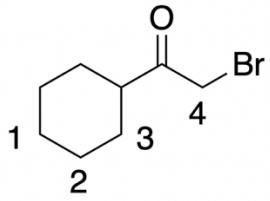

Bromoacetyl bromide (**92**) (0.24 mL, 2.72 mmol, 1 equiv.) in DCM (5 mL) was added dropwise to a solution of piperidine (0.27 mL, 1 equiv.) in DCM (20 mL) at 0 °C. This was allowed to warm to room temperature before washing with H_2O (20 mL), 1 M citric acid solution (20 mL) and saturated $NaHCO_3$ (20 mL). The organic layer was dried with sodium sulphate and concentrated under reduced pressure to give the ethanone (**93**) as a brown oil (443 mg, 79% yield). HRMS (ESI^+): calculated mass for $C_7H_{13}BrNO^+$ = 206.0181, observed [M + H] = 206.0191 Da.

Characterization data matches previously published data.[1]

δ ^{1}H NMR (599 MHz, $CDCl_3$):

δ 3.84 (s, 2H, H_4); 3.55 - 3.38 (m, 4H, H_3); 1.67 - 1.58 (m, 4H, H_2); 1.57 - 1.50 (m, 2H, H_1).

^{13}C NMR (151 MHz, $CDCl_3$):

δ 164.96 (CO-pip); 47.88, 43.21 (CH_2, C_3); 26.16 (CH_2, C_4); 25.33, 24.24 (CH_2, C_{1+2}).

5.3.2 Bromine Displacement with Primary Amines

2-Bromo-1-(piperidin-1-yl)ethenone (**1**) (175 mg, 0.85 mmol, 1 equiv.) was dissolved in MeCN (5 mL) and added dropwise to a solution of primary amine (4 equiv.) in MeCN (10 mL) at 0 °C in an ice bath and under an N_2 atmosphere. The reaction was allowed to warm to room temperature, stirred for 16 h and concentrated under reduced pressure to give an oily residue. No further purification was performed. LC/MS verified the presence of the target compound.

5.3.3 Synthesis of 2-amino-1-(piperidin-1-yl)ethan-1-one (107)

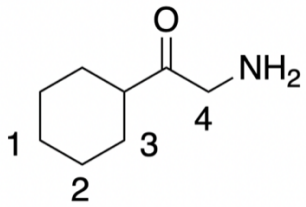

Boc-glycine (**105**) (3.50 g, 20 mmol, 1 equiv.) in THF (40 mL) was stirred in a 100 mL round bottom flask under N_2 at -15 °C using a benzyl alcohol and dry ice bath. *N*-methylmorpholine (NMM) (2.48 mL, 1.1 equiv.) was added followed by dropwise addition of isobutyl chloroformate (2.8 mL, 1.1 equiv.). The solution was allowed to stir for 5 mins before adding piperidine (1.98 mL, 1 equiv.) and NMM (2.48 mL, 1.1 equiv.) simultaneously. The solution was stirred at -15 °C for 30 mins before being allowed to warm to room temperature and left to react for 16 h. The insoluble salt was then removed by vacuum filtration and the filtrate concentrated under reduced pressure before being redissolved in ethyl acetate. This was washed first with 1.0 M sodium hydroxide solution (2 x 20 mL), followed by water (2 x 20 mL) and finally 1.0 M hydrochloric acid solution (2 x 20 mL). The organic phase was dried over sodium sulphate and concentrated under reduced pressure before being dissolved in DCM (10 mL) and cooled to 0 °C in an ice bath. Trifluoroacetic acid (10 mL) was added dropwise, after which the reaction was allowed to warm to room temperature and left to stir for 16 h. The solution was then concentrated under reduced pressure and raised to pH = 12 with 1.0 M sodium hydroxide solution. This was then extracted with DCM and the organic layer dried over sodium sulphate before concentrating under reduced pressure. The crude was then purified by flash column chromatography eluting with 5% MeOH in DCM. This gave **107** as pale-yellow oil (1.12 g, 78%). HRMS (ESI^+): calculated mass for $C_7H_{15}N_2O^+$ = 143.1184, observed [M + H] = 143.1192 Da.

Characterization data matches previously published data.[2]

δ ^{1}H NMR (599 MHz, $CDCl_3$):

δ 3.55 – 3.48 (m, 4H, $H_{4 + 3(ax/eq)}$); 3.27 (t, *J* = 4.4 Hz, 2H, $H_{3\ (ax/eq)}$); 1.66 - 1.59 (m, 2H, H_1); 1.56 – 1.48 (m, 4H, H_2).

^{13}C NMR (151 MHz, $CDCl_3$):

δ 164.96 (CO-pip); 45.19, 43.23 (CH_2, C_3); 26.15 (CH_2, C_4); 25.38, 24.20 (CH_2, C_{1+2}).

5.3.4 General Procedure for Alkylation with Iodoalkanes

An iodoalkane (0.85 mmol, 1 equiv.) was dissolved in MeCN (5 mL) and added dropwise to a solution of 2-amino-1-(piperidin-1-yl)ethan-1-one (**2**) (479 mg, 4 equiv.) in MeCN (10 mL) at 50 °C under an N_2 atmosphere. The reaction was allowed to stir for 16 h and concentrated under reduced pressure to give an oily residue. No further purification was performed. LC/MS verified the presence of the target compound.

5.3.5 General Procedure for Final Acetylation

The products from steps **5.3.2** and **5.3.4** were dissolved in DCM (15 mL) followed by addition of acetyl chloride (2 equiv.) and DIPEA (2 equiv.). This was allowed to stir for 30 mins at room temperature before washing with 1 M citric acid solution (2 x 20 mL) and extracting the aqueous layer thrice with DCM. The organic solutions were combined and dried over sodium sulphate, before being concentrated under reduced pressure, giving the crude model peptoid confirmed by LC/MS.

5.3.6 Purification of Model Peptoids

Purification of the model peptoids was performed via silica gel flash column chromatography. Once the sample was loaded, EtOAc was flushed through the column until no TLC spots were identifiable under a UV lamp. The product was then eluted with 1 – 3% MeOH in DCM. Fractions containing single TLC spots with the same R_f values were combined and concentrated under reduced pressure, giving the pure model peptoid. Products were characterised by LC/MS, Acc Mass, ^{1}H-NMR, ^{13}C-NMR and, where appropriate, ^{19}F-NMR.

5.4 Determination of $K_{cis/trans}$ in Model Peptoid Systems

20 – 40 mg of each pure model peptoid was dissolved in $CDCl_3$, CD_3CN and MeOD for a full set of high field NMR experiments. Protons were independently assigned by ^{1}H-NMR, ^{1}H-*psyche*, and ^{1}H-^{1}H COSY, with rotamers being distinguished by ^{1}H-^{1}H NOESY. Three sets of rotamer peaks were employed to determine an average $K_{cis/trans}$ value. These rotamer peaks arise from the main protons involved in isomerization about the amide bond: (H_5) the terminal acetyl CH_3 group, (H_4) the backbone CH_2 group, and (H_6) the side chain CH_2 group directly appended to nitrogen. Signals arising from the *cis* rotamer gave NOEs between (H_5) and (H_4) whereas peaks from the trans rotamer gave NOEs between (H_5) and (H_6). Two separate

proton spectra were recorded in each solvent giving a total of 6 $K_{cis/trans}$ values, where attainable, for the reported average. $K_{cis/trans}$ for each set of rotamer peaks was taken as the ratio between the area under the *cis* and *trans* signals. Standard deviation was calculated from the individual values arising from each set of rotamer peaks in duplicate experiments. In fluorinated systems, ^{19}F-NMR was used for an additional calculation of $K_{cis/trans}$. These calculations were not employed in the average value of the model but reported separately as further confirmation. $K_{cis/trans}$ from ^{19}F-NMR calculated as a ratio of *cis* to *trans* from a single spectrum. Standard deviation is given only for models **101** and **102** as two fluorine environments are present, giving two *cis* rotamer peaks and two *trans*. Standard deviation was calculated for ^{19}F-NMR values in models **101** and **102**, as two distinct fluorine environments are present. The average value and corresponding standard deviation is given as n = 6. $\Delta G_{cis/trans}$ was calculated at 25 °C using the equation below:

$$\Delta G_{cis/trans} = -RT \ln K_{cis/trans}$$

R = 1.987 x 10^{-3} kcal K^{-1} mol^{-1} and T = 298 K

All individually derived $K_{cis/trans}$ values are displayed in **Table 5.1**, **Table 5.2** and **Table 5.3**.

Table 5.1: Summary of $K_{cis/trans}$ values calculated from each ^{1}H-NMR experiment, alongside $\Delta G_{cis/trans}$ and where appropriate ^{19}F-NMR $K_{cis/trans}$ values, for model peptoids **94** – **104** in $CDCl_3$.

Model	^{1}H-NMR K*cis*/*trans* Values						Average K*cis*/*trans*	$\Delta G_{cis/trans}$ (kcal/mol)	^{19}F-NMR Values
	H_4 (1)	H_4 (2)	H_5 (1)	H_5 (2)	H_6 (1)	H_6 (2)			
94	0.19	0.19	0.18	0.18	-	-	0.18 ± 0.01	1.00 ± 0.02	-
95	0.17	0.18	0.17	0.17	-	-	0.17 ± 0.01	1.04 ± 0.02	-
96	0.17	0.19	0.17	0.20	-	-	0.18 ± 0.02	1.01 ± 0.05	-
97	0.18	0.19	0.19	0.19	-	-	0.19 ± 0.01	0.99 ± 0.02	-
98	0.78	0.77	0.89	0.86	-	-	0.83 ± 0.06	0.12 ± 0.04	0.88
99	0.53	0.54	0.52	0.50	-	-	0.52 ± 0.02	0.38 ± 0.02	0.62
100	0.38	0.42	0.38	0.38	-	-	0.39 ± 0.02	0.56 ± 0.03	- [a]
101	0.64	0.63	0.65	0.66	-	-	0.65 ± 0.01	0.26 ± 0.01	0.92 ± 0.04
102	0.98	0.97	0.93	0.91	-	-	0.95 ± 0.03	0.03 ± 0.02	0.94 ± 0.02
103	3.16	3.18	3.11	3.12	3.40	3.40	3.23 ± 0.14	-0.69 ± 0.02	3.23
104	0.80	0.80	0.80	0.75	-	-	0.79 ± 0.03	0.14 ± 0.02	0.79

[a] Overlap in ^{19}F-NMR prevents $K_{cis/trans}$ being calculated.

Table 5.2: Summary of $K_{cis/trans}$ values calculated from each ^{1}H-NMR experiment, alongside $\Delta G_{cis/trans}$ and where appropriate ^{19}F-NMR $K_{cis/trans}$ values, for model peptoids **94** – **104** in CD_3OD.

Model	^{1}H-NMR K*cis*/*trans* Values						Average K*cis*/*trans*	$\Delta G_{cis/trans}$ (kcal/mol)	^{19}F-NMR Values
	H_4 (1)	H_4 (2)	H_5 (1)	H_5 (2)	H_6 (1)	H_6 (2)			
94	0.49	0.50	0.51	0.49	-	-	0.50 ± 0.01	0.41 ± 0.01	-
95	0.53	0.51	0.54	0.50	-	-	0.52 ± 0.02	0.39 ± 0.02	-
96	0.46	0.50	0.52	0.52	-	-	0.50 ± 0.03	0.41 ± 0.03	-
97	0.55	0.58	0.58	0.59	0.57	0.57	0.57 ± 0.01	0.33 ± 0.01	-
98	1.34	1.32	1.36	1.34	-	-	1.34 ± 0.02	-0.17 ± 0.01	1.25
99	1.03	1.02	0.88	0.93	-	-	0.97 ± 0.07	0.02 ± 0.04	~1.00 [b]
100	0.75	0.74	0.76	0.77	0.83	0.79	0.77 ± 0.03	0.15 ± 0.02	- [a]
101	2.18	2.13	1.98	2.0	2.25	2.16	2.12 ± 0.11	-0.44 ± 0.03	2.17 ± 0.01
102	1.64	1.64	1.57	1.60	1.58	1.59	1.60 ± 0.03	-0.28 ± 0.01	1.60 ± 0.05
103	3.21	3.14	3.27	3.33	3.41	3.30	3.28 ± 0.09	-0.70 ± 0.02	3.60
104	1.47	1.45	-	-	-	-	1.46 ± 0.01	-0.22 ± 0.01	1.51

[a] Overlap in ^{19}F-NMR prevents $K_{cis/trans}$ being calculated.
[b] $K_{cis/trans}$ from ^{19}F-NMR approximated to 1.00 as *cis* and *trans* peaks cannot be distinguished by integration alone.

Table 5.3: Summary of $K_{cis/trans}$ values calculated from each ^{1}H-NMR experiment, alongside $\Delta G_{cis/trans}$ and where appropriate ^{19}F-NMR $K_{cis/trans}$ values, for model peptoids **94** – **104** in CD_3CN.

Model	^{1}H-NMR K*cis*/*trans* Values						Average K*cis*/*trans*	$\Delta G_{cis/trans}$ (kcal/mol)	^{19}F-NMR Values
	H_4 (1)	H_4 (2)	H_5 (1)	H_5 (2)	H_6 (1)	H_6 (2)			
94	0.70	0.70	0.69	0.70	0.71	0.72	0.70 ± 0.01	0.21 ± 0.01	-
95	0.74	0.74	0.72	0.74	0.75	0.74	0.74 ± 0.01	0.18 ± 0.01	-
96	-	-	0.77	0.75	0.79	0.73	0.76 ± 0.03 [d]	0.16 ± 0.01	-
97	0.85	0.84	0.83	0.87	0.86	0.83	0.85 ± 0.02	0.10 ± 0.01	-
98	1.90	1.95	2.04	2.13	-	-	2.01 ± 0.10 [d]	-0.41 ± 0.03	1.67
99	1.32	1.35	1.34	1.40	-	-	1.35 ± 0.03 [d]	-0.18 ± 0.01	1.48
100	1.05	1.11	1.19	1.08	-	-	1.11 ± 0.06 [d]	-0.06 ± 0.03	- [a]
101	4.00	4.02	-	-	-	-	4.01 ± 0.01 [e]	-0.82 ± 0.00	3.93 ± 0.11
102	2.20	2.13	2.17	2.15	-	-	2.17 ± 0.05 [d]	-0.91 ± 0.01	2.02 [b]
103	6.23	6.25	6.21	6.19	-	-	6.22 ± 0.03 [d]	-1.08 ± 0.00	6.09
104	2.24	2.27	2.22	2.29	-	-	2.26 ± 0.03 [d]	-0.48 ± 0.01	2.29

[a] Overlap in ^{19}F-NMR prevents $K_{cis/trans}$ being calculated.
[b] $K_{cis/trans}$ from ^{19}F-NMR calculated from one set of peaks due to overlap in the spectra, hence no standard deviation reporte

5.5 Solid Phase Synthesis of Peptoid Oligomers

5.5.1 General Solid Phase Peptoid Synthesis

All peptoids were synthesised using the well-established submonomer method. Fmoc-protected Rink Amide resin (typically 60 mg, 0.10 mmol, loading 0.84 mol g^{-1}) in a pre-fritted 20 mL cartridge was left to swell in DMF (2 mL) at 400 rpm for 30 mins. The vessel was drained, followed by Fmoc deprotection with 20% piperidine in DMF (2 mL, 2 x 15 mins). After draining again, the resin was washed with DMF (4 x 2mL x 2 mins) before acylation with bromoacetic acid (2 mL, 0.6 M in DMF) and DIC (0.2 mL) shaking at 400 rpm for 15 minutes. The resin was again drained and washed with DMF (4 x 2mL x 2 mins) followed by bromine displacement with the desired amine (2 mL, 1.2 M in DMF) for 30 mins at 400 rpm.

For peptoids **114** – **116**, microwave irradiation was employed in the bromine displacement step. The resin was transferred into a 5 mL microwave vial with a magnetic stirrer bar and manually drained using a syringe. The desired amine was then added (2 mL, 1.2 M in DMF) and stirred for 15 mins at 80 °C in a Biotage® Initiator+ Microwave synthesizer. The reaction was allowed to cool before being transferred back into a fritted cartridge, drained and washed with DMF (4 x 2mL x 2 mins).

Acylation and bromine displacement steps were alternated, growing the oligomer to the desired length. After the final bromine displacement, the resin was washed with DMF (4 x 2mL x 2 mins), MeOH (3 x 10 mL), DCM (3 x 10 mL) and diethyl ether (3 x 10 mL). Completed peptoids were kept refrigerated in their cartridges until being cleaved from the resin. When a pause in the peptoid synthesis was required, the bromine displacement step was completed, and the resin washed and stored as though it were the final bromine displacement step. To resume chain growth, the resin was re-swelled in DMF (2 mL) at 400 rpm for 30 mins before re-initiating the synthesis with acylation. Pauses were made whenever required except following the second bromine displacement, as the resin-peptoid conjugate may form a cyclic diketopiperazine side-product.

5.5.2 General Cleavage of Peptoids from Resin

The resin hosting the fully grown oligomer was treated with a cleavage cocktail (2 mL, TFA/TIPS/H_2O (95:2.5:2.5 v/v/v)) for 10 mins at 400 rpm, and subsequently drained into a round-bottom flask. The resin was shaken with DCM (2 mL) for 2 mins and again drained into

the flask to wash through any remaining peptoid. The solution was concentrated under reduced pressure to yield a viscous oil, which was then precipitated with diethyl ether forming a white solid on the edge of the glassware. The diethyl ether was decanted and the solid dissolved in H_2O:MeCN (5 mL, 50:50 v/v) before being transferred to a pre-weighed Falcon tube. The solution was frozen and lyophilized to give the crude peptoid product as a white solid confirmed by LC/MS.

5.6 Procedure for Peptoid Purification

5.6.1 General Procedure for Peptoid Purification by RP-HPLC

Th crude peptoid was dissolved in a solution of 50:50 H_2O:MeCN (10 mL) (with the addition of 2 – 3% TFA for fluorinated peptoids **113** – **116**) and purified by preparative RP-HPLC using an InterChim Puriflash purification system equipped with a Waters XBridge C_{18} 5 µm (19 mm x 100 mm) column. Separation was achieved using gradient elution at a flow rate of 17 mL/min with eluent A (0.1% HCOOH in water) and eluent B (acetonitrile) linearly increasing from 10 – 90% B over 10 mins before being held at this composition for 5 mins. A diode array detector monitored the absorption of the eluent and fractions were collected when a threshold of 5 mAU was achieved at 220 nm. Relevant fractions were collected, lyophilised and analysed by LC-MS.

5.6.2 Analysis of Purified Peptoids by Analytical RP-HPLC

Pure peptoids were dissolved in H_2O to create solutions of 1 mg/mL and their purities assessed by analytical HPLC using an X-Bridge C_{18} 5.3 µm,(4.6 x 100 mm) column at 40 °C using a Perking-Elmer 200 series lc system supplied with auto-sampler, UV/Vis detector and a Peltier column oven. A linear gradient rising from solvent A (95:5:0.05 v/v/v H_2O:MeCN:TFA) to 100% of solvent B (5:95:0.03% v/v/v H_2O:MeCN:TFA) over 30 mins was applied at a flow rate of 1 mL/min. Detection was performed at λ= 220 nm.

5.7 Circular Dichroism (CD) Analysis of Peptoids

All CD spectra were recorded on a Jasco J-1500 spectrometer, fitted with a Jasco MCB- 100 mini circulation bath. All samples were recorded as the average of 3 accumulations (1.0 nm data pitch, continuous scanning mode, 50 nm/min scanning speed, 3 nm bandwidth) using a

QS high precision cell with a 0.1 cm of path length from Hellma Analytics. For CD measurements, a 250 μM solution of each peptoid in H_2O was prepared and to every raw recorded spectrum, the signal arising from the solvent was subtracted. Finally, all curves were smoothed using Means-Movement smoothing on Spectral Manager II software (JASCO, UK).

5.8 Characterization Data for Chapter 2

5.8.1 Model Peptoid NMR and MS Data

Please note: both *cis* and *trans* isomers also appear as rotamers.

Compound 94: *N*-propyl-*N*-(2-oxo-2-(piperidin-1-yl)ethyl)acetamide

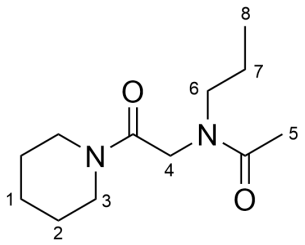

2-Bromo-1-(piperidin-1-yl)ethenone (**93**) was dissolved in MeCN (5 mL) and added dropwise to a solution of propylamine (201 mg, 4 equiv.) in MeCN (10 mL) at 0 °C under an N_2 atmosphere. The reaction was allowed to warm to room temperature and stirred for 16 h following the general protocol described in **Section 5.3.2**. The reaction was then concentrated under reduced pressure and acetylated as per **Section 5.3.5**, before purification by flash column chromatography (**Section 5.3.6**). This gave *N*-propyl-*N*-(2-oxo-2-(piperidin-1-yl)ethyl)acetamide (**94**) as a yellow oil (117 mg, 61%). HRMS (ESI^+): calculated for $C_{12}H_{22}N_2O_2^+$ 227.1760 $[M+H]^+$, found: 227.1749 Da.

^{1}H NMR (599 MHz, $CDCl_3$)

cis (minor): δ 4.01 (s, 2H, H_4); 3.50 (t, *J* = 5.6 Hz, 2H, $H_{3\ (ax/eq)}$); 3.36 (t, *J* = 5.6 Hz, 2H, $H_{3\ (ax/eq)}$); 1.96 (s, 3H, H_5); 1.68 – 1.45 (m, 8H, H_{1+2+7}); 0.86 (t, *J* = 7.4 Hz, 3H, H_8).

Note: H_6 peak unassignable for *cis* rotamer

trans (major): δ 4.13 (s, 2H, H_4); 3.50 (t, *J* = 5.6 Hz, 2H, $H_{3\ (ax/eq)}$); 3.36 (t, *J* = 5.6 Hz, 2H, $H_{3\ (ax/eq)}$); 3.30 (t, *J* = 7.7 Hz, 2H, H_6); 2.12 (s, 3H, H_5); 1.68 – 1.45 (m, 8H, H_{1+2+7}); 0.90 (t, *J* = 7.4 Hz, 3H, H_8).

^{13}C NMR (151 MHz, $CDCl_3$)

cis (minor): δ 171.34 (CO-CH_3); 165.85 (CO-pip); 50.08 (C_4, CH_2); 49.13 (C_6, CH_2); 45.82, 43.46 (C_3, CH_2); 26.59, 25.62 (C_2, CH_2); 24.44 (C_1, CH_2); 21.68 (C_7, CH_2); 20.90 (C_5, CH_3); 11.44 (C_8, CH_3).

trans (major): δ 170.90 (CO-CH_3); 166.49 (CO-pip); 51.21 (C_6, CH_2); 46.43 (C_4, CH_2); 46.09, 43.17 (C_3, CH_2); 26.37, 25.54 (C_2, CH_2); 24.54 (C_1, CH_2); 21.68 (C_7, CH_2); 21.19 (C_5, CH_3); 11.29 (C_8, CH_3).

^{1}H NMR (599 MHz, CD_3CN)

cis (minor): δ 4.10 (s, 2H, H_4); 3.51 – 3.42 (m, 2H, $H_{3\,(ax/eq)}$); 3.38 – 3.32 (m, 2H, $H_{3\,(ax/eq)}$); 3.18 (t, *J* = 7.6 Hz, 2H, H_6); 1.84 (s, 3H, H_5); 1.67 – 1.40 (m, 8H, H_{1+2+7}); 0.83 (t, *J* = 7.4 Hz, 3H, H_8).

trans (major): δ 4.08 (s, 2H, H_4); 3.51 – 3.42 (m, 2H, $H_{3\,(ax/eq)}$); 3.38 – 3.32 (m, 2H, $H_{3\,(ax/eq)}$); 3.23 (t, *J* = 8.0 Hz, 2H, H_6); 2.04 (s, 3H, H_5); 1.67 – 1.40 (m, 8H, H_{1+2+7}); 0.88 (t, *J* = 7.4 Hz, 3H, H_8).

^{13}C NMR (151 MHz, CD_3CN)

cis (minor): δ 172.03 (CO-CH_3); 167.21 (CO-pip); 50.72 (C_4, CH_2); 49.33 (C_6, CH_2); 46.23, 43.76 (C_3, CH_2); 27.04, 26.42 (C_2, CH_2); 25.10 (C_1, CH_2); 21.81 (C_5, CH_3); 21.55 (C_7, CH_2); 11.59 (C_8, CH_3).

trans (major): δ 171.09 (CO-CH_3); 167.26 (CO-pip); 51.83 (C_6, CH_2); 47.31 (C_4, CH_2); 46.32, 43.46 (C_3, CH_2); 26.98, 26.38 (C_2, CH_2); 25.16 (C_1, CH_2); 22.31 (C_5, CH_3); 21.36 (C_7, CH_2); 11.37 (C_8, CH_3).

^{1}H NMR (599 MHz, CD_3OD)

cis (minor): δ 4.30 (s, 2H, H_4); 3.58 – 3.49 (m, 2H, $H_{3\,(ax/eq)}$); 3.49 – 3.43 (m, 2H, $H_{3\,(ax/eq)}$); 3.31 – 3.25 (m, 2H, H_6); 1.96 (s, 3H, H_5); 1.75 – 1.43 (m, 8H, H_{1+2+7}); 0.89 (t, *J* = 7.4 Hz, 3H, H_8).

trans (major): δ 4.21 (s, 2H, H_4); 3.58 – 3.49 (m, 2H, $H_{3\,(ax/eq)}$); 3.49 – 3.43 (m, 2H, $H_{3\,(ax/eq)}$); 3.35 – 3.29 (m, 2H, H_6); 2.15 (s, 3H, H_5); 1.75 – 1.43 (m, 8H, H_{1+2+7}); 0.94 (t, *J* = 7.4 Hz, 3H, H_8).

^{13}C NMR (151 MHz, CD_3OD)

cis (minor): δ 173.02 (CO-CH_3); 166.70 (CO-pip); 49.83 (CH_2, C_4); 49.11 (CH_2, C_6); 45.40, 43.09 (CH_2, C_3); 26.02, 25.32 (CH_2, C_2); 23.92 (CH_2, C_1); 20.26 (CH_2, C_7); 20.06 (CH_3, C_5); 10.18 (CH_3, C_8).

trans (major): δ 172.22 (CO-CH_3); 166.84 (CO-pip); 51.42 (CH_2, C_6); 46.61 (CH_2, C_4); 45.57, 42.91 (CH_2, C_3); 25.82, 25.21 (CH_2, C_2); 23.98 (CH_2, C_1); 21.08 (CH_2, C_7); 19.62 (CH_3, C_5); 9.97 (CH_3, C_8).

Compound 95: *N*-butyl-*N*-(2-oxo-2-(piperidin-1-yl)ethyl)acetamide

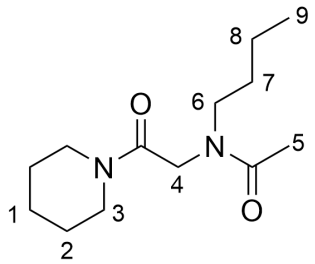

2-Bromo-1-(piperidin-1-yl)ethenone (**93**) was dissolved in MeCN (5 mL) and added dropwise to a solution of butylamine (249 mg, 4 equiv.) in MeCN (10 mL) at 0 °C under an N_2 atmosphere. The reaction was allowed to warm to room temperature and stirred for 16 h following the general protocol described in **Section 5.3.2**. The reaction was then concentrated under reduced pressure and acetylated as per **Section 5.3.5**, before purification by flash column chromatography (**Section 5.3.6**). This gave *N*-butyl-*N*-(2-oxo-2-(piperidin-1-yl)ethyl)acetamide (**95**) as a yellow oil (86 mg, 42%). HRMS (ESI$^+$): calculated for $C_{13}H_{24}N_2O_2^+$ 241.1916 $[M+H]^+$, found: 241.1909 Da.

^{1}H NMR (599 MHz, $CDCl_3$)

cis (minor): δ 4.02 (s, 2H, H_4); 3.58 – 3.45 (m, 2H, $H_{3\,(ax/eq)}$); 3.43 – 3.26 (m, 2H, $H_{3\,(ax/eq)}$); 1.97 (s, 2H, H_5); 1.73 – 1.40 (m, 8H, H_{1+2+7}); 1.36 – 1.26 (m, 2H, H_8); 0.89 (t, *J* = 7.3 Hz, 3H, H_9).

Note: H_6 peak unassignable for *cis* rotamer

trans (major): δ 4.14 (s, 2H, H_4); 3.58 – 3.45 (m, 2H, $H_{3\,(ax/eq)}$); 3.43 – 3.26 (m, 4H, $H_{3\,(ax/eq)\,+\,6}$); 2.14 (s, 2H, H_5); 1.73 – 1.40 (m, 8H, H_{1+2+7}); 1.36 – 1.26 (m, 2H, H_8); 0.93 (t, *J* = 7.3 Hz, 3H, H_9).

^{13}C NMR (151 MHz, $CDCl_3$)

cis (minor): δ 171.19 (CO-CH_3); 165.73 (CO-pip); 49.88 (CH_2, C_4); 47.13 (CH_2, C_6); 45.73, 43.37 (CH_2, C_3); 29.69 (CH_2, C_7); 26.48, 25.51 (CH_2, C_2); 24.33 (CH_2, C_1); 21.57 (CH_3, C_5); 20.17 (CH_2, C_8); 13.86 (CH_3, C_9).

trans (major): δ 170.75 (CO-CH_3); 166.40 (CO-pip); 49.29 (CH_2, C_6); 46.33 (CH_2, C_4); 45.99, 43.08 (CH_2, C_3); 30.50 (CH_2, C_7); 26.26, 25.43 (CH_2, C_2); 24.43 (CH_2, C_1); 21.04 (CH_3, C_5); 20.02 (CH_2, C_8); 13.78 (CH_3, C_9).

^{1}H NMR (599 MHz, CD_3CN)

cis (minor): δ 4.09 (s, 2H, H_4); 3.51 – 3.41 (m, 2H, $H_{3\,(ax/eq)}$); 3.40 – 3.31 (m, 2H, $H_{3\,(ax/eq)}$); 3.22 (t, *J* = 7.5 Hz, 2H, H_6); 1.84 (s, 3H, H_5); 1.69 – 1.36 (m, 8H, H_{1+2+7}); 1.36 – 1.20 (m, 2H, H_8); 0.90 (t, *J* = 7.4 Hz, 3H, H_9).

trans (major): δ 4.08 (s, 2H, H_4); 3.51 – 3.41 (m, 2H, $H_{3\ (ax/eq)}$); 3.40 – 3.31 (m, 2H, $H_{3\ (ax/eq)}$); 3.26 (t, *J* = 7.7 Hz, 2H, H_6); 2.04 (s, 3H, H_5); 1.69 – 1.36 (m, 8H, H_{1+2+7}); 1.36 – 1.20 (m, 2H, H_8); 0.92 (t, *J* = 7.4 Hz, 3H, H_9).

^{13}C NMR (151 MHz, CD_3CN)

cis (minor): δ 171.00 (CO-CH_3); 166.24 (CO-pip); 49.67 (CH_2, C_4); 46.37 (CH_2, C_6); 45.28, 42.80 (CH_2, C_3); 29.53 (CH_2, C_7); 26.08, 25.45 (CH_2, C_2); 24.14 (CH_2, C_1); 20.85 (CH_3, C_5); 19.84 (CH_2, C_8); 13.22 (CH_3, C_9).

trans (major): δ 170.06 (CO-CH_3); 166.30 (CO-pip); 49.09 (CH_2, C_6); 46.39 (CH_2, C_4); 45.36, 42.50 (CH_2, C_3); 30.30 (CH_2, C_7); 26.02, 25.41 (CH_2, C_2); 24.19 (CH_2, C_1); 20.37 (CH_3, C_5); 19.70 (CH_2, C_8); 13.14 (CH_3, C_9).

^{1}H NMR (599 MHz, CD_3OD)

cis (minor): δ 4.30 (s, 2H, H_4); 3.58 – 3.50 (m, 2H, $H_{3\ (ax/eq)}$); 3.49 – 3.42 (m, 2H, $H_{3\ (ax/eq)}$); 3.39 – 3.29 (m, 2H, H_6); 1.96 (s, 3H, H_5); 1.75 – 1.45 (m, 8H, H_{1+2+7}); 1.42 – 1.25 (m, 2H, H_8); 0.93 (t, *J* = 7.4 Hz, 3H, H_9).

Note: H_6 peak overlapped with solvent for *cis* rotamer

trans (major): δ 4.20 (s, 2H, H_4); 3.58 – 3.50 (m, 2H, $H_{3\ (ax/eq)}$); 3.49 – 3.42 (m, 2H, $H_{3\ (ax/eq)}$); 3.35 (t, *J* = 7.7 Hz, 2H, H_6); 2.15 (s, 3H, H_5); 1.75 – 1.45 (m, 8H, H_{1+2+7}); 1.42 – 1.25 (m, 2H, H_8); 0.97 (t, *J* = 7.4 Hz, 3H, H_9).

^{13}C NMR (151 MHz, CD_3OD)

cis (minor): δ 172.98 (CO-CH_3); 166.70 (CO-pip); 49.77 (CH_2, C_4); 45.42, 43.11 (CH_2, C_3); 29.23 (CH_2, C_7); 26.02, 25.32 (CH_2, C_2); 23.91 (CH_2, C_1); 20.06 (CH_3, C_5); 12.79 (CH_3, C_9).

trans (major): δ 172.18 (CO-CH_3); 166.85 (CO-pip); 49.69 (CH_2, C_6); 46.65 (CH_2, C_4); 45.58, 42.93 (CH_2, C_3); 30.07 (CH_2, C_7); 25.82, 25.20 (CH_2, C_2); 23.97 (CH_2, C_1); 19.73 (CH_3, C_5); 19.60 (CH_2, C_8); 12.72 (CH_3, C_9).

Note: C_6 and C_8 peaks unassignable for *cis* rotamer.

Compound 96: *N*-amyl-*N*-(2-oxo-2-(piperidin-1-yl)ethyl)acetamide

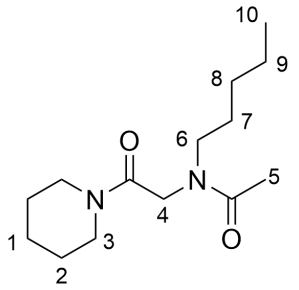

2-Bromo-1-(piperidin-1-yl)ethenone (**93**) was dissolved in MeCN (5 mL) and added dropwise to a solution of amylamine (296 mg, 4 equiv.) in MeCN (10 mL) at 0 °C under an N_2 atmosphere. The reaction was allowed to warm to room temperature and stirred for 16 h following the general protocol described in **Section 5.3.2**. The reaction was then concentrated under reduced pressure and acetylated as per **Section 5.3.5**, before purification by flash column chromatography (**Section 5.3.6**). This gave *N*-amyl-*N*-(2-oxo-2-(piperidin-1-yl)ethyl)acetamide (**96**) as a yellow oil (121 mg, 56%). HRMS (ESI^+): calculated for $C_{14}H_{26}N_2O_2^+$ 255.2084 $[M+H]^+$, found: 255.2082 Da.

^{1}H NMR (599 MHz, $CDCl_3$)

cis (minor): δ 4.02 (s, 2H, H_4); 3.58 – 3.49 (m, 2H, $H_{3\,(ax/eq)}$); 3.40 – 3.30 (m, 2H, $H_{3\,(ax/eq)}$); 1.97 (s, 2H, H_5); 1.70 – 1.43 (m, 8H, H_{1+2+7}); 1.37 – 1.21 (m, 4H, H_{8+9}); 0.92 - 0.83 (m, 3H, H_{10}).

Note: H_6 peak unassignable for *cis* rotamer.

trans (major): δ 4.13 (s, 2H, H_4); 3.58 – 3.49 (m, 2H, $H_{3\,(ax/eq)}$); 3.40 – 3.30 (m, 2H, $H_{3\,(ax/eq)\,+\,6}$); 2.13 (s, 2H, H_5); 1.70 – 1.43 (m, 8H, H_{1+2+7}); 1.37 – 1.21 (m, 4H, H_{8+9}); 0.92 - 0.83 (m, 3H, H_{10}).

^{13}C NMR (151 MHz, $CDCl_3$)

cis (minor): δ 171.22 ($CO\text{-}CH_3$); 165.74 (CO-pip); 49.89 (CH_2, C_4); 47.37 (CH_2, C_6); 46.74, 43.38 (CH_2, C_3); 29.11 (CH_2, C_8); 27.27 (CH_2, C_7); 26.49, 25.52 (CH_2, C_2); 24.34 (CH_2, C_1); 22.47 (CH_2, C_9); 21.58 (CH_3, C_5); 14.01 (CH_3, C_{10}).

trans (major): δ 170.79 ($CO\text{-}CH_3$); 166.41 (CO-pip); 49.51 (CH_2, C_6); 46.32 (CH_2, C_4); 46.00, 43.09 (CH_2, C_3); 28.95 (CH_2, C_8); 28.09 (CH_2, C_7); 26.27, 25.44 (CH_2, C_2); 24.43 (CH_2, C_1); 22.40 (CH_2, C_9); 21.07 (CH_3, C_5); 13.96 (CH_3, C_{10}).

^{1}H NMR (599 MHz, CD_3CN)

cis (minor): δ 4.09 (s, 2H, H_4); 3.51 – 3.41 (m, 2H, $H_{3\,(ax/eq)}$); 3.39 – 3.32 (m, 2H, $H_{3\,(ax/eq)}$); 3.21 (t, J = 7.5 Hz, 2H, H_6); 1.84 (s, 2H, H_5); 1.70 – 1.39 (m, 8H, H_{1+2+7}); 1.39 – 1.15 (m, 4H, H_{8+9}); 0.93 - 0.85 (m, 3H, H_{10}).

trans (major): δ 4.08 (s, 2H, H_4); 3.51 – 3.41 (m, 2H, $H_{3\ (ax/eq)}$); 3.39 – 3.32 (m, 2H, $H_{3\ (ax/eq)}$); 3.25 (t, *J* = 7.8 Hz, 2H, H_6); 2.04 (s, 2H, H_5); 1.70 – 1.39 (m, 8H, H_{1+2+7}); 1.39 – 1.15 (m, 4H, H_{8+9}); 0.93 - 0.85 (m, 3H, H_{10}).

^{13}C NMR (151 MHz, CD_3CN)

cis (minor): δ 171.00 ($CO\text{-}CH_3$); 166.26 (CO-pip); 49.69 (CH_2, C_4); 46.66 (CH_2, C_6); 45.29, 42.81 (CH_2, C_3); 28.88 (CH_2, C_8); 27.08 (CH_2, C_7); 26.10, 25.47 (CH_2, C_2); 24.15 (CH_2, C_1); 22.23 (CH_2, C_9); 20.87 (CH_3, C_5); 13.37 (CH_3, C_{10}).

trans (major): δ 170.06 ($CO\text{-}CH_3$); 166.31 (CO-pip); 49.29 (CH_2, C_6); 46.35 (CH_2, C_4); 45.38, 42.52 (CH_2, C_3); 28.68 (CH_2, C_8); 27.87 (CH_2, C_7); 26.04, 25.42 (CH_2, C_2); 24.20 (CH_2, C_1); 22.18 (CH_2, C_9); 20.39 (CH_3, C_5); 13.33 (CH_3, C_{10}).

^{1}H NMR (599 MHz, CD_3OD)

cis (minor): δ 4.29 (s, 2H, H_4); 3.60 – 3.42 (m, 2H, $H_{3\ (ax/eq)}$); 3.40 – 3.25 (m, 2H, H_6); 1.95 (s, 2H, H_5); 1.73 – 1.46 (m, 8H, H_{1+2+7}); 1.42 – 1.22 (m, 4H, H_{8+9}); 0.96 - 0.87 (m, 3H, H_{10}).

trans (major): δ 4.20 (s, 2H, H_4); 3.60 – 3.42 (m, 2H, $H_{3\ (ax/eq)}$); 3.40 – 3.25 (m, 2H, H_6); 2.14 (s, 2H, H_5); 1.73 – 1.46 (m, 8H, H_{1+2+7}); 1.42 – 1.22 (m, 4H, H_{8+9}); 0.96 - 0.87 (m, 3H, H_{10}).

^{13}C NMR (151 MHz, CD_3OD)

cis (minor): δ 172.96 ($CO\text{-}CH_3$); 166.71 (CO-pip); 49.89 (CH_2, C_4); 45.43, 43.11 (CH_2, C_3); 28.81 (CH_2, C_8); 26.78 (CH_2, C_7); 26.04, 25.33 (CH_2, C_2); 23.93 (CH_2, C_1); 22.12 (CH_2, C_9); 20.07 (CH_3, C_5); 12.94 (CH_3, C_{10}).

Note: C_6 peak not detected for *cis* rotamer.

trans (major): δ 172.16 ($CO\text{-}CH_3$); 166.86 (CO-pip); 49.79 (CH_2, C_6); 46.65 (CH_2, C_4); 45.60, 42.93 (CH_2, C_3); 28.64 (CH_2, C_8); 27.67 (CH_2, C_7); 25.84, 25.22 (CH_2, C_2); 23.99 (CH_2, C_1); 22.09 (CH_2, C_9); 19.62 (CH_3, C_5); 12.93 (CH_3, C_{10}).

Compound 97: *N*-^{i}butyl-*N*-(2-oxo-2-(piperidin-1-yl)ethyl)acetamide

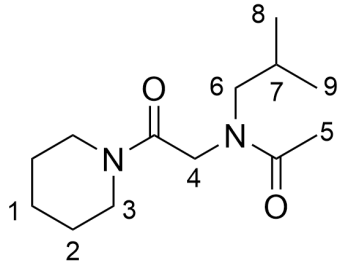

2-Bromo-1-(piperidin-1-yl)ethenone (**93**) was dissolved in MeCN (5 mL) and added dropwise to a solution of isobutylamine (249 mg, 4 equiv.) in MeCN (10 mL) at 0 °C under an N_2 atmosphere. The reaction was allowed to warm to room temperature and stirred for 16 h

following the general protocol described in **Section 5.3.2**. The reaction was then concentrated under reduced pressure and acetylated as per **Section 5.3.5**, before purification by flash column chromatography (**Section 5.3.6**). This gave *N*-^{i}butyl-*N*-(2-oxo-2-(piperidin-1-yl)ethyl)acetamide (**97**) as a yellow oil (63 mg, 31%). HRMS (ESI^{+}): calculated for $C_{13}H_{24}N_2O_2^{+}$ 241.1916 $[M+H]^{+}$, found: 241.1931 Da.

^{1}H NMR (599 MHz, $CDCl_3$)

cis (minor): δ 4.02 (s, 2H, H_4); 3.57 – 3.44 (m, 2H, $H_{3\,(ax/eq)}$); 3.39 – 3.29 (m, 2H, $H_{3\,(ax/eq)}$); 1.97 (s, 2H, H_5); 1.93 – 1.80 (m, 1H, H_7); 1.70 – 1.43 (m, 6H, H_{1+2}); 0.86 (d, *J* = 6.6 Hz, 6H, H_{8+9}).

Note: H_6 peak not detected for *cis* rotamer

trans (major): δ δ 4.12 (s, 2H, H_4); 3.57 – 3.44 (m, 2H, $H_{3\,(ax/eq)}$); 3.39 – 3.29 (m, 2H, $H_{3\,(ax/eq)}$); 3.17 (d, *J* = 7.5 Hz, 2H, H_6); 2.12 (s, 2H, H_5); 1.93 – 1.80 (m, 1H, H_7); 1.70 – 1.43 (m, 6H, H_{1+2}); 0.91 (d, *J* = 6.7 Hz, 6H, H_{8+9}).

^{13}C NMR (151 MHz, $CDCl_3$)

cis (minor): δ 171.65 (CO-CH_3); 165.70 (CO-pip); 54.54 (CH_2, C_6); 50.44 (CH_2, C_4); 45.70, 43.35 (CH_2, C_3); 27.05 (CH, C_7); 26.47, 25.50 (CH_2, C_2); 24.31 (CH_2, C_1); 21.62 (CH_3, C_5); 20.16 (CH_3, C_{8+9}).

trans (major): δ 171.34 (CO-CH_3); 166.27 (CO-pip); 56.86 (CH_2, C_6); 46.64 (CH_2, C_4); 45.94, 43.06 (CH_2, C_3); 27.55 (CH, C_7); 26.24, 25.41 (CH_2, C_2); 24.42 (CH_2, C_1); 21.33 (CH_3, C_5); 20.04 (CH_3, C_{8+9}).

^{1}H NMR (599 MHz, CD_3CN)

cis (minor): δ 4.09 (s, 2H, H_4); 3.50 – 3.42 (m, 2H, $H_{3\,(ax/eq)}$); 3.38 – 3.31 (m, 2H, $H_{3\,(ax/eq)}$); 3.06 (d, *J* = 7.4 Hz, 2H, H_6); 1.86 (s, 2H, H_5); 1.85 – 1.79 (m, 1H, H_7); 1.68 – 1.42 (m, 6H, H_{1+2}); 0.85 (d, *J* = 6.6 Hz, 6H, H_{8+9}).

trans (major): δ 4.07 (s, 2H, H_4); 3.50 – 3.42 (m, 2H, $H_{3\,(ax/eq)}$); 3.38 – 3.31 (m, 2H, $H_{3\,(ax/eq)}$); 3.11 (d, *J* = 7.5 Hz, 2H, H_6); 2.04 (s, 2H, H_5); 1.92 – 1.87 (m, 1H, H_7); 1.70 – 1.43 (m, 6H, H_{1+2}); 0.85 (d, *J* = 6.6 Hz, 6H, H_{8+9}).

^{13}C NMR (151 MHz, CD_3CN)

cis (minor): δ 171.44 (CO-CH_3); 53.83 (CH_2, C_6); 50.19 (CH_2, C_4); 45.26, 42.79 (CH_2, C_3); 28.60 (CH, C_7); 26.07, 25.46 (CH_2, C_2); 24.14 (CH_2, C_1); 20.92 (CH_3, C_5); 19.44 (CH_3, C_{8+9}).

Note: CO-pip peak not detected for *cis* rotamer

trans (major): δ 170.53 (CO-CH_3); 166.19 (CO-pip); 56.51 (CH_2, C_6); 46.71 (CH_2, C_4); 45.35, 42.50 (CH_2, C_3); 27.34 (CH, C_7); 26.02, 25.42 (CH_2, C_2); 24.20 (CH_2, C_1); 20.71 (CH_3, C_5); 19.23 (CH_3, C_{8+9}).

^{1}H NMR (599 MHz, CD_3OD)

cis (minor): δ 4.30 (s, 2H, H_4); 3.58 – 3.50 (m, 2H, $H_{3\ (ax/eq)}$); 3.49 – 3.42 (m, 2H, $H_{3\ (ax/eq)}$); 3.16 (d, *J* = 7.5 Hz, 2H, H_6); 1.97 (s, 2H, H_5); 1.96 – 1.85 (m, 1H, H_7); 1.76 – 1.48 (m, 6H, H_{1+2}); 0.90 (d, *J* = 6.7 Hz, 6H, H_{8+9}).

trans (major): δ 4.20 (s, 2H, H_4); 3.58 – 3.50 (m, 2H, $H_{3\ (ax/eq)}$); 3.49 – 3.42 (m, 2H, $H_{3\ (ax/eq)}$); 3.20 (d, *J* = 7.6 Hz, 2H, H_6); 2.15 (s, 2H, H_5); 1.96 – 1.85 (m, 1H, H_7); 1.76 – 1.48 (m, 6H, H_{1+2}); 0.96 (d, *J* = 6.7 Hz, 6H, H_{8+9}).

^{13}C NMR (151 MHz, CD_3OD)

cis (minor): δ 173.40 (CO-CH_3); 166.63 (CO-pip); 54.50 (CH_2, C_6); 50.23 (CH_2, C_4); 45.40, 43.09 (CH_2, C_3); 26.72 (CH, C_7); 26.02, 25.32 (CH_2, C_2); 23.92 (CH_2, C_1); 20.12 (CH_3, C_5); 19.10 (CH_3, C_{8+9}).

trans (major): δ 172.66 (CO-CH_3); 166.74 (CO-pip); 57.00 (CH_2, C_6); 46.93 (CH_2, C_4); 45.60, 42.93 (CH_2, C_3); 27.30 (CH, C_7); 25.82, 25.21 (CH_2, C_2); 23.99 (CH_2, C_1); 19.95 (CH_3, C_5); 18.86 (CH_3, C_{8+9}).

Compound 98: *N*-(3,3,3-trifluoropropyl)-*N*-(2-oxo-2-(piperidin-1-yl)ethyl)acetamide

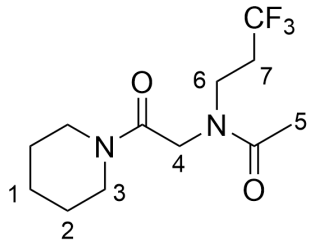

2-Bromo-1-(piperidin-1-yl)ethenone (**93**) was dissolved in MeCN (5 mL) and added dropwise to a solution of 3,3,3-trifluoropropylamine (384 mg, 4 equiv.) in MeCN (10 mL) at 0 °C under an N_2 atmosphere. The reaction was allowed to warm to room temperature and stirred for 16 h following the general protocol described in **Section 5.3.2**. The reaction was then concentrated under reduced pressure and acetylated as per **Section 5.3.5**, before purification by flash column chromatography (**Section 5.3.6**). This gave *N*-(3,3,3-trifluoropropyl)-*N*-(2-oxo-2-(piperidin-1-yl)ethyl)acetamide (**98**) as a yellow oil (28 mg, 12%). HRMS (ESI$^+$): calculated for $C_{12}H_{19}F_3N_2O_2^+$ 281.1486 $[M+H]^+$, found: 281.1487 Da.

^{1}H NMR (599 MHz, $CDCl_3$)

cis (minor): δ 4.08 (s, 2H, H_4); 3.59 – 3.55 (m, 2H, $H_{3\ (ax/eq)}$); 3.52 (t, *J* = 7.1 Hz, 2H, H_6); 3.41 – 3.32 (m, 2H, $H_{3\ (ax/eq)}$); 2.55 – 2.41 (m, 2H, H_7); 1.98 (s, 2H, H_5); 1.75 – 1.48 (m, 6H, H_{1+2}).

Note: Overlap between $H_{3\ (ax/eq)}$ and H_6 for *cis* rotamer.

trans (major): δ 4.14 (s, 2H, H_4); 3.66 (t, *J* = 7.4 Hz, 2H, H_6); 3.59 – 3.55 (m, 2H, $H_{3\ (ax/eq)}$); 3.41 – 3.32 (m, 2H, $H_{3\ (ax/eq)}$); 2.55 – 2.41 (m, 2H, H_7); 2.18 (s, 2H, H_5); 1.75 – 1.48 (m, 6H, H_{1+2}).

^{13}C NMR (151 MHz, $CDCl_3$)

cis (minor): δ 171.56 (CO-CH_3); 165.39 (CO-pip); 126.15 (m, CF_3); 51.56 (CH_2, C_4); 45.75, 43.45 (CH_2, C_3); 42.68 – 45.52 (m, CH_2, C_6); 32.06 (q, *J* = 27.7 Hz, CH_2, C_7); 26.44, 25.48 (CH_2, C_2); 24.27 (CH_2, C_1); 21.46 (CH_3, C_5).

trans (major): δ 170.69 (CO-CH_3); 165.86 (CO-pip); 126.15 (m, CF_3); 47.00 (CH_2, C_4); 43.32 – 43.21 (m, CH_2, C_6); 46.04, 43.19 (CH_2, C_3); 33.06 (q, J = 27.9 Hz, CH_2, C_7); 26.25, 25.40 (CH_2, C_2); 24.37 (CH_2, C_1); 20.90 (CH_3, C_5).

^{19}F NMR (376 MHz, $CDCl_3$)

δ -65.17 (t, *J* = 11.2 Hz, CF_3 *cis*); -65.39 (t, *J* = 10.7 Hz, CF_3 *trans*).

^{1}H NMR (599 MHz, CD_3CN)

cis (major): δ 4.16 (s, 2H, H_4); 3.52 – 3.43 (m, 2H, $H_{3\ (ax/eq)}$ + H_6); 3.39 – 3.31 (m, 2H, $H_{3\ (ax/eq)}$); 2.61 – 2.35 (m, 2H, H_7); 1.86 (s, 2H, H_5); 1.70 – 1.40 (m, 6H, H_{1+2}).

Note: Overlap between $H_{3\ (ax/eq)}$ and H_6 for *cis* rotamer.

trans (minor): δ 4.10 (s, 2H, H_4); 3.58 (t, *J* = 7.9 Hz, 2H, H_6); 3.52 – 3.43 (m, 2H, $H_{3\ (ax/eq)}$); 3.39 – 3.41 (m, 2H, $H_{3\ (ax/eq)}$); 2.61 – 2.35 (m, 2H, H_7); 2.08 (s, 2H, H_5); 1.70 – 1.40 (m, 6H, H_{1+2}).

^{13}C NMR (151 MHz, CD_3CN)

cis (major): δ 171.52 (CO-CH_3); 165.99 (CO-pip); 126.84 (q, *J* = 275.7 Hz, CF_3); 50.74 (CH_2, C_4); 45.27, 42.83 (CH_2, C_3); 41.04 (q, *J* = 3.9 Hz, CH_2, C_6); 31.33 (q, *J* = 27.3 Hz, CH_2, C_7); 25.99, 25.39 (CH_2, C_2); 24.09 (CH_2, C_1); 20.73 (CH_3, C_5).

trans (minor): δ 170.23 (CO-CH_3); 126.37 (q, *J* = 276.5 Hz, CF_3); 46.67 (CH_2, C_4); 42.77 – 42.63 (m, CH_2, C_6); 45.36, 42.56 (CH_2, C_3); 32.14 (q, *J* = 27.2 Hz, CH_2, C_7); 25.98, 25.37 (CH_2, C_2); 24.15 (CH_2, C_1); 20.25 (CH_3, C_5).

Note: CO-pip not detected for *trans* rotamer.

^{19}F NMR (376 MHz, CD_3CN)

δ -65.96 (t, *J* = 11.2 Hz, CF_3 *trans*); -66.08 (t, *J* = 11.4 Hz, CF_3 *cis*).

^{1}H NMR (599 MHz, CD_3OD)

cis (major): δ 4.37 (s, 2H, H_4); 3.60 – 3.50 (m, 2H, $H_{3\ (ax/eq)}$ + H_6); 3.49 – 3.39 (m, 2H, $H_{3\ (ax/eq)}$); 2.68 – 2.53 (m, 2H, H_7); 1.97 (s, 2H, H_5); 1.80 – 1.44 (m, 6H, H_{1+2}).

Note: Overlap between $H_{3\ (ax/eq)}$ and H_6 for *cis* rotamer.

trans (minor): δ 4.24 (s, 2H, H_4); 3.66 (t, *J* = 7.7 Hz, 2H, H_6); 3.60 – 3.50 (m, 2H, $H_{3\ (ax/eq)}$); 3.49 – 3.39 (m, 2H, $H_{3\ (ax/eq)}$); 2.68 – 2.53 (m, 2H, H_7); 2.19 (s, 2H, H_5); 1.80 – 1.44 (m, 6H, H_{1+2}).

^{13}C NMR (151 MHz, CD_3OD)

cis (major): δ 177.26 ($CO\text{-}CH_3$); 170.48 (CO-pip); 130.40 (q, *J* = 275.6 Hz, CF_3); 54.65 (CH_2, C_4); 49.35, 47.06 (CH_2, C_3); 45.60 – 45.41 (m, CH_2, C_6); 35.03 (q, *J* = 27.8 Hz, CH_2, C_7); 29.89, 29.22 (CH_2, C_2); 27.82 (CH_2, C_1); 23.90 (CH_3, C_5).

trans (minor): δ 176.21 ($CO\text{-}CH_3$); 170.54 (CO-pip); 129.82 (q, *J* = 276.9 Hz, CF_3); 50.65 (CH_2, C_4); 49.53, 46.90 (CH_2, C_3); 35.67 (q, *J* = 27.8 Hz, CH_2, C_7); 29.73, 29.22 (CH_2, C_2); 27.90 (CH_2, C_1); 23.42 (CH_3, C_5).

Note: C_6 not detected for *trans* rotamer.

^{19}F NMR (376 MHz, CD_3OD)

δ -66.86 (t, *J* = 11.0 Hz, CF_3 *trans*); -67.10 (t, *J* = 11.1 Hz, CF_3 *cis*).

Compound 99: *N*-(4,4,4-trifluorobutyl)-*N*-(2-oxo-2-(piperidin-1-yl)ethyl)acetamide

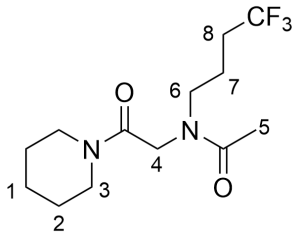

2-Bromo-1-(piperidin-1-yl)ethenone (**93**) was dissolved in MeCN (5 mL) and added dropwise to a solution of 4,4,4-trifluorobutylamine (432 mg, 4 equiv.) in MeCN (10 mL) at 0 °C under an N_2 atmosphere. The reaction was allowed to warm to room temperature and stirred for 16 h following the general protocol described in **Section 5.3.2**. The reaction was then concentrated under reduced pressure and acetylated as per **Section 5.3.5**, before purification by flash column chromatography (**Section 5.3.6**). This gave *N*-(4,4,4-trifluorobutyl)-*N*-(2-oxo-2-(piperidin-1-yl)ethyl)acetamide (**99**) as a yellow oil (46 mg, 18%). HRMS (ESI^+): calculated for $C_{13}H_{21}F_3N_2O_2^+$ 295.1642 $[M+H]^+$, found: 295.1641 Da.

^{1}H NMR (599 MHz, $CDCl_3$)

cis (minor): δ 4.04 (s, 2H, H_4); 3.60 – 3.49 (m, 2H, $H_{3\ (ax/eq)}$); 3.48 – 3.41 (m, 2H, H_6); 3.41 – 3.33 (m, 2H, $H_{3\ (ax/eq)}$); 2.14 – 2.08 (m, 2H, H_8); 1.99 (s, 2H, H_5); 1.79 – 1.71 (m, 2H, H_7); 1.71 – 1.50 (m, 6H, H_{1+2}).

Note: Overlap between H_6 peaks of the *cis* and *trans* rotamers.

trans (major): δ 4.13 (s, 2H, H_4); 3.60 – 3.49 (m, 2H, $H_{3\ (ax/eq)}$); 3.48 – 3.41 (m, 2H, H_6); 3.41 – 3.33 (m, 2H, $H_{3\ (ax/eq)}$); 2.15 (s, 2H, H_5); 2.14 – 2.08 (m, 2H, H_8); 1.89 – 1.81 (m, 2H, H_7); 1.71 – 1.50 (m, 6H, H_{1+2}).

^{13}C NMR (151 MHz, $CDCl_3$)

cis (minor): δ 171.70 (CO-CH_3); 165.39 (CO-pip); 127.13 (q, *J* = 275.6 Hz, CF_3); 50.14 (CH_2, C_4); 48.32 (CH_2, C_6); 45.75, 43.44 (CH_2, C_3); 31.30 (q, *J* = 28.8 Hz, CH_2, C_8); 26.48, 25.48 (CH_2, C_2); 24.29 (CH_2, C_1); 21.48 (CH_3, C_5); 20.54 – 20.35 (m, CH_2, C_7).

Note: Only one peak detected for C_6.

trans (major): δ 170.72 (CO-CH_3); 166.01 (CO-pip); 126.76 (q, *J* = 275.6 Hz, CF_3); 48.32 (CH_2, C_6); 46.35 (CH_2, C_4); 46.02, 43.14 (CH_2, C_3); 30.85 (q, 29.3 Hz, CH_2, C_8); 26.26, 25.40 (CH_2, C_2); 24.39 (CH_2, C_1); 21.11 – 21.05 (m, CH_2, C_7); 21.03 (CH_3, C_5).

^{19}F NMR (376 MHz, $CDCl_3$)

δ -65.98 (t, *J* = 10.7 Hz, CF_3 *trans*); -66.25 (t, *J* = 11.0 Hz, CF_3 *cis*).

^{1}H NMR (599 MHz, CD_3CN)

cis (major): δ 4.12 (s, 2H, H_4); 3.51 – 3.42 (m, 2H, $H_{3\ (ax/eq)}$); 3.39 – 3.33 (m, 2H, $H_{3\ (ax/eq)}$); 3.32 (t, *J* = 7.1 Hz, 2H, H_6); 2.28 – 2.21 (m, 2H, H_8); 1.86 (s, 2H, H_5); 1.74 – 1.66 (m, 2H, H_7); 1.66 – 1.42 (m, 6H, H_{1+2}).

Note: Overlap between $H_{3\ (ax/eq)}$ and H_6 peak for the *trans* rotamer.

trans (minor): δ 4.08 (s, 2H, H_4); 3.51 – 3.42 (m, 2H, $H_{3\ (ax/eq)}$); 3.39 – 3.33 (m, 2H, $H_{3\ (ax/eq)\ +\ 6}$); 2.28 – 2.21 (m, 2H, H_8); 2.05 (s, 2H, H_5); 1.84 – 1.75 (m, 2H, H_7); 1.66 – 1.42 (m, 6H, H_{1+2}).

^{13}C NMR (151 MHz, CD_3CN)

cis (major): δ 171.70 (CO-CH_3); 165.39 (CO-pip); 127.76 (q, *J* = 276.8 Hz, CF_3); 50.14 (CH_2, C_4); 48.32 (CH_2, C_6); 45.28, 42.84 (CH_2, C_3); 30.68 (q, *J* = 28.7 Hz, CH_2, C_8); 26.05, 25.44 (CH_2, C_2); 24.29 (CH_2, C_1); 21.48 (CH_3, C_5); 20.22 (q, *J* = 3.0 Hz, CH_2, C_7).

Note: Only one peak detected for C_6.

trans (minor): δ 171.61 (CO-CH_3); 166.17 (CO-pip); 127.62 (q, *J* = 278.8 Hz, CF_3); 50.05 (CH_2, C_4); 45.69 (CH_2, C_6); 45.36, 42.55 (CH_2, C_3); 30.18 (q, *J* = 28.6 Hz, CH_2, C_8); 26.01, 25.40 (CH_2, C_2); 24.11 (CH_2, C_1); 20.85 (q, *J* = 2.9 Hz, CH_2, C_7); 20.39 (CH_3, C_5).

^{19}F NMR (376 MHz, CD_3CN)

δ -61.46 (t, *J* = 11.3 Hz, CF_3 *trans*); -61.65 (t, *J* = 11.4 Hz, CF_3 *cis*).

^{1}H NMR (599 MHz, CD_3OD)

cis (minor): δ 4.33 (s, 2H, H_4); 3.58 – 3.51 (m, 2H, $H_{3\ (ax/eq)}$); 3.48 – 3.43 (m, 2H, $H_{3\ (ax/eq)}$); 3.41 (t, *J* = 7.2 Hz, 2H, H_6); 2.30 – 2.17 (m, 2H, H_8); 1.97 (s, 2H, H_5); 1.80 – 1.73 (m, 2H, H_7); 1.73 – 1.51 (m, 6H, H_{1+2}).

Note: Overlap between $H_{3\ (ax/eq)}$ and H_6 peak for the *trans* rotamer.

trans (major): δ 4.22 (s, 2H, H_4); 3.58 – 3.51 (m, 2H, $H_{3\ (ax/eq)}$); 3.48 – 3.43 (m, 2H, $H_{3\ (ax/eq)\ +\ 6}$); 2.30 – 2.17 (m, 2H, H_8); 2.16 (s, 2H, H_5); 1.90 – 1.82 (m, 2H, H_7); 1.73 – 1.51 (m, 6H, H_{1+2}).

^{13}C NMR (151 MHz, CD_3OD)

cis (minor): δ 173.48 ($CO\text{-}CH_3$); 166.62 (CO-pip); 127.35 (q, *J* = 275.9 Hz, CF_3); 50.12 (CH_2, C_4); 46.47 (CH_2, C_6); 45.42, 43.13 (CH_2, C_3); 30.11 (q, *J* = 29.3 Hz, CH_2, C_8); 25.80, 25.19 (CH_2, C_2); 23.97 (CH_2, C_1); 20.09 – 20.03 (m, CH_3, C_7); 20.02 (CH_2, C_5).

trans (major): δ 172.25 ($CO\text{-}CH_3$); 166.72 (CO-pip); 127.25 (q, *J* = 279.6 Hz, CF_3); 48.65 (CH_2, C_6); 46.83 (CH_2, C_4); 45.58, 42.95 (CH_2, C_3); 30.66 (q, *J* = 29.3 Hz, CH_2, C_8); 25.99, 25.30 (CH_2, C_2); 23.90 (CH_2, C_1); 20.80 – 20.63 (m, CH_3, C_7); 19.57 (CH_2, C_5).

^{19}F NMR (376 MHz, CD_3OD)

δ -67.67 (t, *J* = 11.1 Hz, CF_3); -67.95 (t, *J* = 11.2 Hz, CF_3).

Note: No major rotamer present in ^{19}F NMR making *cis* and *trans* indistinguishable.

Compound 100: *N*-(5,5,5-trifluoroamyl)-*N*-(2-oxo-2-(piperidin-1-yl)ethyl)acetamide

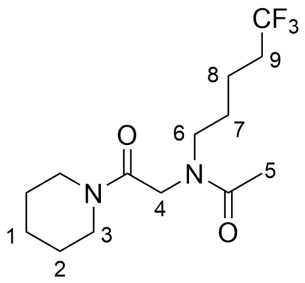

1,1,1-trifluoro-5-iodopentane (214 mg, 1 equiv.) was dissolved in MeCN (5 mL) and added dropwise to a solution of 2-amino-1-(piperidin-1-yl)ethan-1-one (**107**) in MeCN (10 mL) at 0 °C under an N_2 atmosphere. The reaction was allowed to warm to room temperature and stirred for 16 h following the general protocol described in **Section 5.3.4**. The reaction was then concentrated under reduced pressure and acetylated as per **Section 5.3.5**, before purification by flash column chromatography (**Section 5.3.6**). This gave *N*-(5,5,5-trifluoroamyl)-*N*-(2-oxo-2-(piperidin-1-yl)ethyl)acetamide (**100**) as a yellow oil (32 mg, 12%). HRMS (ESI$^+$): calculated for $C_{14}H_{23}F_3N_2O_2^+$ 309.1790 $[M+H]^+$, found: 309.1053 Da.

^{1}H NMR (599 MHz, $CDCl_3$)

cis (minor): δ 4.03 (s, 2H, H_4); 3.60 – 3.47 (m, 2H, $H_{3\,(ax/eq)}$); 3.44 – 3.25 (m, 2H, $H_{3\,(ax/eq)}$); 2.12 – 2.05 (m, 2H, H_9); 1.98 (s, 2H, H_5); 1.75 – 1.47 (m, 10H, $H_{1+2+7+8}$).

Note: H_6 peak unassignable for the *cis* rotamer.

trans (major): δ 4.14 (s, 2H, H_4); 3.60 – 3.47 (m, 2H, $H_{3\,(ax/eq)}$); 3.44 – 3.25 (m, 2H, $H_{3\,(ax/eq)\,+\,6}$); 2.14 (s, 2H, H_5); 2.12 – 2.05 (m, 2H, H_9); 1.75 – 1.47 (m, 6H, $H_{1+2+7+8}$).

^{13}C NMR (151 MHz, $CDCl_3$)

cis (minor): δ 171.39 (CO-CH_3); 165.54 (CO-pip); 129.93 – 123.85 (m, CF_3); 50.24 (CH_2, C_4); 47.01 (CH_2, C_6); 45.73, 43.41 (CH_2, C_3); 33.74 – 32.98 (m, CH_2, C_9); 26.64 (CH_2, C_8); 26.12, 25.51 (CH_2, C_2); 24.31 (CH_2, C_1); 21.53 (CH_3, C_5); 19.50 – 19.28 (m, CH_2, C_7).

trans (major): δ 170.66 (CO-CH_3); 166.19 (CO-pip); 129.93 – 123.85 (m, CF_3); 49.15 (CH_2, C_6); 46.47 (CH_2, C_4); 46.03, 43.12 (CH_2, C_3); 33.74 – 32.98 (m, CH_2, C_9); 27.53 (CH_2, C_8); 26.28, 25.43 (CH_2, C_2); 24.41 (CH_2, C_1); 21.08 (CH_3, C_5); 19.50 – 19.28 (m, CH_2, C_7).

^{19}F NMR (376 MHz, $CDCl_3$)

δ -66.21 - -66.37 (m, CF_3 *cis* + *trans*)

Note: Overlap between *cis* and *trans* rotamers in ^{19}F NMR.

^{1}H NMR (599 MHz, CD_3CN)

cis (major): δ 4.11 (s, 2H, H_4); 3.53 – 3.44 (m, 2H, $H_{3\,(ax/eq)}$); 3.41 – 3.34 (m, 2H, $H_{3\,(ax/eq)}$); 3.34 – 3.26 (m, 2H, H_6); 2.27 – 2.14 (m, 2H, H_9); 1.87 (s, 2H, H_5); 1.72 – 1.45 (m, 10H, $H_{1+2+7+8}$).

trans (minor): δ 4.10 (s, 2H, H_4); 3.53 – 3.44 (m, 2H, $H_{3\,(ax/eq)}$); 3.41 – 3.34 (m, 2H, $H_{3\,(ax/eq)}$); 3.34 – 3.26 (m, 2H, H_6); 2.27 – 2.14 (m, 2H, H_9); 2.07 (s, 2H, H_5); 1.72 – 1.45 (m, 10H, $H_{1+2+7+8}$).

^{13}C NMR (151 MHz, CD_3CN)

cis (major): δ 171.33 (CO-CH_3); 166.18 (CO-pip); 127.79 (q, J = 280.0 Hz, CF_3); 49.79 (CH_2, C_4); 46.52 (CH_2, C_6); 45.29, 42.83 (CH_2, C_3); 33.11 – 32.37 (m, CH_2, C_9); 26.36 (CH_2, C_8); 26.07, 25.45 (CH_2, C_2); 24.14 (CH_2, C_1); 20.83 (CH_3, C_5); 19.06 – 18.92 (m, CH_2, C_7).

trans (minor): δ 170.15 (CO-CH_3); 166.23 (CO-pip); 127.66 (q, J = 277.9 Hz, CF_3); 48.90 (CH_2, C_6); 45.98 (CH_2, C_4); 45.38, 42.54 (CH_2, C_3); 33.11 – 32.37 (m, CH_2, C_9); 27.18 (CH_2, C_8); 26.02, 25.41 (CH_2, C_2); 24.19 (CH_2, C_1); 20.40 (CH_3, C_5); 19.06 – 18.92 (m, CH_2, C_7).

^{19}F NMR (376 MHz, CD_3CN)

δ -66.88 – 67.09 (m, CF_3 *cis* + *trans*)

Note: Overlap between *cis* and *trans* rotamers in ^{19}F NMR.

^{1}H NMR (599 MHz, CD_3OD)

cis (minor): δ 4.31 (s, 2H, H_4); 3.58 – 3.50 (m, 2H, $H_{3\ (ax/eq)}$); 3.49 – 3.42 (m, 2H, $H_{3\ (ax/eq)}$); 3.36 (t, *J* = 7.1 Hz, 2H, H_6); 2.27 – 2.17 (m, 2H, H_9); 1.97 (s, 2H, H_5); 1.74 – 1.50 (m, 10H, $H_{1+2+7+8}$).

trans (major): δ 4.21 (s, 2H, H_4); 3.58 – 3.50 (m, 2H, $H_{3\ (ax/eq)}$); 3.49 – 3.42 (m, 2H, $H_{3\ (ax/eq)}$); 3.39 (t, *J* = 7.8 Hz, 2H, H_6); 2.12 – 2.05 (m, 2H, H_9); 2.16 (s, 2H, H_5); 1.75 – 1.47 (m, 6H, $H_{1+2+7+8}$).

^{13}C NMR (151 MHz, CD_3OD)

cis (minor): δ 173.24 ($CO\text{-}CH_3$); 166.66 (CO-pip); 127.35 (q, *J* = 282.0 Hz, CF_3); 49.84 (CH_2, C_4); 46.71 (CH_2, C_6); 45.42, 43.12 (CH_2, C_3); 33.04 – 32.30 (m, CH_2, C_9); 26.17 (CH_2, C_8); 26.00 (CH_2, C_1); 25.31, 23.91 (CH_2, C_2); 20.01 (CH_3, C_5); 19.02 – 18.91 (m, CH_2, C_7).

trans (major): δ 172.23 ($CO\text{-}CH_3$); 166.80 (CO-pip); 127.30 (q, *J* = 275.1 Hz, CF_3); 49.44 (CH_2, C_6); 46.76 (CH_2, C_4); 45.59, 42.94 (CH_2, C_3); 33.04 – 32.30 (m, CH_2, C_9); 26.98 (CH_2, C_8); 25.81 (CH_2, C_1); 25.20, 23.98 (CH_2, C_2); 19.61 (CH_3, C_5); 19.02 – 18.91 (m, CH_2, C_7).

^{19}F NMR (376 MHz, CD_3OD)

δ -67.93 - -68.02 (m, CF_3 *cis* + *trans*)

Note: Overlap between *cis* and *trans* rotamers in ^{19}F NMR.

Compound 101: *N*-(2,2,3,3,3-pentafluoropropyl)-*N*-(2-oxo-2-(piperidin-1-yl)ethyl)acetamide

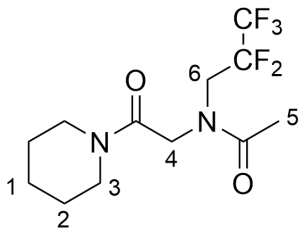

2-Bromo-1-(piperidin-1-yl)ethenone (**93**) was dissolved in MeCN (5 mL) and added dropwise to a solution of 2,2,3,3,3-pentafluoropropylamine (507 mg, 4 equiv.) in MeCN (10 mL) at 0 °C under an N_2 atmosphere. The reaction was allowed to warm to room temperature and stirred for 16 h following the general protocol described in **Section 5.3.2**. The reaction was then concentrated under reduced pressure and acetylated as per **Section 5.3.5**, before purification by flash column chromatography (**Section 5.3.6**). This gave *N*-(2,2,3,3,3-pentafluoropropyl)-*N*-(2-oxo-2-(piperidin-1-yl)ethyl)acetamide (**101**) as a yellow oil (23 mg, 9%). HRMS (ESI^+): calculated for $C_{12}H_{17}F_5N_2O_2^+$ 317.1290 $[M+H]^+$, found: 317.1290 Da.

^{1}H NMR (599 MHz, $CDCl_3$)

cis (minor): δ 4.21 (s, 2H, H_4); 4.10 (s, 2H, H_6); 3.62 – 3.49 (m, 2H, $H_{3\ (ax/eq)}$); 3.40 – 3.33 (m, 2H, $H_{3\ (ax/eq)}$); 2.05 (s, 3H, H_5); 1.75 – 1.53 (m, 6H, H_{1+2})

trans (major): δ 4.30 (s, 2H, H_4); 4.10 (s, 2H, H_6); 3.62 – 3.49 (m, 2H, $H_{3\ (ax/eq)}$); 3.40 – 3.33 (m, 2H, $H_{3\ (ax/eq)}$); 2.20 (s, 3H, H_5); 1.75 – 1.53 (m, 6H, H_{1+2})

^{13}C NMR (151 MHz, $CDCl_3$)

cis (minor): δ 172.20 ($CO\text{-}CH_3$); 164.80 (CO-pip); 50.55 (CH_2, C_4); 45.71, 43.48 (CH_2, C_3); 44.83 (t, J = 22.3 Hz, CH_2, C_6); 26.44, 25.50 (CH_2, C_2); 24.26 (CH_2, C_1); 20.90 (CH_3, C_5)

trans (major): δ 172.00 ($CO\text{-}CH_3$); 165.58 (CO-pip); 48.41 (t, J = 21.1 Hz, CH_2, C_6); 47.34 (CH_2, C_4); 45.87, 43.18 (CH_2, C_3); 26.20, 25.37 (CH_2, C_2); 24.34 (CH_2, C_1); 21.05 (CH_3, C_5)

Note: CF_3 and CF_2 peaks not detected for both *cis* and *trans* rotamers.

^{19}F NMR (376 MHz, $CDCl_3$)

δ -85.51 (s, CF_3 *trans*); -85.66 (s, CF_3 *cis*); -118.08 (t, J = 19.1 Hz, CF_2 *cis*); -118.30 (t, J = 18.2 Hz, CF_2, *trans*)

^{1}H NMR (599 MHz, CD_3CN)

cis (major): δ 4.29 (s, 2H, H_4); 4.17 – 4.04 (m, 2H, H_6); 3.54 – 3.45 (m, 2H, $H_{3\ (ax/eq)}$); 3.39 – 3.32 (m, 2H, $H_{3\ (ax/eq)}$); 1.98 – 1.95 (m, 3H, H_5 + CD_3CN); 1.70 – 1.49 (m, 6H, H_{1+2})

Note: Overlap between H_5 *cis* and CD_3CN solvent peak.

trans (minor): δ 4.24 (s, 2H, H_4); 4.17 – 4.04 (m, 2H, H_6); 3.54 – 3.45 (m, 2H, $H_{3\ (ax/eq)}$); 3.39 – 3.32 (m, 2H, $H_{3\ (ax/eq)}$); 2.13 (s, 3H, H_5); 1.70 – 1.49 (m, 6H, H_{1+2})

^{13}C NMR (151 MHz, CD_3CN)

cis (major): δ 172.90 ($CO\text{-}CH_3$); 165.33 (CO-pip); 51.16 (CH_2, C_4); 45.23, 44.88 (CH_2, C_3); 44.73 (t, J = 22.4 Hz, CH_2, C_6); 45.23, 42.87 (CH_2, C_3); 25.94, 25.36 (CH_2, C_2); 24.06 (CH_2, C_1); 20.43 (CH_3, C_5)

trans (minor): δ 171.74 (CO-CH3); 48.14 (CH_2, C_4); 42.62 (CH_2, C_3); 25.94, 24.12 (CH_2, C_1); 20.32 (CH_3, C_5)

Note: CO-pip, C_2 and C_6 peaks undetected for *trans* rotamer, and only one peak detected for C_3 *trans*. CF_3 and CF_2 peaks undetected for both *cis* and *trans* rotamers.

^{19}F NMR (376 MHz, CD_3CN)

δ -79.89 (s, CF_3 *trans*); -80.03 (s, CF_3 *cis*); -115.82 (t, J = 15.9 Hz, CF_2 *cis*); -116.21 (t, J = 16.1 Hz, CF_2, *trans*)

^{1}H NMR (599 MHz, CD_3OD)

cis (major): δ 4.47 (s, 2H, H_4); 4.14 (t, *J* = 15.6 Hz, 2H, H_6); 3.58 – 3.51 (m, 2H, $H_{3\ (ax/eq)}$); 3.47 – 3.41 (m, 2H, $H_{3\ (ax/eq)}$); 2.04 (s, 3H, H_5); 1.73 – 1.52 (m, 6H, H_{1+2})

trans (minor): δ 4.33 (s, 2H, H_4); 4.24 (t, *J* = 15.9 Hz, 2H, H_6); 3.58 – 3.51 (m, 2H, $H_{3\ (ax/eq)}$); 3.47 – 3.41 (m, 2H, $H_{3\ (ax/eq)}$); 2.20 (s, 3H, H_5); 1.73 – 1.52 (m, 6H, H_{1+2})

^{13}C NMR (151 MHz, CD_3OD)

cis (major): δ 174.29 ($CO\text{-}CH_3$); 165.97 (CO-pip); 50.95 (CH_2, C_4); 45.36, 43.13 (CH_2, C_3); 44.88 (t, *J* = 22.6 Hz, CH_2, C_6); 25.89, 25.25 (CH_2, C_2); 23.87 (CH_2, C_1); 19.68 (CH_3, C_5)

trans (minor): δ 173.41 ($CO\text{-}CH_3$); 166.08 (CO-pip); 48.33 (CH_2, C_4); 45.55, 42.99 (CH_2, C_3); 25.76, 25.16 (CH_2, C_2); 23.95 (CH_2, C_1); 19.58 (CH_3, C_5)

Note: C_6 peaks unassignable for the *trans* rotamer due to overlap with the solvent peak. CF_2 and CF_3 peaks not detected for both *cis* and *trans* rotamers.

^{19}F NMR (376 MHz, CD_3OD)

δ -86.02 (s, CF_3 *trans*); -86.13 (s, CF_3 *cis*); -121.57 (t, *J* = 15.7 Hz, CF_2 *cis*), -122.03 (t, *J* = 16.0 Hz, CF_2 *trans*)

Compound 102: *N*-(3,3,4,4,4-pentafluorobutyl)-*N*-(2-oxo-2-(piperidin-1-yl)ethyl)acetamide

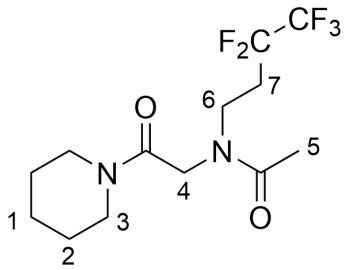

2-Bromo-1-(piperidin-1-yl)ethenone (**93**) was dissolved in MeCN (5 mL) and added dropwise to a solution of 3,3,4,4,4-pentafluorobutylamine (555 mg, 4 equiv.) in MeCN (10 mL) at 0 °C under an N_2 atmosphere. The reaction was allowed to warm to room temperature and stirred for 16 h following the general protocol described in **Section 5.3.2**. The reaction was then concentrated under reduced pressure and acetylated as per **Section 5.3.5**, before purification by flash column chromatography (**Section 5.3.6**). This gave *N*-(3,3,4,4,4-pentafluorobutyl)-*N*-(2-oxo-2-(piperidin-1-yl)ethyl)acetamide (**102**) as a yellow oil (65 mg, 23%). HRMS (ESI^+): calculated for $C_{13}H_{19}F_5N_2O_2^+$ 331.1448 $[M+H]^+$, found: 331.1449 Da.

^{1}H NMR (599 MHz, $CDCl_3$)

cis (minor): δ 4.08 (s, 2H, H_4); 3.59 – 3.48 (m, 4H, H_6 + $H_{3\ (ax/eq)}$); 3.39 – 3.31 (m, 2H, $H_{3\ (ax/eq)}$); 2.48 – 2.35 (m, 2H, H_7); 1.96 (s, 3H, H_5); 1.70 – 1.49 (m 6H, H_{1+2})

trans (major): δ 4.12 (s, 2H, H_4); 3.69 (t, *J* = 8.0 Hz, 2H, H_6); 3.59 – 3.48 (m, 2H, $H_{3\ (ax/eq)}$); 3.39 – 3.31 (m, 2H, $H_{3\ (ax/eq)}$); 2.48 – 2.35 (m, 2H, H_7); 2.16 (s, 3H, H_5); 1.70 – 1.49 (m 6H, H_{1+2})

^{13}C NMR (151 MHz, $CDCl_3$)

cis (minor): δ 170.65 ($CO\text{-}CH_3$); 165.80 (CO-pip); 120.32 – 112.74 (m, CF_3 + CF_2); 51.52 (CH_2, C_4); 46.03, 43.19 (CH_2, C_3); 41.49 (t, *J* = 4.7 Hz, CH_2, C_6); 28.74 (t, *J* = 21.1 Hz, CH_2, C_7); 26.22, 25.36 (CH_2, C_2); 24.23 (CH_2, C_1); 20.86 (CH_3, C_5).

trans (major): δ 171.64 ($CO\text{-}CH_3$); 165.35 (CO-pip); 120.32 – 112.74 (m, CF_3 + CF_2); 47.16 (CH_2, C_4); 45.74, 43.44 (CH_2, C_3); 42.21 (t, *J* = 4.6 Hz, CH_2, C_6); 29.90 (t, *J* = 21.3 Hz, CH_2, C_7); 26.41, 25.45 (CH_2, C_2); 24.33 (CH_2, C_1); 21.43 (CH_3, C_5).

^{19}F NMR (376 MHz, $CDCl_3$)

δ -85.55 (s, CF_3 *cis*); -85.69 (s, CF_3 *trans*); -118.13 (t, *J* = 19.1 Hz, CF_2 *cis*), -118.33 (t, *J* = 18.2 Hz, CF_2 *trans*)

^{1}H NMR (599 MHz, CD_3CN)

cis (major): δ 4.18 (s, 2H, H_4); 3.57 – 3.42 (m, 4H, $H_{6\ +\ 3\ (ax/eq)}$); 3.39 – 3.31 (m, 2H, $H_{3\ (ax/eq)}$); 2.57 – 2.32 (m, 2H, H_7); 1.87 (s, 3H, H_5); 1.68 – 1.44 (m, 6H, H_{1+2})

trans (minor): δ 4.12 (s, 2H, H_4); 3.65 (t, *J* = 7.9 Hz, 2H, H_6); 3.57 – 3.42 (m, 2H, $H_{3\ (ax/eq)}$); 3.39 – 3.31 (m, 2H, $H_{3\ (ax/eq)}$); 2.57 – 2.32 (m, 2H, H_7); 2.09 (s, 3H, H_5); 1.68 – 1.44 (m, 6H, H_{1+2})

^{13}C NMR (151 MHz, CD_3CN)

cis (major): δ 171.64 ($CO\text{-}CH_3$); 166.04 (CO-pip); 122.57 – 113.32 (m, CF_3 + CF_2); 50.90 (CH_2, C_4); 45.29, 42.85 (CH_2, C_3); 40.11 (t, *J* = 4.6 Hz, CH_2, C_6); 28.23 (t, *J* = 20.9 Hz, CH_2, C_7); 25.99, 25.39 (CH_2, C_2); 24.08 (CH_2, C_1); 20.73 (CH_3, C_5).

trans (minor): δ 170.31 ($CO\text{-}CH_3$); 122.57 – 113.32 (m, CF_3 + CF_2); 46.86 (CH_2, C_4); 45.39, 42.59 (CH_2, C_3); 41.65 (t, *J* = 4.5 Hz, CH_2, C_6); 29.15 (t, *J* = 20.9 Hz, CH_2, C_7); 25.97, 25.36 (CH_2, C_2); 24.14 (CH_2, C_1); 20.28 (CH_3, C_5).

Note: CO-pip not detected for *trans* rotamer.

^{19}F NMR (376 MHz, CD_3CN)

δ -86.45 (s, CF_3 *trans*); -86.49 (s, CF_3 *cis*); -118.76 - -118.96 (m, CF_2 *cis* + *trans*)

Note: Overlap between the *cis* and *trans* signals from CF_2 in ^{19}F-NMR.

^{1}H NMR (599 MHz, CD_3OD)

cis (major): δ 4.39 (s, 2H, H_4); 3.60 (t, *J* = 7.6 Hz, 2H, H_6); 3.58 – 3.52 (m, 4H, $H_{6\ +3\ (ax/eq)}$); 3.50 – 3.42 (m, 2H, $H_{3\ (ax/eq)}$); 2.66 – 2.39 (m, 2H, H_7); 1.98 (s, 3H, H_5); 1.74 – 1.52 (m, 6H, H_{1+2})

trans (minor): δ 4.26 (s, 2H, H_4); 3.73 (t, *J* = 7.7 Hz, 2H, H_6); 3.58 – 3.52 (m, 4H, $H_{6\ +3\ (ax/eq)}$); 3.50 – 3.42 (m, 2H, $H_{3\ (ax/eq)}$); 2.66 – 2.39 (m, 2H, H_7); 2.19 (s, 3H, H_5); 1.74 – 1.52 (m, 6H, H_{1+2})

^{13}C NMR (151 MHz, CD_3OD)

cis (major): δ 173.32 ($CO\text{-}CH_3$); 166.56 (CO-pip); 122.50 – 113.01 (m, CF_3 + CF_2); 50.86 (CH_2, C_4); 45.42, 43.12 (CH_2, C_3); 40.62 (t, *J* = 4.7 Hz, CH_2, C_6); 27.98 (t, *J* = 21.1 Hz, CH_2, C_7); 25.95, 25.28 (CH_2, C_2); 23.88 (CH_2, C_1); 19.98 (CH_3, C_5).

trans (minor): δ 172.18 ($CO\text{-}CH_3$); 166.63 (CO-pip); 122.50 – 113.01 (m, CF_3 + CF_2); 46.91 (CH_2, C_4); 45.60, 42.96 (CH_2, C_3); 42.01 (t, *J* = 4.6 Hz, CH_2, C_6); 28.79 (t, *J* = 21.0 Hz, CH_2, C_7); 25.79, 25.18 (CH_2, C_2); 23.95 (CH_2, C_1); 19.51 (CH_3, C_5).

^{19}F NMR (376 MHz, CD_3OD)

δ -87.19 (s, CF_3 *trans*); -87.29 (s, CF_3 *cis*); -119.54 (t, *J* = 18.9 Hz, CF_2 *trans*), -119.66 (t, *J* = 19.0 Hz, CF_2 *cis*)

Compound 103: *N*-(3,3,3-trifluoro-2-trifluoromethyl-butyl)-*N*-(2-oxo-2-(piperidin-1-yl)ethyl)acetamide

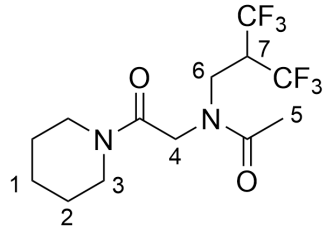

1,1,1-trifluoro-2-trifluoromethyl-3-iodobutane (248 mg, 1 equiv.) was dissolved in MeCN (5 mL) and added dropwise to a solution of 2-amino-1-(piperidin-1-yl)ethan-1-one (**107**) in MeCN (10 mL) at 0 °C under an N_2 atmosphere. The reaction was allowed to warm to room temperature and stirred for 16 h following the general protocol described in **Section 5.3.4**. The reaction was then concentrated under reduced pressure and acetylated as per **Section 5.3.5**, before purification by flash column chromatography (**Section 5.3.6**). This gave *N*-(3,3,3-trifluoro-2-trifluoromethyl-butyl)-*N*-(2-oxo-2-(piperidin-1-yl)ethyl)acetamide (**93**) as a yellow oil (50 mg, 18%). HRMS (ESI^+): calculated for $C_{13}H_{18}F_6N_2O_2^+$ 349.1352 $[M+H]^+$, found: 349.1357 Da.

^{1}H NMR (599 MHz, $CDCl_3$)

cis (major): δ 4.09 (s, 2H, H_4); 3.83 – 3.74 (m, 1H, H_7); 3.71 (d, *J* = 6.5 Hz, 2H, H_6); 3.59 – 3.50 (m, 2H, $H_{3\ (ax/eq)}$); 3.42 – 3.28 (m, 2H, $H_{3\ (ax/eq)}$); 1.99 (s, 3H, H_5); 1.72 – 1.53 (m, 6H, H_{1+2})

trans (minor): δ 4.13 (s, 2H, H_4); 3.93 (d, *J* = 5.6 Hz, 2H, H_6); 3.59 – 3.50 (m, 2H, $H_{3\ (ax/eq)}$); 3.42 – 3.28 (m, 2H, $H_{3\ (ax/eq)}$); 2.20 (s, 3H, H_5); 1.72 – 1.53 (m, 6H, H_{1+2})

Note: H_7 peak unassignable for *trans* rotamer.

^{13}C NMR (151 MHz, $CDCl_3$)

cis (major): δ 172.39 ($CO\text{-}CH_3$); 165.13 (CO-pip); 126.63 – 119.90 (m, CF_3); 52.11 (CH_2, C_4); 46.19 (CH_2, C_3); 46.48 – 45.55 (m, CH, C_7); 45.72, 43.45 (CH_2, C_3); 44.36 – 44.22 (m, CH_2, C_6); 26.40, 25.44 (CH_2, C_2); 24.23 (CH_2, C_1); 21.49 (CH_3, C_5).

trans (minor): δ 171.15 ($CO\text{-}CH_3$); 165.67 (CO-pip); 126.63 – 119.90 (m, CF_3); 47.09 (CH_2, C_4); 47.70 – 47.14 (m, CH, C_7); 46.01, 43.34 (CH_2, C_3); 44.55 – 44.37 (m, CH_2, C_6); 26.24, 25.40 (CH_2, C_2); 24.35 (CH_2, C_1); 20.80 (CH_3, C_5).

Note: Overlap between C_7 *cis* multiplet and C_3 peaks.

^{19}F NMR (376 MHz, $CDCl_3$)

δ -66.19 (d, *J* = 8.0 Hz, CF_3 *cis*); -66.28 (d, *J* = 8.1 Hz, CF_3 *trans*)

^{1}H NMR (599 MHz, CD_3CN)

cis (major): δ 4.18 (s, 2H, H_4); 3.88 – 3.77 (m, 1H, H_7); 3.72 (d, *J* = 6.3 Hz, 2H, H_6); 3.51 – 3.44 (m, 2H, $H_{3\ (ax/eq)}$); 3.40 – 3.30 (m, 2H, $H_{3\ (ax/eq)}$); 1.90 (s, 3H, H_5); 1.69 – 1.42 (m, 6H, H_{1+2})

trans (minor): δ 4.12 (s, 2H, H_4); 3.95 - 3.89 (m, 3H, H_{6+7}); 3.51 – 3.44 (m, 2H, $H_{3\ (ax/eq)}$); 3.40 – 3.30 (m, 2H, $H_{3\ (ax/eq)}$); 2.11 (s, 3H, H_5); 1.69 – 1.42 (m, 6H, H_{1+2})

^{13}C NMR (151 MHz, CD_3CN)

cis (major): δ 172.58 ($CO\text{-}CH_3$); 165.66 (CO-pip); 126.81 – 120.62 (m, CF_3); 51.38 (CH_2, C_4); 46.67 – 45.32 (m, CH, C_7); 45.28, 42.87 (CH_2, C_3); 42.54 – 42.35 (CH_2, C_6); 25.96, 25.37 (CH_2, C_2); 24.06 (CH_2, C_1); 20.81 (CH_3, C_5).

trans (minor): δ 170.83 ($CO\text{-}CH_3$); 165.73 (CO-pip); 126.81 – 120.62 (m, CF_3); 46.44 (CH_2, C_4); 45.28 (CH_2, C_3); 43.83 – 43.70 (m, CH_2, C_6); 42.68 (CH_2, C_3); 24.12 (CH_2, C_1); 20.22 (CH_3, C_5).

Note: One C_3 peak unassignable for *trans* rotamer due to overlap with C_7 *cis*. C_2 peaks not detected for *trans* isomer.

^{19}F NMR (376 MHz, CD_3CN)

δ -66.80 (d, *J* = 8.7 Hz, CF_3 *trans*); -67.01 (d, *J* = 8.3 Hz, CF_3 *cis*)

^{1}H NMR (599 MHz, CD_3OD)

cis (major): δ 4.38 (s, 2H, H_4); 3.97 – 3.88 (m, 1H, H_7); 3.82 (d, *J* = 6.3 Hz, 2H, H_6); 3.58 – 3.51 (m, 2H, $H_{3\ (ax/eq)}$); 3.49 – 3.41 (m, 2H, $H_{3\ (ax/eq)}$); 1.99 (s, 3H, H_5); 1.73 – 1.52 (m, 6H, H_{1+2})

trans (minor): δ 4.25 (s, 2H, H_4); 3.98 (d, *J* = 6.1 Hz, 2H, H_6); 3.58 – 3.51 (m, 2H, $H_{3\ (ax/eq)}$); 3.49 – 3.41 (m, 2H, $H_{3\ (ax/eq)}$); 2.20 (s, 3H, H_5); 1.73 – 1.52 (m, 6H, H_{1+2})

Note: H_7 peak unassignable for *trans* rotamer.

^{13}C NMR (151 MHz, CD_3OD)

cis (major): δ 174.05 ($CO\text{-}CH_3$); 166.26 (CO-pip); 127.41 – 119.95 (m, CF_3); 50.98 (CH_2, C_4); 46.08 – 45.45 (m, CH, C_7); 45.40, 43,14 (CH_2, C_3); 42.48 – 42.26 (m, CH_2, C_6); 25.90, 25.25 (CH_2, C_2); 23.86 (CH_2, C_1); 20.04 (CH_3, C_5).

trans (minor): δ 172.68 ($CO\text{-}CH_3$); 166.24 (CO-pip); 127.41 – 119.95 (m, CF_3); 46.18 (CH_2, C_4); 44.04 – 43.55 (m, CH_2, C_6); 43.03 (CH_2, C_3); 25.83, 25.20 (CH_2, C_2); 23.94 (CH_2, C_1); 19.48 (CH_3, C_5).

Note: C_7 and one C_3 peak not detected for *trans* isomer.

^{19}F NMR (376 MHz, CD_3OD)

δ -67.55 (d, *J* = 8.3 Hz, CF_3 *trans*); -67.82 (d, *J* = 8.3 Hz, CF_3 *cis*)

Compound 104: *N*-(4,4,4-trifluoro-3-trifluoromethyl-amyl)-*N*-(2-oxo-2-(piperidin-1-yl)ethyl)acetamide

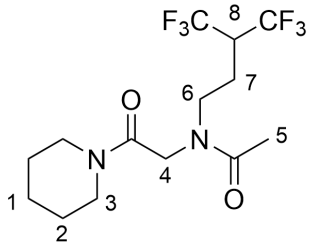

1,1,1-trifluoro-2-trifluoromethyl-4-iodopentane (260 mg, 1 equiv.) was dissolved in MeCN (5 mL) and added dropwise to a solution of 2-amino-1-(piperidin-1-yl)ethan-1-one (**107**) in MeCN (10 mL) at 0 °C under an N_2 atmosphere. The reaction was allowed to warm to room temperature and stirred for 16 h following the general protocol described in **Section 5.3.4**. The reaction was then concentrated under reduced pressure and acetylated as per **Section 5.3.5**, before purification by flash column chromatography (**Section 5.3.6**). This gave *N*-(4,4,4-trifluoro-3-trifluoromethyl-amyl)-*N*-(2-oxo-2-(piperidin-1-yl)ethyl)acetamide (**104**) as a yellow oil (20 mg, 7%). HRMS (ESI^+): calculated for $C_{14}H_{20}F_6N_2O_2^+$ 363.1480 $[M+H]^+$, found: 363.1509 Da.

^{1}H NMR (599 MHz, $CDCl_3$)

cis (minor): δ 4.04 (s, 2H, H_4); 3.62 – 3.47 (m, 4H, $H_{6 + 3\ (ax/eq)}$); 3.41 – 3.33 (m, 2H, $H_{3\ (ax/eq)}$); 3.22 – 3.13 (m, 1H, H_8); 2.14 – 2.04 (m, 2H, H_7); 1.99 (s, 3H, H_5); 1.73 – 1.51 (m, 6H, H_{1+2})

trans (major): 4.12 (s, 2H, H_4); 3.62 – 3.47 (m, 4H, $H_{6 + 3\ (ax/eq)}$); 3.41 – 3.33 (m, 2H, $H_{3\ (ax/eq)}$); 3.03 – 2.90 (m, 1H, H_8); 2.16 (s, 3H, H_5); 2.14 – 2.04 (m, 2H, H_7); 1.73 – 1.51 (m, 6H, H_{1+2})

^{13}C NMR (151 MHz, $CDCl_3$)

cis (minor): δ 172.01 ($CO\text{-}CH_3$); 165.23 (CO-pip); 125.14 – 122.51 (m, CF_3); 50.75 (CH_2, C_4); 47.05, 46.03 (CH_2, C_3); 43.50 (CH_2, C_6); 26.47, 25.49 (CH_2, C_2); 24.29 (CH_2, C_1); 22.04 (CH_2, C_7); 21.47 (CH_3, C_5)

trans (major): δ 170.80 ($CO\text{-}CH_3$); 165.79 (CO-pip); 125.14 – 122.51 (m, CF_3); 46.55 (CH_2, C_4); 46.08, 45.78 (CH_2, C_3); 43.22 (CH_2, C_6); 26.28, 25.40 (CH_2, C_2); 24.39 (CH_2, C_1); 22.65 (CH_2, C_7); 20.87 (CH_3, C_5)

Note: C_8 peaks undistinguishable for the *cis* and *trans* isomers due to weak, crowded signals.

^{19}F NMR (376 MHz, $CDCl_3$)

δ -66.90 (d, J = 8.1 Hz, CF_3 *trans*); -67.16 (d, J = 8.2 Hz, CF_3 *cis*)

^{1}H NMR (599 MHz, CD_3CN)

cis (major): δ 4.14 (s, 2H, H_4); 3.52 – 3.30 (m, 4H, $H_{6 + 3\ (ax/eq)}$); 2.05 – 2.01 (m, 2H, H_7); 1.87 (s, 3H, H_5); 1.68 – 1.44 (m, 6H, H_{1+2})

trans (minor): δ 4.10 (s, 2H, H_4); 3.52 – 3.30 (m, 4H, $H_{6 + 3\ (ax/eq)}$); 2.15 – 2.10 (m, 2H, H_7); 2.06 (s, 3H, H_5); 1.68 – 1.44 (m, 6H, H_{1+2})

Note: H_8 peak not detected for both *cis* and *trans* rotamers.

^{13}C NMR (151 MHz, CD_3CN)

cis (major): δ 172.05 ($CO\text{-}CH_3$); 166.04 (CO-pip); 50.46 (CH_2, C_4); 45.30, 42.87 (CH_2, C_3); 45.08 (CH_2, C_6); 26.05, 25.43 (CH_2, C_2); 24.09 (CH_2, C_1); 21.67 (CH_2, C_7); 20.80 (CH_3, C_5)

trans (minor): δ 170.25 ($CO\text{-}CH_3$); 166.11 (CO-pip); 46.84 (CH_2, C_6); 46.81 (CH_2, C_4); 45.41, 42.59 (CH_2, C_3); 26.02, 25.40 (CH_2, C_2); 24.16 (CH_2, C_1); 22.34 (CH_2, C_7); 20.25 (CH_3, C_5)

Note: C_8 peaks undistinguishable for the *cis* and *trans* isomers due to weak, crowded signals. CF_3 and CF_2 peaks undetected for both isomers.

^{19}F NMR (376 MHz, CD_3CN)

δ -67.66 (d, J = 8.4 Hz, CF_3 *trans*); -67.94 (d, J = 8.6 Hz, CF_3 *cis*)

^{1}H NMR (599 MHz, CD_3OD)

cis (major): δ 4.35 (s, 2H, H_4); 3.60 – 3.43 (m, 4H, $H_{6 + 3 (ax/eq)}$); 2.12 – 2.06 (m, 2H, H_7); 1.98 (s, 3H, H_5); 1.74 – 1.52 (m, 6H, H_{1+2})

trans (minor): δ 4.23 (s, 2H, H_4); 3.71 – 3.61 (m, 1H, H_8); 3.60 – 3.43 (m, 4H, $H_{6 + 3 (ax/eq)}$); 2.21 – 2.13 (m, 5H, H_{5+7}); 1.74 – 1.52 (m, 6H, H_{1+2})

Note: H_8 peak unassignable for *cis* rotamer.

^{13}C NMR (151 MHz, CD_3OD)

cis (major): δ 173.67 ($CO\text{-}CH_3$); 166.53 (CO-pip); 50.47 (CH_2, C_4); 45.88 – 44.57 (m, C_6 + C_8); 45.44, 43.15 (CH_2, C_3); 26.00, 25.31 (CH_2, C_2); 23.89 (CH_2, C_1); 21.42 (CH_2, C_7); 19.98 (CH_3, C_5)

trans (minor): δ 172.15 ($CO\text{-}CH_3$); 166.65 (CO-pip); 47.04 (CH_2, C_4); 45.88 – 44.57 (m, C_6 + C_8); 45.61, 42.99 (CH_2, C_3); 25.83, 25.20 (CH_2, C_2); 23.96 (CH_2, C_1); 22.16 (CH_2, C_7); 19.43 (CH_3, C_5)

Note: Overlap between C_6 and C_8 signals makes them indistinguishable. CF_3 and CF_2 peaks undetected for both isomers.

^{19}F NMR (376 MHz, CD_3OD)

δ -64.50 (d, J = 8.5 Hz, CF_3 *trans*); -64.72 (d, J = 8.5 Hz, CF_3 *cis*)

Compound 107: *N*-(2,2,2-trifluoroethyl)-*N*-(2-oxo-2-(piperidin-1-yl)ethyl)acetamide

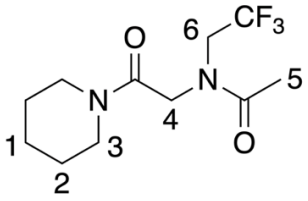

2-Bromo-1-(piperidin-1-yl)ethenone (**93**) was dissolved in MeCN (5 mL) and added dropwise to a solution of 2,2,2-trifluoroethylamine (337 mg, 4 equiv.) in MeCN (10 mL) at 0 °C under an N_2 atmosphere. The reaction was allowed to warm to room temperature and stirred for 16 h following the general protocol described in **Section 5.3.2**. The reaction was then concentrated under reduced pressure and acetylated as per **Section 5.3.5**, before purification by flash column chromatography (**Section 5.3.6**). This gave *N*-(2,2,2-trifluoroethyl)-*N*-(2-oxo-2-(piperidin-1-yl)ethyl)acetamide (**107**) as a yellow oil (31 mg, 14%). LCMS (ESI^+): calculated for $C_{11}H_{17}F_3N_2O_2^+$ 267.12 $[M+H]^+$, found: 267.13 Da. Characterization matches previously published data.[1]

^{1}H NMR (599 MHz, $CDCl_3$)

cis (minor): δ 4.19 (s, 2H, H_4); 4.10 – 3.99 (m, 2H, H_6); 3.62 – 3.47 (m, 4H, $H_{3\ (ax/eq)}$); 3.39 – 3.32 (m, 2H, $H_{3\ (ax/eq)}$); 2.05 (s, 3H, H_5); 1.76 – 1.48 (m, 6H, H_{1+2})

trans (major): 4.28 (s, 2H, H_4); 4.10 – 3.99 (m, 2H, H_6); 3.62 – 3.47 (m, 4H, $H_{3\ (ax/eq)}$); 3.39 – 3.32 (m, 2H, $H_{3\ (ax/eq)}$); 2.22 (s, 3H, H_5); 1.76 – 1.48 (m, 6H, H_{1+2})

^{13}C NMR (151 MHz, $CDCl_3$)

cis (minor): δ 172.06 (CO-CH_3); 164.77 (CO-pip); 50.29 (CH_2, C_4); 46.65 (CH_2, C_6); 45.71, 43.47 (CH_2, C_3); 26.20, 25.38 (CH_2, C_2); 24.26 (CH_2, C_1); 21.09 (CH_3, C_5)

trans (major): δ 171.76 (CO-CH_3); 165.54 (CO-pip); 50.51 (CH_2, C_6); 46.79 (CH_2, C_4); 45.85, 43.16 (CH_2, C_3); 26.44, 25.50 (CH_2, C_2); 24.34 (CH_2, C_1); 21.02 (CH_3, C_5)

Note: CF_3 peaks unassignable for both *cis* and *trans* rotamers due to weak signals.

^{19}F NMR (376 MHz, $CDCl_3$)

δ -70.14 (t, *J* = 9.3 Hz, CF_3 *cis*); -70.70 (t, *J* = 8.8 Hz, CF_3 *trans*)

5.8.2 Model Peptoid X-Ray Crystallography

Model peptoids **98** and **100** – **103** were dissolved in a minimal amount of ethyl acetate, dichloromethane or chloroform to form a saturated solution. Hexane was added dropwise until precipitation was observed then the solution re-cleared with polar solvent. The solutions were left to crystalise by slow evaporation until diffraction quality crystals were obtained.

Suitable single crystals were selected and analysed on a Bruker D8 Venture diffractometer (Photon100 CMOS detector, IμS-microsource, focusing mirrors) equipped with a Cryostream (Oxford Cryosystems) open-flow nitrogen cryostat at the temperature 120 K. All structures were solved by direct methods and refined by full-matrix least squares on F2 for all data using Olex2[3] software.

Crystal structures of these models reported at a 50% thermal ellipsoid probability as well as crystal data and structure refinement paramters are shown in **Figure 5.1** – **5.5** and **Table 5.4** – **5.8** respectively.

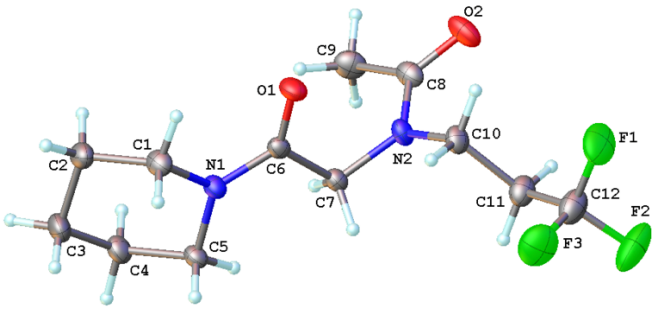

Figure 5.1: Crystal structure of model peptoid **98** reported with a 50% thermal ellipsoid probability

Table 5.4: Crystal data and structure refinement parameters of model peptoid **98**

Empirical formula	$C_{12}H_{19}F_3N_2O_2$	**μ/mm^{-1}**	0.118
Formula weight	280.29	**F(000)**	592.0
Temperature/K	120.00	**Crystal size/mm^3**	0.38 × 0.31 × 0.23
Crystal system	triclinic	**Radiation**	Mo Kα (λ = 0.71073)
Space group	P-1	**2Θ range for data collection/°**	4.064 to 60
a/Å	9.0771(3)	**Index ranges**	-12 ≤ h ≤ 12, -16 ≤ k ≤ 16, -19 ≤ l ≤ 19
b/Å	11.7768(4)	**Reflections collected**	49987
c/Å	13.6604(5)	**Independent reflections**	8045 [R_{int} = 0.0369, R_{sigma} = 0.0251]
α/°	106.0231(14)	**Data/restraints/parameters**	8045/0/495
β/°	91.7987(15)	**Goodness-of-fit on F^2**	1.016
γ/°	98.0982(15)	**Final R indexes [I>=2σ (I)]**	R_1 = 0.0426, wR_2 = 0.1018
Volume/Å^3	1385.76(8)	**Final R indexes [all data]**	R_1 = 0.0503, wR_2 = 0.1065
Z	4	**Largest diff. peak/hole / e Å^{-3}**	0.37/-0.31
ρ_{calc}g/cm^3	1.343		

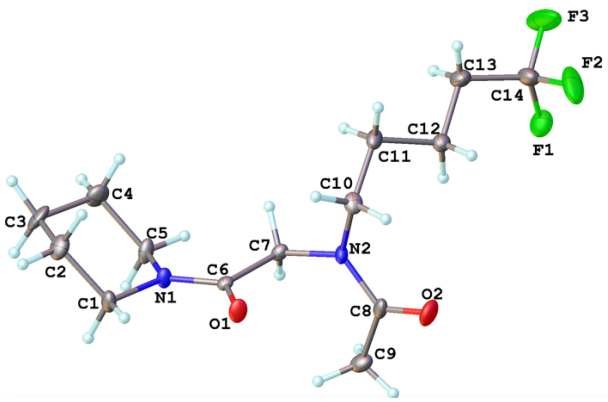

Figure 5.2: Crystal structure of model peptoid **100** reported with a 50% thermal ellipsoid probability

Table 5.5: Crystal data and structure refinement parameters of model peptoid **100**

Empirical formula	$C_{14}H_{23}F_3N_2O_2$	**μ/mm^{-1}**	0.112
Formula weight	308.34	**F(000)**	1312.0
Temperature/K	120.00	**Crystal size/mm^3**	0.17 × 0.02 × 0.01
Crystal system	orthorhombic	**Radiation**	Mo Kα (λ = 0.71073)
Space group	Pbca	**2Θ range for data collection/°**	4.652 to 51.998
a/Å	10.6919(3)	**Index ranges**	-13 ≤ h ≤ 13, -11 ≤ k ≤ 11, -37 ≤ l ≤ 37
b/Å	9.5338(2)	**Reflections collected**	49147
c/Å	30.5005(7)	**Independent reflections**	3048 [R_{int} = 0.0855, R_{sigma} = 0.0325]
α/°	90	**Data/restraints/parameters**	3048/0/282
β/°	90	**Goodness-of-fit on F^2**	1.258
γ/°	90	**Final R indexes [I>=2σ (I)]**	R_1 = 0.0825, wR_2 = 0.1441
Volume/Å^3	3109.05(13)	**Final R indexes [all data]**	R_1 = 0.0913, wR_2 = 0.1479
Z	8	**Largest diff. peak/hole / e Å^{-3}**	0.28/-0.30
ρ_{calc}g/cm^3	1.317		

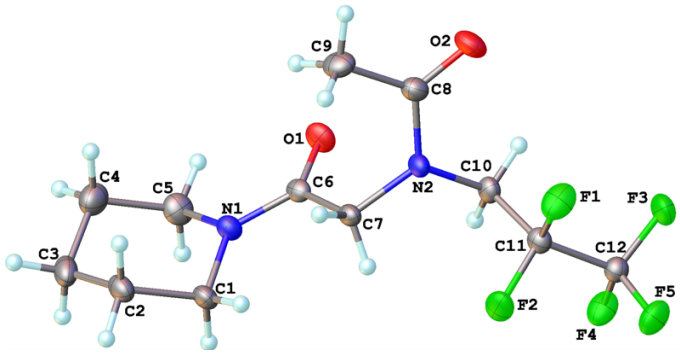

Figure 5.3: Crystal structure of model peptoid **101** reported with a 50% thermal ellipsoid probability

Table 5.6: Crystal data and structure refinement parameters of model peptoid **101**

Empirical formula	$C_{12}H_{17}F_5N_2O_2$	**μ/mm^{-1}**	0.140
Formula weight	316.27	**F(000)**	656.0
Temperature/K	120.00	**Crystal size/mm^3**	0.39 × 0.07 × 0.02
Crystal system	monoclinic	**Radiation**	Mo Kα (λ = 0.71073)
Space group	$P2_1/c$	**2Θ range for data collection/°**	4.74 to 59.988
a/Å	12.1732(4)	**Index ranges**	-17 ≤ h ≤ 17, -17 ≤ k ≤ 17, -13 ≤ l ≤ 13
b/Å	12.7115(4)	**Reflections collected**	34000
c/Å	9.8431(3)	**Independent reflections**	4239 [R_{int} = 0.0734, R_{sigma} = 0.0430]
α/°	90	**Data/restraints/parameters**	4239/0/258
β/°	106.6099(11)	**Goodness-of-fit on F^2**	1.130
γ/°	90	**Final R indexes [I>=2σ (I)]**	R_1 = 0.0560, wR_2 = 0.1157
Volume/Å^3	1459.56(8)	**Final R indexes [all data]**	R_1 = 0.0690, wR_2 = 0.1215
Z	4	**Largest diff. peak/hole / e Å^{-3}**	0.58/-0.27
ρ_{calc}g/cm^3	1.439		

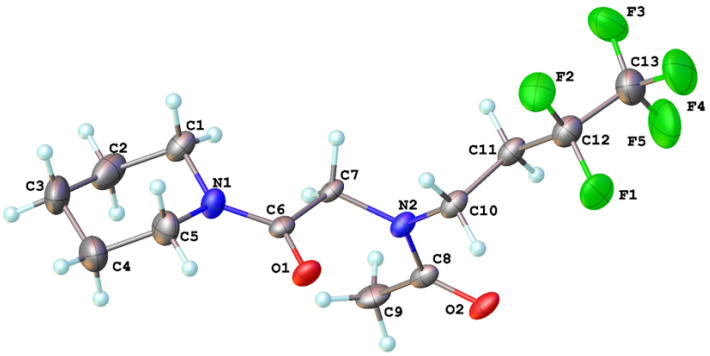

Figure 5.4: Crystal structure of model peptoid **102** reported with a 50% thermal ellipsoid probability

Table 5.7: Crystal data and structure refinement parameters of model peptoid **102**

Empirical formula	$C_{13}H_{19}F_5N_2O_2$	**μ/mm^{-1}**	0.133
Formula weight	330.30	**F(000)**	688.0
Temperature/K	120.00	**Crystal size/mm^3**	0.23 × 0.18 × 0.15
Crystal system	monoclinic	**Radiation**	Mo Kα (λ = 0.71073)
Space group	$P2_1/c$	**2Θ range for data collection/°**	4.354 to 51.996
a/Å	13.7707(6)	**Index ranges**	-16 ≤ h ≤ 16, -16 ≤ k ≤ 16, -10 ≤ l ≤ 11
b/Å	13.3300(6)	**Reflections collected**	22798
c/Å	8.9593(4)	**Independent reflections**	3077 [R_{int} = 0.0754, R_{sigma} = 0.0543]
α/°	90	**Data/restraints/parameters**	3077/0/200
β/°	107.5670(18)	**Goodness-of-fit on F^2**	1.066
γ/°	90	**Final R indexes [I>=2σ (I)]**	R_1 = 0.0666, wR_2 = 0.1612
Volume/Å^3	1567.90(12)	**Final R indexes [all data]**	R_1 = 0.1014, wR_2 = 0.1756
Z	4	**Largest diff. peak/hole / e Å^{-3}**	0.45/-0.25
ρ_{calc}g/cm^3	1.399		

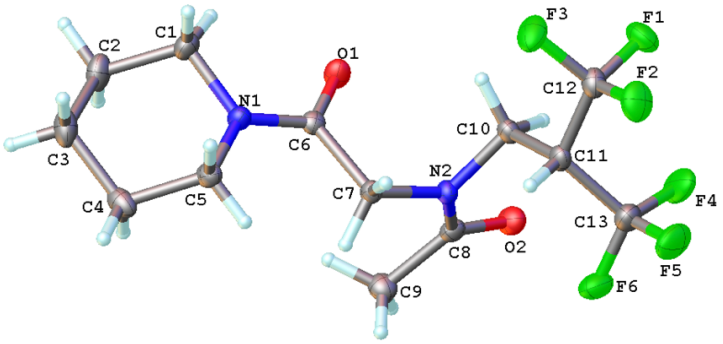

Figure 5.5: Crystal structure of model peptoid **103** reported with a 50% thermal ellipsoid probability

Table 5.8: Crystal data and structure refinement parameters of model peptoid **103**

Empirical formula	$C_{13}H_{18}F_6N_2O_2$	**μ/mm^{-1}**	0.149
Formula weight	348.29	**F(000)**	720.0
Temperature/K	120.00	**Crystal size/mm^3**	0.29 × 0.1 × 0.04
Crystal system	monoclinic	**Radiation**	Mo Kα (λ = 0.71073)
Space group	$P2_1/c$	**2Θ range for data collection/°**	4.518 to 57.98
a/Å	12.8996(4)	**Index ranges**	-17 ≤ h ≤ 17, -18 ≤ k ≤ 18, -12 ≤ l ≤ 12
b/Å	13.6278(4)	**Reflections collected**	29842
c/Å	9.3846(3)	**Independent reflections**	4103 [R_{int} = 0.0598, R_{sigma} = 0.0362]
α/°	90	**Data/restraints/parameters**	4103/0/280
β/°	111.2755(10)	**Goodness-of-fit on F^2**	1.148
γ/°	90	**Final R indexes [I>=2σ (I)]**	R_1 = 0.0518, wR_2 = 0.1079
Volume/Å^3	1537.31(8)	**Final R indexes [all data]**	R_1 = 0.0638, wR_2 = 0.1129
Z	4	**Largest diff. peak/hole / e Å^{-3}**	0.36/-0.26
ρ_{calc}g/cm^3	1.505		

5.9 Characeterization Data for Chapter 3

Peptoids **110** – **116** were all synthesised on a 0.10 mmol scale using the protocol outlined in **Section 5.5.1**. They were subsequently cleaved as described in **Section 5.5.2** to give the crude product, 100 mg of which was purified by RP-HPLC using the procedure detailed in **Section 5.6.1**. Pure fractions were combined and lyophilized to give the pure peptoids as white solids. **Figure 5.6** gives the full structures of **110** – **116** and **Table 5.9** gives the characterization data of each sequence.

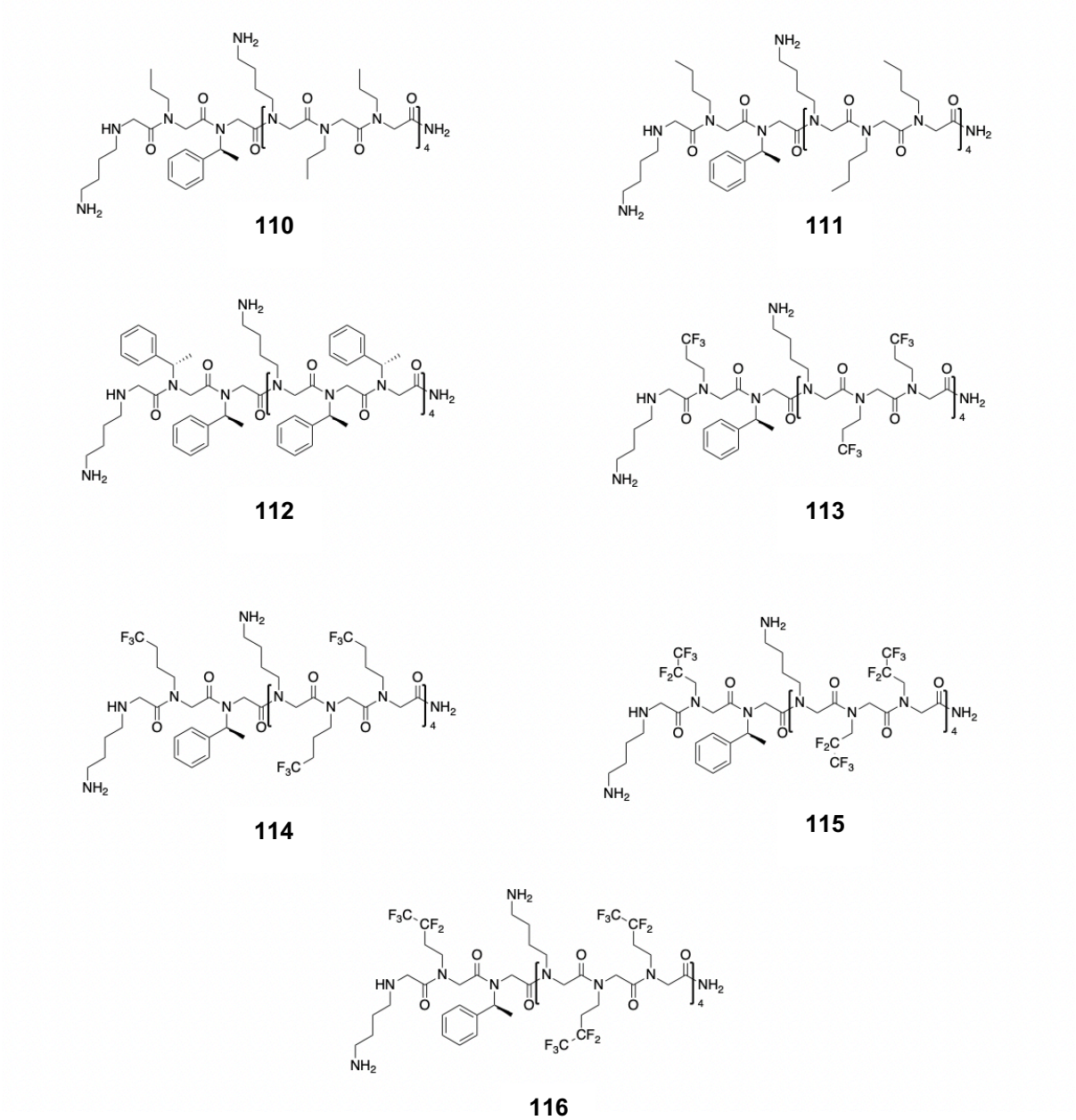

Figure 5.6: Structure of peptoid oligomers **110** – **116** synthesised for **Chapter 3**.

Table 5.9: Characterization data for peptoid oligomers **110** - **116**

Peptoid	Sequence	Analytical HPLC		Yields*			Accurate Mass Spectrometry	
		Retention Time	Purity (%)	Crude Mass (mg)	Isolated Mass (mg)	Isolated Yield (%)	Calculated Mass $[M+2H]^{2+}$ (Da)	Observed Mass (Da)
110	[*N*Lys-*N*Pro-*N*spe][*N*Lys-*N*Pro-*N*Pro]$_4$	16.47	≥95	172	45	26.3	856.1061	856.1084
111	[*N*Lys-*N*Bu-*N*spe][*N*Lys-*N*Bu-*N*Bu]$_4$	21.25	≥95	206	38	20.7	919.1758	919.1788
112	[*N*Lys-*N*spe-*N*spe][*N*Lys-*N*spe-*N*spe]$_4$	25.38	≥95	263	10	4.4	1135.1788	1135.1747
113	[*N*Lys-*N*3fPro-*N*spe][*N*Lys-*N*3fPro-*N*3fPro]$_4$	20.86	≥95	109	12	5.5	1098.9760	1098.9812
114	[*N*Lys-*N*3fBu-*N*spe][*N*Lys-*N*3fBu-*N*3fBu]$_4$	23.37	≥95	175	21	9.0	1162.0531	1162.0516
115	[*N*Lys-*N*5fPro-*N*spe][*N*Lys-*N*5fPro-*N*5fPro]$_4$	24.91	≥95	232	6	2.4	1260.8947	1260.8964
116	[*N*Lys-*N*5fBu-*N*spe][*N*Lys-*N*5fBu-*N*5fBu]$_4$	27.48	≥98	212	12	4.5	1323.9597	1323.9668

*Note only 100 mg of crude peptoid was purified for each compound. Yield is given for the mass of pure peptoid obtained from 100 mg of crude compound.

5.10 References

1 D. Gimenez, J. A. Aguilar, E. H. C. Bromley and S. L. Cobb, *Angew Chem Int Ed*, 2018, **57**, 10549–10553.

2 F. Wen and Z. Li, *Synth Commun*, 2020, **50**, 3462–3474.

3 O. v. Dolomanov, L. J. Bourhis, R. J. Gildea, J. A. K. Howard and H. Puschmann, *J Appl Crystallogr*, 2009, **42**, 339–341.